

# Heavy-ion tumor therapy: Physical and radiobiological benefits

Dieter Schardt and Thilo Elsässer

GSI Helmholtzzentrum für Schwerionenforschung mbH (GSI), D-64291 Darmstadt, Germany

Daniela Schulz-Ertner

Markus-Krankenhaus, MVZ Radiologisches Institut, D-60431 Frankfurt/M., Germany

(Published 19 February 2010)

High-energy beams of charged nuclear particles (protons and heavier ions) offer significant advantages for the treatment of deep-seated local tumors in comparison to conventional megavolt photon therapy. Their physical depth-dose distribution in tissue is characterized by a small entrance dose and a distinct maximum (Bragg peak) near the end of range with a sharp fall-off at the distal edge. Taking full advantage of the well-defined range and the small lateral beam spread, modern scanning beam systems allow delivery of the dose with millimeter precision. In addition, projectiles heavier than protons such as carbon ions exhibit an enhanced biological effectiveness in the Bragg peak region caused by the dense ionization of individual particle tracks resulting in reduced cellular repair. This makes them particularly attractive for the treatment of radio-resistant tumors localized near organs at risk. While tumor therapy with protons is a well-established treatment modality with more than 60 000 patients treated worldwide, the application of heavy ions is so far restricted to a few facilities only. Nevertheless, results of clinical phase I-II trials provide evidence that carbon-ion radiotherapy might be beneficial in several tumor entities. This article reviews the progress in heavy-ion therapy, including physical and technical developments, radiobiological studies and models, as well as radiooncological studies. As a result of the promising clinical results obtained with carbon-ion beams in the past ten years at the Heavy Ion Medical Accelerator facility (Japan) and in a pilot project at GSI Darmstadt (Germany), the plans for new clinical centers for heavy-ion or combined proton and heavy-ion therapy have recently received a substantial boost.

DOI: [10.1103/RevModPhys.82.383](https://doi.org/10.1103/RevModPhys.82.383)

PACS number(s): 34.50.Gb, 87.50.–a, 87.53.Kn, 87.55.–x

## CONTENTS

	3. Dependencies of RBE	405
	4. RBE determined from <i>in vivo</i> measurements	406
	5. Dependence on oxygen status	407
I. Introduction	383	
II. Physical Aspects of Radiotherapy with Ion Beams	384	
A. Energy deposition and dose	384	
1. Stopping of high-energy ions	385	
2. Energy-loss and range straggling	386	
3. Lateral beam spread	387	
4. Nuclear fragmentation	388	
5. Neutron dose	389	
B. Accelerators for ion-beam therapy	390	
C. Beam delivery systems	391	
1. Passive beam shaping	391	
2. Scanning systems	392	
3. Gantries	394	
4. Irradiation of moving organs	395	
D. Treatment planning and dose verification	397	
1. Dose optimization	398	
2. Heavy-ion dosimetry	399	
3. <i>In vivo</i> PET monitoring	399	
E. Future directions	402	
III. Biological Effects of Ion Irradiation	402	
A. Relative biological effectiveness	402	
1. Radiation damage by photons and heavy ions	403	
a. Microscopic track structure of ion beams	403	
b. DNA damage and cell inactivation	404	
2. Definition of RBE	404	
	B. Biophysical models in heavy-ion therapy	407
	1. Biological optimization at LBL	408
	2. HIMAC approach	408
	3. Local effect model (GSI)	409
	a. Basic assumptions	409
	b. Integration into the treatment planning system	411
	c. Choice of parameters for clinical treatments	411
	4. Alternative approaches	411
	C. Implications for treatment planning	412
	D. Future directions	413
	IV. Clinical Experiences	414
	A. Clinical trials investigating heavy-ion radiation therapy	414
	B. Future directions	416
	V. Conclusion	416
	Acknowledgments	417
	References	417
	<b>I. INTRODUCTION</b>	
	Radiotherapy plays an important role in the treatment of cancer. After surgery it is the most frequently and most successfully applied form of therapy. More than	

50% of all patients with localized malignant tumors are treated with radiation. In radiotherapy the key problem is to deliver the dose in such a way that ideally the planned target volume receives 100% of the dose needed to kill all cancer cells in the tumor, while the surrounding normal tissue should not receive any dose. In practice, this cannot be achieved because of the unavoidable dose deposition in the entrance channel of the radiation. In the past 50 years much progress has been made to improve dose delivery towards the ideal situation and to thereby increase the tumor control rate. These achievements would not have been possible without the strong and fruitful interdisciplinary collaboration of scientists in the fields of oncology and radiation medicine, radiation biology, accelerator technology, and engineering, as well as atomic and nuclear physics.

The application of high-energy beams of heavy charged particles to radiotherapy was first considered in 1946 when Robert R. Wilson investigated the depth-dose characteristics of proton beams (primarily for shielding purposes) (Wilson, 1946). He recognized the potential benefits of proton beams and predicted “that precision exposures of well-defined small volumes within the body will soon be feasible.” Two years later the 184 in. synchrocyclotron at Lawrence Berkeley Laboratory (LBL), Berkeley (USA) became available for experiments and the physical and radiobiological properties of proton beams were thoroughly investigated by Tobias (1967). Patient treatments started in 1954 at LBL Berkeley, first with protons and later with helium beams. Radiotherapy with heavier ions started in 1975 at the Bevalac facility at LBL. There most of the patient treatments were performed with beams of  $^{20}\text{Ne}$  (670 MeV/u), which at that time appeared to be most attractive because of their high relative biological effectiveness (RBE) combined with a low oxygen enhancement ratio (OER) in the treatment target volume (Chen, Castro, and Quivey, 1981; Petti and Lennox, 1994). The beams were delivered to the patient by passive beam shaping systems, including scattering devices, substituted later on by magnetic wobblers, and a number of other passive elements like ridge filters, range modulators, collimators, and boli (Chu *et al.*, 1993). Until its closure in 1992 the Bevalac was the only facility worldwide using heavy ions<sup>1</sup> for radiotherapy of localized deep-seated tumors. The treatments with  $^{20}\text{Ne}$  beams included a total of 433 patients.

In 1994 the Heavy Ion Medical Accelerator (HIMAC) (Hirao *et al.*, 1992) dedicated to radiotherapy started with carbon ions at National Institute of Radiological

Science (NIRS) Chiba (Japan), using similar technical concepts as those pioneered at Berkeley. At the same time new technical solutions were developed almost in parallel at Paul-Scherrer-Institute (PSI) in Switzerland and Gesellschaft für Schwerionenforschung (GSI) in Germany, differing significantly from the previous designs at the Bevalac and HIMAC. The implementation of active beam scanning techniques [“spot scanning” at PSI (Pedroni *et al.*, 1995), “raster scanning” at GSI (Haberer *et al.*, 1993), see Sec. II.C.2] resulted in the achievement of a high degree of conformation, guiding the biologically most effective ions to the target volume and minimizing the dose to the surrounding normal tissue. In spite of the challenging technical concept the pencil beam scanning has proven to operate reliably since the first patient treatments in 1996 at PSI and 1997 at GSI.

For the carbon-ion treatments at GSI the variation of the biological effectiveness across the irradiated volume was taken into account individually for each voxel by the treatment planning system TRiP (Krämer and Scholz, 2000; Krämer *et al.*, 2000) that includes the local effect model (LEM). This model was specifically designed to estimate the RBE by including several important parameters such as the dose level, the biological end point, and the irradiated tissue. This development reflects the progress in radiobiology based on extended experimental studies and improvements in modeling of the RBE, as well as in the development of powerful computer algorithms for treatment planning.

The physical properties of heavy-ion beams, technical solutions, and dose verification techniques are discussed in Sec. II, followed by an overview of radiobiological studies, modeling of the biological effect, and its application in treatment planning in Sec. III. Finally, Sec. IV presents recent clinical results from carbon-ion studies and comparison with other treatment modalities.

## II. PHYSICAL ASPECTS OF RADIOTHERAPY WITH ION BEAMS

### A. Energy deposition and dose

The main reason for using heavy charged particles in radiotherapy is their favorable depth-dose profile (“Bragg curve”), named after Sir William Henri Bragg who investigated the slowing down of  $\alpha$  particles in air (Bragg, 1905). Many years later Wilson (1946) proposed the application of protons and heavier ions for precision exposures in radiotherapy. A comparison of depth-dose profiles for electromagnetic radiation (x rays and megavolt photon beams) and particle beams (protons and carbon ions) is displayed in Fig. 1. Low-energy x rays show a steep exponential decrease of dose with depth (absorption law). For high-energy photons (mostly used in conventional therapy nowadays) the initial dose buildup, mainly caused by forward scattered Compton electrons, shifts the peak dose by a few centimeters away from the surface of the patient’s body, thereby improving the target-to-entrance dose and sparing the radiosensitive

<sup>1</sup>The term “heavy ions” is commonly used in the particle therapy community to characterize ions heavier than protons, although they are relatively light considering the full mass range of nuclei. The radiation techniques which make use of beams of charged nuclei are defined by different authors with different names. On top of “light-ion therapy and heavy-ion therapy,” the most used ones are “hadron therapy” and “particle therapy.”

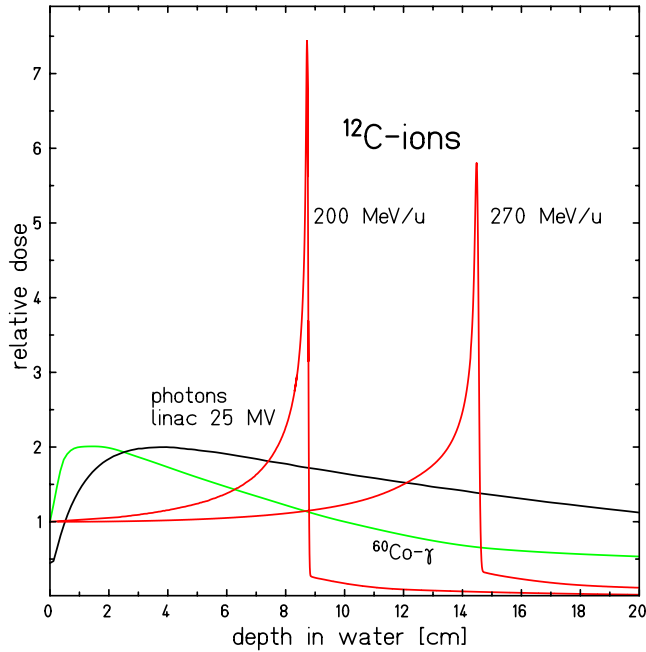


FIG. 1. (Color online) Depth-dose profiles of  $^{60}\text{Co}$   $\gamma$  radiation, megavolt photons, and  $^{12}\text{C}$  ions in water.

skin. In contrast to photons, the dose profiles of protons and heavier ions are characterized by a distinct narrow peak (“Bragg peak”) at the end of their path. The position of this peak can be precisely adjusted to the desired depth in tissue by changing the kinetic energy of the incident ions. Protons and heavier ions differ in two features essentially: First, protons have a similar biological effect as photons (at the same absorbed dose), while heavy ions show higher effectiveness, ranging from low RBE values in the plateau region to a significant enhancement in the Bragg peak (Kraft, 2000). Second, heavy ions (unlike protons) exhibit a characteristic dose tail behind the Bragg peak, which is caused by secondary fragments produced in nuclear reactions along the stopping path of the ions, resulting in a complex radiation field (Schardt *et al.*, 1996).

The dose deposited in tissue is the most important physical quantity in radiotherapy. It is defined (ICRU, 1993) by the term *absorbed dose* (unit Gray [Gy]) as the mean energy  $d\epsilon$  deposited by ionizing radiation in a mass element  $dm$ ,

$$D = \frac{d\epsilon}{dm} \quad [1 \text{ Gy} = 1 \text{ J/kg}]. \quad (1)$$

In radiation therapy (RT) water is used as tissue reference medium. Dose measurements are normally performed with air-filled ionization chambers and have to be converted to the absorbed dose in water by correction factors. For a parallel beam with particle fluence  $F$  the dose deposited in a thin slice of an absorber material with mass density  $\rho$  can be calculated as follows:

$$D[\text{Gy}] = 1.6 \times 10^{-9} \times \frac{dE}{dx} \left[ \frac{\text{keV}}{\mu\text{m}} \right] \times F[\text{cm}^{-2}] \times \frac{1}{\rho} \left[ \frac{\text{cm}^3}{\text{g}} \right], \quad (2)$$

where  $dE/dx$  is the energy loss of the particles per unit path length (specific energy loss or “stopping power”). A similar related quantity is the linear energy transfer (LET), unit  $\text{keV}/\mu\text{m}$ , which refers to the energy deposited in the stopping medium by the slowing-down particle.

For particle therapy the photon-equivalent dose, sometimes referred to as biological dose or Gray-equivalent dose, defined as the product of absorbed dose and RBE, is most significant because it includes the larger efficacy of ions. The units are named Cobalt-Gray-Equivalent (CGE) or Gray-Equivalent (GyE). According to recent recommendations (ICRU, 2007) for proton beam therapy, now the term “RBE-weighted” dose and the unit Gy (RBE) should be used. Similar recommendations for heavy-ion therapy are in progress, but presently still the unit GyE is commonly used within the clinical community.

### 1. Stopping of high-energy ions

In this section the basic formulas describing the stopping of ions in a thick absorber are recalled. The theory of stopping and range of ions in matter has been treated in extended reviews (Fano, 1963; Ahlen, 1980; Sigmund, 2004; Ziegler *et al.*, 2008). Radiotherapy of deep-seated tumors requires ion beam ranges in tissue of up to 30 cm corresponding to specific energies up to 220 MeV/u for protons and helium ions, 430 MeV/u for carbon ions, and 600 MeV/u for neon ions with particle velocities  $\beta \equiv v/c \approx 0.7$ . At these velocities the energy-loss rate  $dE/dx$  in the slowing-down process is dominated by inelastic collisions with the target electrons (electronic stopping) and can be well described by the Bethe-Bloch formula (Bethe, 1930; Bloch, 1933a, 1933b), here given in the relativistic version described by Fano (1963), including the shell correction term  $C/Z_t$  and the density effect correction term  $\delta/2$ ,

$$\frac{dE}{dx} = \frac{4\pi e^4 Z_p Z_t^2}{m_e v^2} \left[ \ln \frac{2m_e v^2}{\langle I \rangle} - \ln(1 - \beta^2) - \beta^2 - \frac{C}{Z_t} - \frac{\delta}{2} \right]. \quad (3)$$

$Z_p$  and  $Z_t$  denote the nuclear charges of the projectile and target,  $m_e$  and  $e$  are the mass and charge of the electron, and  $\langle I \rangle$  is the mean ionization energy of the target atom or molecule. For liquid water the value  $\langle I \rangle = 79.7 \text{ eV}$  was obtained from energy-loss measurements with 70 MeV protons (Bichsel and Hiraoka, 1992; Bichsel *et al.*, 2000). From recent precision Bragg curve measurements for protons and various heavier ions values of 75–78 eV were deduced (Kumazaki *et al.*, 2007; Paul, 2007; Schardt *et al.*, 2008). Stopping-power curves for

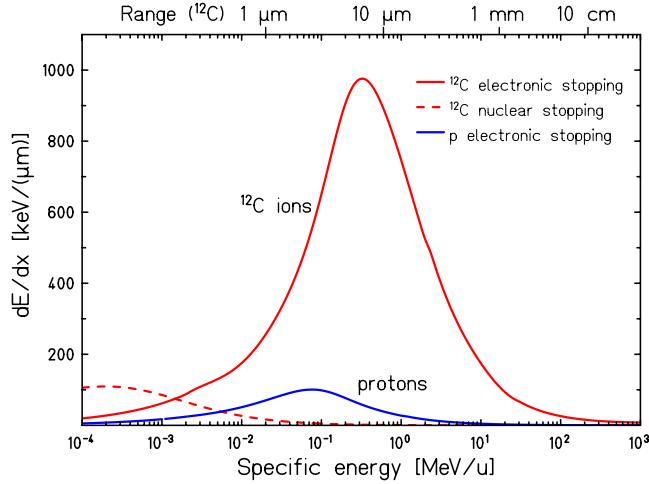


FIG. 2. (Color online) Specific energy loss  $dE/dx$  of  $^{12}\text{C}$  ions and protons in water. The range of  $^{12}\text{C}$  ions in water corresponding to their specific energy is indicated at the top.

protons and  $^{12}\text{C}$  ions in water are shown in Fig. 2.

Due to the  $1/\beta^2$  dependence the energy loss increases with decreasing particle energy. At high velocities the atomic electrons are completely stripped off and the projectile charge is equal to the atomic charge number  $Z_p$ . At lower velocities (for light ions below about 10 MeV/u), the mean charge state decreases due to the interplay of ionization and recombination processes and  $Z_p$  in Eq. (3) has to be replaced by the effective charge  $Z_{\text{eff}}$ , which can be described by the empirical formula (Barkas, 1963)

$$Z_{\text{eff}} = Z_p [1 - \exp(-125\beta Z_p^{-2/3})]. \quad (4)$$

The maximum energy-loss rate, corresponding to the Bragg peak, is reached at a projectile velocity of

$$v_p \approx Z_p^{2/3} v_0, \quad (5)$$

where  $v_0 = e^2/\hbar$  is the Bohr velocity and the corresponding  $\beta$  value is  $e^2/\hbar c = 1/137$ . For  $^{12}\text{C}$  ions this maximum occurs at a specific energy of  $\approx 350$  keV/u. At still lower projectile energies ( $E_p \leq 10$  keV/u) elastic collisions with target nuclei begin to contribute significantly to the energy loss and dominate the stopping process at the very end of the particle path (the last few  $\mu\text{m}$ ). The corresponding dose contribution is, however, very small and can be neglected in radiotherapy applications (Elsässer *et al.*, 2009).

The total path length of the particle's trajectory in the absorber is given by

$$R(E) = \int_0^E \left( \frac{dE'}{dx} \right)^{-1} dE', \quad (6)$$

which for heavy charged projectiles is nearly the same as the mean range  $R$ , i.e., the average traversed absorber thickness, because heavy ions are very little scattered and travel almost on a straight line. Ranges of various ion beams in water are shown in Fig. 3. The range of

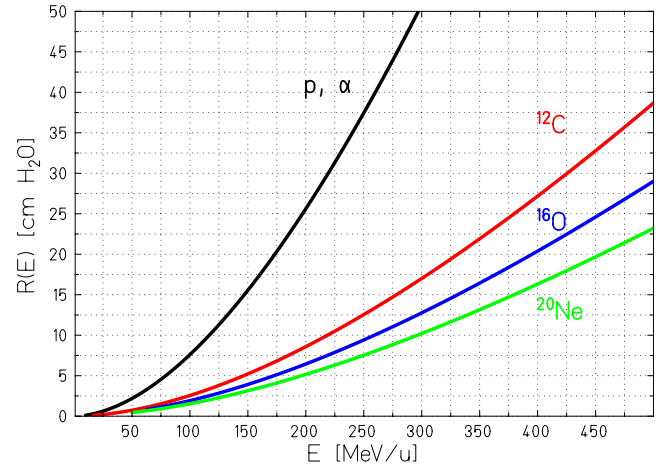


FIG. 3. (Color online) Mean range of heavy ions in water.

ions with the same specific energy scales with a factor of  $A/Z^2$ .

## 2. Energy-loss and range straggling

According to Eq. (3) the energy loss of a *single* carbon ion plotted as a function of absorber depth would result in a very sharp peak near the stopping point. For example, for an incident 300 MeV/u carbon ion the  $dE/dx$  peak-to-entrance value is about 80 (see Fig. 2). However, statistical fluctuations of the energy loss in the large number of collisions of the slowing-down process result in a broadening of the Bragg peak for an ion beam consisting of many particles. These fluctuations are described by the (asymmetric) Vavilov distribution (Vavilov, 1957) for charged particles passing through a thin layer of matter (energy-loss straggling). In the limit of many collisions the Vavilov distribution becomes a Gaussian (Bohr, 1940; Ahlen, 1980),

$$f(\Delta E) = \frac{1}{\sqrt{2\pi}\sigma} \exp \left( -\frac{(\Delta E - \overline{\Delta E})^2}{2\sigma^2} \right) \quad (7)$$

with

$$\sigma = 4\pi Z_{\text{eff}} Z_t e^4 N \Delta x \left[ \frac{1 - \beta^2/2}{1 - \beta^2} \right]. \quad (8)$$

The variance  $\sigma_R^2$  of the range straggling is related to the variance  $\sigma_E^2$  of the energy-loss straggling by

$$\sigma_R^2 = \int_0^{E_i} \left( \frac{d\sigma_E}{dx} \right) \left( \frac{dE}{dx} \right)^{-3} dE. \quad (9)$$

The ratio of the straggling width  $\sigma_R$  and mean range  $R$  is nearly constant and can be described by

$$\frac{\sigma_R}{R} = \frac{1}{\sqrt{M}} f \left( \frac{E}{Mc^2} \right), \quad (10)$$

where  $f$  is a slowly varying function depending on the absorber (Rossi, 1952) and  $E$  and  $M$  are the particle energy and mass. For light ions stopped in water the relative straggling  $\sigma_R/R$  is of the order of  $10^{-3}$ . Because

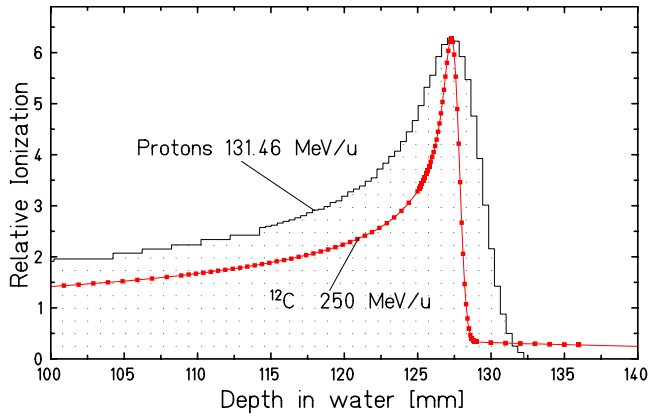


FIG. 4. (Color online) Measured Bragg peaks of protons and  $^{12}\text{C}$  ions having the same mean range in water (Schardt *et al.*, 2008).

of the  $1/\sqrt{M}$  dependence it is smaller for heavier ions than for protons, e.g., a factor of 3.5 for  $^{12}\text{C}$  ions (Fig. 4). In practice, however, the profile of the Bragg peaks is broader, mainly due to the density inhomogeneities of the penetrated tissue. Furthermore, for scanning beam delivery systems using slice-by-slice irradiation of the target volume, it can be even advantageous to widen the sharp Bragg peaks by passive systems in order to reduce the treatment time (Weber and Kraft, 1999).

### 3. Lateral beam spread

The small lateral deflection of heavy ions penetrating through an absorber is a particular advantage of heavy ions in comparison to protons and is of clinical relevance for treatments near organs at risk (OAR). The beam spread is mainly caused by elastic Coulomb interactions with the target nuclei, while scattering due to electronic interactions, which dominate the stopping process, can be neglected. The statistical distribution function  $F(\theta, d)$  for the resulting scattering angle  $\theta$  at penetration depth  $d$  can be obtained from the integral equation given by Bothe (1921). An analytical solution of this equation was given by Molière (1948) for a shielded Coulomb potential. A thorough analysis of a large set of proton beam spread data obtained over many years at the Harvard proton therapy center (Gottschalk *et al.*, 1993) was found to be in very good agreement with the Molière theory.

For small angles the higher-order terms in Molière's solution can be neglected and the angular distribution can be approximated by a Gaussian function with a standard deviation given by Highland (1975, 1979)

$$\sigma_{\theta}[\text{rad}] = \frac{14.1 \text{ MeV}}{\beta pc} Z_p \sqrt{\frac{d}{L_{\text{rad}}}} \left[ 1 + \frac{1}{9} \log_{10} \left( \frac{d}{L_{\text{rad}}} \right) \right]. \quad (11)$$

The absorber material is characterized by the thickness  $d$  and the radiation length  $L_{\text{rad}}$ . Values of  $L_{\text{rad}}$  for common materials can be found in Tsai (1974) and can be easily computed for compounds (e.g., water 36.08, Al

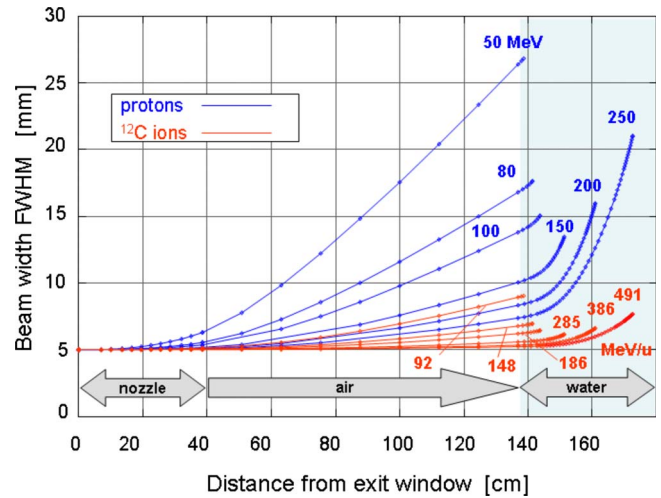


FIG. 5. (Color online) Calculated beam spread for  $^{12}\text{C}$  ions and protons in a typical treatment beam line. It was assumed that an initially parallel particle beam (5 mm full width at half maximum) passes through the nozzle (including a thin vacuum window and beam monitors) and enters a water absorber (patient) at 1 m distance from nozzle exit. At small depth (i.e., small particle energies) the width is mainly determined by scattering in the nozzle, while at higher energies the scattering in the water absorber dominates. Carbon ions show a much smaller spread than protons at the same penetration depth. Figure courtesy of U. Weber, Rhön-Klinikum AG.

24.01, Fe 13.83, Pb 6.37  $\text{g}/\text{cm}^2$ ). Targets containing heavy elements cause a larger angular spread than targets of light elements with the same thickness (in units of  $\text{g cm}^{-2}$ ). The angular spread for heavy charged particles is small (of the order of 1 mrad for a thin target), but increases significantly towards low energies due to the  $\beta pc$  term in the denominator of Eq. (11). Comparing beams with the same range in water (e.g., 150 MeV protons and 285 MeV/u  $^{12}\text{C}$  ions with  $R=15.6$  cm) shows that the angular spread ( $\sigma_{\theta}$ ) for protons is more than three times larger than that for  $^{12}\text{C}$  ions.

In practice two different contributions to the angular beam spreading have to be considered: (i) scattering caused by materials in front of the patient (e.g., vacuum exit window, beam monitor, beam shaping devices) and (ii) scattering in tissue between entrance point and stopping depth. At low energies (i) represents the dominant contribution because even a small angular spread translates in a significant broadening of the beam spot due to the traveling distance of typically 0.5–1.0 m before entering the patient. This is critical in particular for protons and scanning systems using narrow pencil-like beams. Therefore the material in the beam path in front of the patient should be kept as thin as possible, not contain heavy elements, and be located as close as possible towards the patient. At higher energies contribution (i) becomes less important or even negligible while (ii) increases due to the larger penetration depths in tissue. The calculations shown in Fig. 5 demonstrate the much smaller beam spread of  $^{12}\text{C}$  ions compared to protons (Weber and Kraft, 2009). Detailed measurements

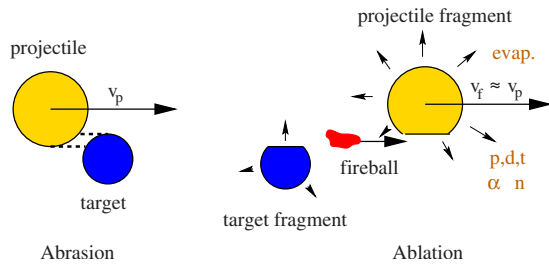


FIG. 6. (Color online) Illustration of the abrasion-ablation model of peripheral collisions at high energies according to Serber (1947). Adapted from Gunzert-Marx *et al.* (2008).

confirmed these calculations (Weber, 1996). It should be kept in mind, however, that in irradiations of tissues with large density inhomogeneities even a small lateral spread may translate into a considerable range broadening.

#### 4. Nuclear fragmentation

While the stopping process of high-energy ions penetrating a thick absorber is governed by collisions with atomic electrons, the probability of nuclear reactions is much smaller, but leads to significant effects at large penetration depths. At energies of several hundred MeV/u violent nuclear spallation reactions may result in a complete disintegration of both projectile and target nuclei (e.g., in central head-on collisions) or in partial fragmentations. For geometrical reasons peripheral collisions, where the beam particle loses one or several nucleons, are the most frequent nuclear reactions occurring along the stopping path of the ions. They can be well described by the abrasion-ablation model (Serber, 1947) as a two-step process (Fig. 6).

In the first step nucleons are abraded in the overlapping reaction zone (the “fireball”) while the outer (“spectator”) nucleons are only slightly affected. The remaining projectile and target fragments then deexcite by evaporation of nucleons or clusters in the second step (ablation). Fragmentation reactions have been extensively studied in nuclear physics [see, e.g., Goldhaber and Heckman (1978), Hüfner (1985), and Lynch (1987)] and experimental data are available for many projectile-target combinations and for a wide range of beam energies (Friedländer and Heckmann, 1985). Some important conclusions can be drawn for the effects of fragmentation relevant to radiotherapy with high-energy ion beams: (i) Nuclear reactions cause a loss of primary beam particles and a buildup of lower- $Z$  fragments, these effects becoming more and more important with increasing penetration depth. (ii) The secondary (or higher-order) projectilelike fragments are moving with about the same velocity as the primary ions. They have in general longer ranges and produce a dose tail behind the Bragg peak. (iii) The angular distributions of fragments are mainly determined by reaction kinematics and forward directed, but much broader than the lateral spread of the primary ions caused by multiple Coulomb scattering (Golovkov *et al.*, 1997; Matsufuji *et al.*, 2005).

TABLE I. Total reaction cross section  $\sigma_R$  (Kox *et al.*, 1987) and mean free path in water  $\lambda$  of high-energy ions with about 25 cm range in water.

Ion	$E$ (MeV/u)	$\sigma_R$ (mb)	$\lambda$ (cm)
$p$	200	352	85.2
${}^4\text{He}$	200	767	38.6
${}^{12}\text{C}$	380	1424	20.8
${}^{20}\text{Ne}$	530	1929	15.5

Dedicated fragmentation studies for applications in radiotherapy began at Princeton (Maccabee and Ritter, 1974) and were performed over many years at the Bevalac at LBL Berkeley (Schimmerling *et al.*, 1983, 2008; Llacer, Tobias, *et al.*, 1984; Llacer *et al.*, 1990). for the characterization of 670 MeV/u beams of  ${}^{20}\text{Ne}$  which were used for patient treatments. The measured fluence and LET data (Shavers *et al.*, 1990, 1993) as a function of depth in water were compared with transport theories (Wilson *et al.*, 1984, 1990).

Similar fragmentation studies were performed later at the HIMAC facility and at the SIS-18 synchrotron at GSI Darmstadt. In a comparative experimental study of the fragmentation characteristics of  ${}^{10}\text{B}$ ,  ${}^{12}\text{C}$ ,  ${}^{14}\text{N}$ ,  ${}^{16}\text{O}$ , and  ${}^{20}\text{Ne}$ , the total (nuclear) cross section for reactions changing the proton number  $Z$  was found to be even smaller for  ${}^{12}\text{C}$  than that of  ${}^{10}\text{B}$ , while the value for  ${}^{14}\text{N}$  was relatively high (Schall *et al.*, 1996). This indicates that shell-structure effects are still visible in high-energy reactions. Nevertheless, at larger penetration depths a substantial fraction of primary ions is lost by nuclear reactions. For a 400 MeV/u  ${}^{20}\text{Ne}$  beam, for example, only 38% of the primary ions reach the Bragg peak at 16 cm depth in water, the number of surviving  ${}^{12}\text{C}$  ions at the same range being 52%. Regarding fragmentation, carbon ions thus offer relatively good conditions. Furthermore, the positron-emitting fragments  ${}^{10}\text{C}$  and  ${}^{11}\text{C}$  can be utilized for *in vivo* range monitoring with position emission tomography (PET) techniques (see Sec. II.C.2).

The total reaction cross sections  $\sigma_R$  at high energies can be well described by semiempirical geometrical models (Kox *et al.*, 1987; Sihver *et al.*, 1993; Tsao *et al.*, 1993) and are almost constant over a wide energy range down to about 100 MeV/u. Typical values for various ions and the corresponding mean free paths in water are shown in Table I. At lower energies  $\sigma_R$  rises due to the contributions of other reaction mechanisms like deep-inelastic collisions or fusion reactions.

The partial cross sections for production of lower- $Z$  fragments can be derived from the characteristic shapes of their fluence profiles as a function of depth. These buildup and decay curves can be described by solutions of a diffusion equation, the so-called “transport equation,” which is in a similar way applied to the transport

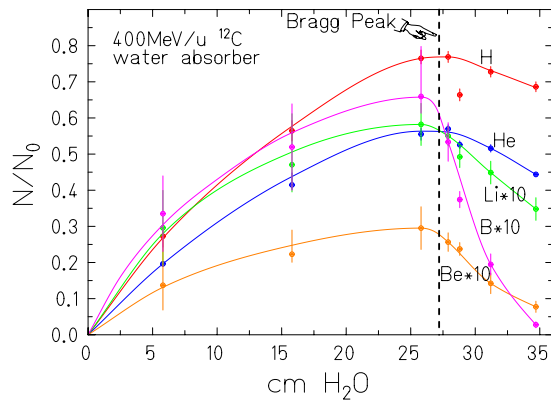


FIG. 7. (Color online) Buildup of secondary fragments produced by 400 MeV/u  $^{12}\text{C}$  ions stopping in water. From Haettner *et al.*, 2006.

of galactic cosmic rays through the atmosphere (Shapiho and Silberberg, 1970; Allkofer and Heinrich, 1974; Wilson *et al.*, 1987). With the simplifying assumption of energy-independent cross sections the elemental fragment distributions as a function of absorber depth can be described by a homogeneous system of differential equations. Partial nuclear reaction cross sections can then be obtained from fitting to experimental buildup data (Schall *et al.*, 1996). As an example, measured (Haettner *et al.*, 2006) buildup curves for charged fragments of primary  $^{12}\text{C}$  ions with  $Z=1$  to 5 are shown in Fig. 7. Hydrogen and helium fragments are most abundantly produced. The heavier fragments like boron are slowed down shortly after the Bragg peak, while hydrogen and helium fragments with much longer ranges produce the longer part of the dose tail.

The fluence of primary  $^4\text{He}$ ,  $^{12}\text{C}$ ,  $^{20}\text{Ne}$ ,  $^{28}\text{Si}$ , and  $^{40}\text{Ar}$  ions and secondary fragments as a function of penetration depth in a polymethylmethacrylate (PMMA) target was investigated at the HIMAC facility (Matsufuji *et al.*, 2003). Fragments were identified by a  $\Delta E$ - $E$  telescope detector, which was combined with a gas-flow proportional counter for simultaneous LET measurements. Larger discrepancies from calculated fluences were found for the buildup curves of hydrogen fragments.

The impact of nuclear fragmentation on the depth-dose profile is shown in Fig. 8. With increasing penetration depth the peak-to-entrance dose ratio becomes gradually smaller, mainly caused by the exponentially diminishing flux of primary ions. The buildup of lower- $Z$  fragments is clearly visible in the dose tail behind the Bragg peak at larger depths. Additionally, the Bragg peaks are increasingly broadened by straggling.

In comparison to  $^{12}\text{C}$  ions these effects are much more pronounced in the example shown in Fig. 9 for 670 MeV/u  $^{20}\text{Ne}$  ions with a range of about 36 cm in water. The peak-to-entrance dose ratio is only 1.5 in this case. The calculated contributions of the primary ions and second and third generation fragments are based on a semiempirical fragmentation cross-section formula (Sihver *et al.*, 1998).

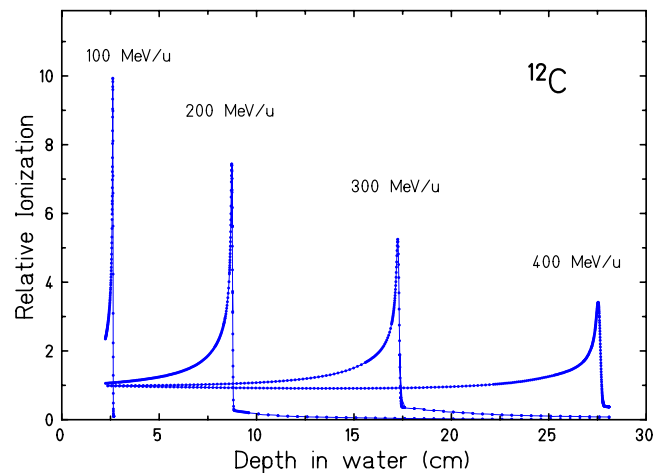


FIG. 8. (Color online) Measured Bragg curves of  $^{12}\text{C}$  ions stopping in water. From Schardt *et al.*, 2008.

### 5. Neutron dose

There is an ongoing discussion about the role of secondary neutrons for the risk of late effects and secondary cancers (Hall, 2006; Hall and Brenner, 2006; Macklis, 2006; Paganetti *et al.*, 2006; Xu *et al.*, 2008). In all modern therapy modalities [intensity-modulated radiation therapy (IMRT), protons, or heavier ions] neutrons may be produced by nuclear interactions either in beam forming elements or (inevitably) in the patient's body. In older facilities where beam modulating elements (e.g., range shifters) were placed near to the patient rather high neutron doses have been reported (Binns and Hough, 1997; Yan *et al.*, 2002). These results were in agreement with Monte Carlo calculations (Agosteo *et al.*, 1998), showing that neutrons emerging from passive beam shaping devices straight ahead to the patient cause the predominant secondary dose contribution, which can be about ten times higher than for fully active scanning systems. It was pointed out, however, that the neutron

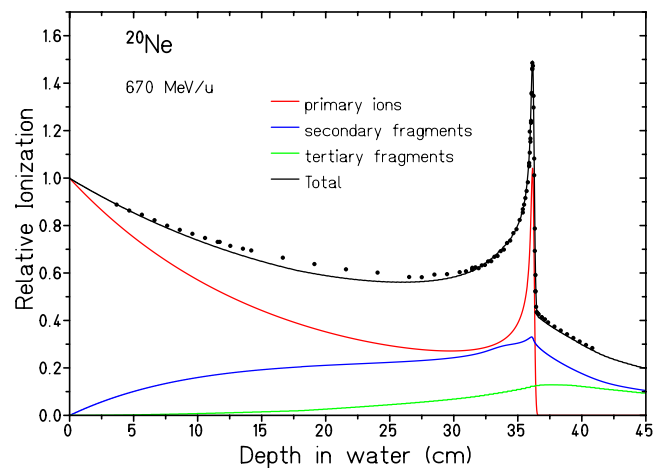


FIG. 9. (Color online) Bragg curve for 670 MeV/u  $^{20}\text{Ne}$  ions in water measured at GSI (circles) and calculated contributions of primary ions, secondary and tertiary fragments. Adapted from Sihver *et al.* (1998).

dose depends on the details of the beam delivery system (Gottschalk, 2006). Neutron doses of 2 mSv per treatment Gy in normal tissue measured at the spot-scanning facility at PSI (Switzerland) are indeed very small and led to the conclusion that such doses are negligible in view of the dose sparing that can be achieved with scanned proton beams in comparison to photons (Schneider *et al.*, 2002).

In case of heavy ions the dose of secondary fragments, in particular the dose tail at large depths, can mainly be attributed to *charged* particles, produced as projectile fragments or emitted in the deexcitation process. Secondary neutrons are produced with similar characteristics as protons: their energy spectrum shows a broad maximum at about half the velocity of the incident primary ions and their emission angles are strongly forward peaked. For a 200 MeV/u  $^{12}\text{C}$  beam stopping in a thick water absorber the forward yield was found to be 0.54 neutrons per primary ion (Gunzert-Marx *et al.*, 2008). Based on this number the neutron dose in typical carbon-ion treatments assuming a medium-sized target volume of 125 cm<sup>3</sup> was estimated as 8 mGy per treatment Gy, i.e., less than 1% of the treatment dose. This is about ten times less than the dose contributed by charged fragments. Direct dose measurements (Iwase *et al.*, 2007) using a wide-energy neutron dosimeter confirmed the above dose estimates. Comparing the neutron doses in proton and carbon-ion therapy (considering only the dose inevitably produced by fragmentation in the patient's body) results in a similar level, although the neutron yield is much higher for carbon ions. This is mainly explained by the fact that a much higher number of protons (more than a factor of 20) is needed to produce the same dose as carbon ions. Studies performed with GEANT4 Monte Carlo calculations, where the complex processes of neutron transport and energy deposition were investigated in detail, arrived at similar results (Pshenichnov *et al.*, 2005). Microdosimetric measurements (Endo *et al.*, 2007) at various angles to the beam axis resulted in neutron doses ranging from  $1.4 \times 10^{-4}$  in forward direction (0° in 9 cm distance behind Bragg peak) to  $8.2 \times 10^{-8}$  backwards (126°) relative to the dose in the Bragg peak.

In conclusion, the dose contribution of secondary neutrons produced by fragmentation reactions in tissue appears to be small, even considering their enhanced biological effectiveness. The absorbed dose due to neutrons is of course included in the measured Bragg curves, entering as basic input data into the physical model used in heavy-ion treatment planning. As discussed above, the production of neutrons in thick absorber materials located in the beam line in front of the patient should be avoided. Therefore, in modern treatment facilities using passive energy degraders or other beam shaping devices the treatment beam is cleaned by deflection units located behind the passive elements before it is sent to the patient.

## B. Accelerators for ion-beam therapy

At the early stage of heavy-ion therapy the Bevalac (combining the heavy-ion linear accelerator SuperHILAC with the Bevatron synchrotron) was the only machine worldwide capable of accelerating heavy ions to kinetic energies of several hundred MeV/u as required for radiotherapy. It was, however, not optimized for the requirements of particle therapy but designed as a forefront tool for nuclear research with relativistic heavy-ion beams. While research machines should offer maximum flexibility, the design of medical machines has to focus on reliability of the machine operation and extreme care in beam control, which are key issues for operation in a clinical environment and patient safety. In the following years a number of proposals for medical heavy-ion accelerator projects were elaborated trying to best meet these demands. Most of these projects were designed as highly versatile facilities, serving also the demands of the physics and nuclear chemistry communities. Except for the Japanese HIMAC-project, however, none of the other projects (USA, Canada, Europe) have been realized.

The choice of the accelerator type, cyclotron or synchrotron, was one important question discussed by accelerator experts. Cyclotrons were considered as easy to operate, highly reliable, and compact machines. They offer extremely stable and regulable beam intensities, but no energy variation, i.e., only by means of passive degraders in the beam line. Synchrotrons, on the other hand, offer fast energy variation (from pulse to pulse), but need an injector and a delicate extraction system and are more complex in operation. For a critical review of projects up to 1991 see Böhne (1992). In Böhne's conclusion the synchrotron is recommended as the most appropriate technical choice at lowest investment cost. This assessment was shared in the final report of a design study for an European Light Ion Medical Accelerator (EULIMA) (Wambersie *et al.*, 1992), where the concept of a superconducting cyclotron was compared to a conventional synchrotron.

Further on, major progress was made in the design of the injection linac [electron cyclotron resonance (ECR) ion source, radio frequency quadrupole (RFQ) and interdigital H-type (IH) structures] and led to a significant reduction in length and cost. Compact accelerators for modern carbon-ion therapy centers such as the HIBMC Hyogo, Japan (designed by Mitsubishi) or Heidelberg Ion Therapy center (HIT) Heidelberg, Germany (GSI design) combine injection linacs less than 10 m long with synchrotron rings of 20–30 m diameter. A compact unit for heavy-ion therapy was designed at CERN in a Proton and Ion Medical Machine Study (PIMMS). Major progress was made in the beam extraction, which is activated through a resonance with a betatron core and results in a flat time structure (Badano *et al.*, 1999, 2000). The new facility CNAO (TERA foundation, Italy), presently under construction, as well as several other projected European ion-therapy centers are based on the PIMMS design (Amaldi and Kraft, 2007). At the

HIMAC facility, a new beam extraction method the RF knock-out slow extraction (“KO extraction”) was developed (Noda *et al.*, 1996), which proved to be an excellent method of achieving highly controllable structure-free spills. This method allows one to switch the extraction on or off within 1 ms and has been used since 1996 for respiration-gated irradiations (See Sec. II.C.4).

The synchrotron solution was chosen for all heavy-ion-therapy centers presently in operation or under construction. Nonetheless, there are ongoing efforts for the design of cyclotrons, which are widely distributed in proton therapy, for heavy-ion therapy as well. The problem of the higher magnetic rigidities for heavy ions might be overcome by superconducting cyclotrons. Recent design studies for a superconducting cyclotron have shown that for heavy ions with  $A/Z=2$  maximum energies of 250–300 MeV/u can be achieved using a conservative and reliable design (Calabretta *et al.*, 2006; Maggiore *et al.*, 2006). This energy range would, however, limit the treatments to a maximum water-equivalent depth of 17 cm. The major difficulty for using cyclotrons, however, is the lack of energy variability. The passive degrader solution applied for protons (see below) is not suitable for carbon-ion beams, as breakup of carbon ions into three  $\alpha$  particles (having the same  $A/Z$  ratio and similar velocity as the carbon ions) has a high cross section and therefore clean degraded carbon beams are difficult to achieve. Another solution proposed by Amaldi and co-workers (Amaldi *et al.*, 2004; Amaldi and Kraft, 2007) is the combination of a cyclotron with a linear accelerator (“cyclinac”), which would bring the maximum energy to 430 MeV/u and additionally provide fast energy variation.

A compilation of particle therapy centers presently in operation, centers under construction, and proposed new centers can be found in PTCOG (2009). Most centers in operation are proton facilities with passive beam delivery systems. The most widely used machines for proton therapy are cyclotrons built by IBA Inc. (Belgium) and synchrotrons built by Optivus Proton Therapy (USA) and Hitachi Ltd. (Japan).

The first superconducting cyclotron for proton therapy (250 MeV) based on the pioneering work at NSCL, MSU (USA) (Kim and Blosser, 2001) started operation in 2007 at the PROSCAN facility (PSI, Switzerland) (Schippers *et al.*, 2007). Fast energy variation required for the spot-scanning technique is accomplished here with a carbon wedge degrader system followed by a cleaning and analyzing section, accepting however significant beam losses and related activation problems. Recently (March 2009) the Rinecker proton therapy center (RPTC), using a superconducting cyclotron of the same type as PSI (built by Accel, Varian), started patient treatments.

A very promising solution is the superconducting synchrocyclotron for proton therapy developed by the Still River Company (Littleton, MA). This machine, operating at an extremely high magnetic field (10 T), weighs not more than 20 tons and can be mounted directly on a gantry. The magnet was successfully tested in February

2009 and the installation at two hospitals in U.S. is scheduled later this year.

Besides the optimization of classical RF machines the investigation of alternative accelerator principles is actively pursued, mainly driven by the demand for more compact machines which ideally would fit into a single treatment room of a clinical center. We mention the dielectric wall accelerator, an induction linac based on high-gradient insulators. A research program aiming at the development of accelerating structures with an average gradient of 100 MV/m is currently in progress (Caporaso *et al.*, 2007) at Livermore (USA), but proton acceleration to clinically relevant energies has not yet been demonstrated. A promising new accelerator type, the laser wakefield particle accelerator is based on the creation of huge electric fields by intense ultrashort laser pulses (Mangles *et al.*, 2004). Laser-induced particle acceleration is a rapidly progressing, very active field of forefront research; see, e.g., Pfotenhauer *et al.* (2008). The difficulties which, however, still have to be overcome for applications in radiotherapy were recently reviewed (Linz and Alonso, 2007). Another type of accelerator, the fixed focusing alternating gradient ring, combining the merits of cyclotron and synchrotron, has been reexamined and its potential for applications in hadrontherapy is presently being investigated in several projects in Japan, UK, and France (Collot *et al.*, 2008).

### C. Beam delivery systems

The beam delivery system transports the particle beams to the treatment area and distributes the beam over the planned target volume (PTV) accurately and homogeneously with the desired dose distribution. Two different basic strategies were followed which in their extreme forms are represented by the fully passive systems with fixed beam modulation or the fully active beam scanning systems. In the first case, the particle beam is adapted in three dimensions to the target volume only by passive nonvariable field shaping elements. In the second case, the target volume is dissected in small volume elements (voxels) and a fine pencil-like beam is used to fill the voxels with the appropriate dose, ideally without any material in the beam path. Many other solutions in between these two extremes are possible and are discussed by Chu *et al.* (1993).

#### 1. Passive beam shaping

The principle of a fully passive system is shown in Fig. 10. The initially narrow beam delivered by the accelerator is first broadened by a scattering device, normally a double-scattering system which generates a flat transversal profile in a most efficient way. The monoenergetic Bragg peak is spread out by a range modulator in order to cover the entire length of the target volume. The whole spread-out Bragg peak (SOBP) can be shifted in depth by absorber plates (“range shifter”). The following two devices are patient specific and need to be precisely fabricated: the collimator cuts out the field area

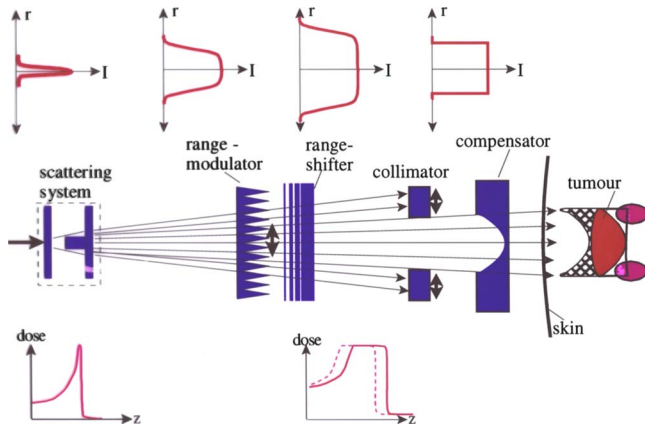


FIG. 10. (Color online) Sketch of a fully passive beam shaping system. The initially narrow beam is broadened by a scattering system and adapted to the target volume by various passive beam shaping devices. Adaption of the dose field to the distal contour of the target volume is achieved by a compensator, but results in unwanted normal-tissue dose in the proximal part (indicated by the doubly hatched area). Figure courtesy of U. Weber, Rhön-Klinikum AG.

defined by the largest target contour as seen in beam's eye view, preventing particles outside the field to pass through. The range compensator adjusts the distal depth pattern, taking into account also the complex tissue composition. Pioneering work was done at the Harvard Cyclotron Laboratory, such as the design of range modulators and compensators and the optimization of range-compensated contoured scattering systems (Koehler *et al.*, 1975, 1977; Gottschalk and Wagner, 1989).

A major limitation of the fully passive modulation system is the fixed width of the SOBP, which may result in significant dose deposition outside the target volume, e.g., in the proximal part when the particle range is adjusted to the distal contours (see Fig. 10). In favorable cases this limitation can be overcome by the stacked irradiation technique: the target volume is divided in layers in depth, which are irradiated consecutively using a "mini-SOBP." The SOBP depth and irradiation area for each layer are defined by a variable range shifter and a variable collimator (Fig. 11). However, this method still

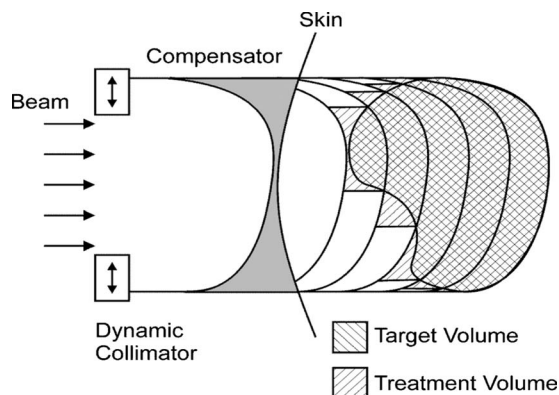


FIG. 11. Stacking of subvolumes using a dynamic range shifter and collimator. Adapted from Chu *et al.*, 1993.

has limitations because the dose level cannot be varied within one layer. This would generally be necessary to compensate for the pre-irradiation of the proximal layers during irradiation of the distal ones. The method works well for the case shown in Fig. 11, but would not work for a reversed left to right target volume with the small part of the volume at distal position.

In most currently operating particle therapy facilities the broad beam technique is applied, either fully passive or in combination with variable (dynamic) beam shaping devices. All these devices have been carefully optimized and refined over the years in order to achieve the highest possible degree of dose conformation to the target volume and maximum protection of the surrounding tissue. For more details the reader is referred to the comprehensive review (Chu *et al.*, 1993) and more recent reviews (Kraft, 2000; Gottschalk and Pedroni, 2008).

The broad beam method is also employed at the two clinical carbon-ion facilities HIMAC (Chiba) and HIBMC (Hyogo) in Japan. The four beam ports at HIMAC (Torikoshi *et al.*, 2007) are equipped with a combination of two wobblers magnets and a scatter foil. The depth profile of the SOBP, generated by special ridge filters, is designed to produce a constant biological effect, taking into account the variation of RBE as a function of depth. The most distal slice corresponds to the highest RBE value because it is irradiated with highly effective stopping ions only. The more proximal slices receive a partial pre-irradiation by traversing ions with lower RBE, which has to be taken into account properly. Therefore the physical dose has to decrease with depth along the SOBP in order to compensate for the increasing RBE. However, in this technique the in-built RBE distribution is derived from measurements for one cell type and the hardware-generated RBE profile cannot account, e.g., for tissue-specific effects.

The adaption of the broad field to the individual patient geometry is accomplished by a combination of two dynamic multileaf collimators and a compensator located just in front of the patient. The dose uniformity was found to be  $\pm 2.5\%$  within a 20-cm<sup>2</sup> field at patient position.

## 2. Scanning systems

For fully active beam delivery the target volume is divided in layers of equal beam energy and each layer is covered by a grid of picture points (voxels). The scanning beam system delivers the dose sequentially to these voxels.

This has several advantages: (i) neither field-specific nor patient-specific hardware (except for immobilization) is needed and in principle any irregular volume can be exactly filled; (ii) the dose can be varied from voxel to voxel allowing to compensate for the pre-irradiation of proximal subvolumes, dose contributions from secondary fragments, and variations of biological effectiveness; and (iii) the material in the beam path can be minimized, reducing beam losses and production of secondary particles like neutrons in front of the patient. On the other

hand, beam scanning implies strict demands on the control and safety systems and places strong requirements on the accelerator performance such as stability and reproducibility of the beam position.

Radiation fields of scanned ion beams are inherently intensity modulated fields and allow for a much greater flexibility in tailoring the dose distribution than passive delivery systems. In analogy to the IMRT techniques used in photon therapy the term “intensity-modulated particle therapy” (IMPT) has been introduced.<sup>2</sup> Each individual field of a treatment plan delivers an optimized and inhomogeneous fluence pattern such that the desired dose distribution in the patient is achieved when all fields are combined. While in IMRT only the fluence in the plane orthogonal to the beam direction is modulated, IMPT has an additional degree of freedom by the beam energy, allowing to position the Bragg peak at the desired depth in beam direction. In contrast to IMRT, dose confirmation to the target can already be achieved with a single IMPT field (see also Sec. II.D.1).

The first so-called spot-scanning system was developed at NIRS (Japan) for 70 MeV protons (Kanai *et al.*, 1983). A collimated beam spot of square shape (1 cm<sup>2</sup>) was produced by a set of four beam defining slits. The target area was divided into squared cells of the same size and filled sequentially by directing the beam to each of the cells using two fast dipole magnets. During repositioning the beam was switched off by a quick beam shutter. The dose was controlled by a parallel-plate ionization chamber placed in front of the target. This system was extended to three dimensions by combining the scanning device with a dynamic range shifter and stacking the doses delivered slice by slice to a homogeneous lucite phantom. These early studies demonstrated the reduction of the integrated normal-tissue dose as compared to fully passive beam delivery. The system was, however, not used for patient treatments.

For a long time only two facilities worldwide have applied pencil beam scanning for tumor therapy: the proton therapy facility at PSI (Switzerland) and the carbon-ion facility at GSI (Germany). The scanning techniques developed almost in parallel at these two centers will be discussed in the following section.

In 1992 a spot-scanning pilot project with 200 MeV proton beams started at PSI (Pedroni *et al.*, 1989, 1995), benefiting from the experience acquired before with the dynamic delivery of pion beams for patient treatments from 1981 to 1992. The proton spot-scanning system (Fig. 12) uses circular-shaped pencil beams with Gaussian profile which are positioned by a fast sweeper magnet in the horizontal direction along the target volume in discrete steps of typically 5 mm. The dose delivered to each single spot is controlled by a beam monitoring system located close to the patient. At completion of one spot the beam is switched off by a fast kicker magnet, the next spot is selected by the sweeper magnet and the

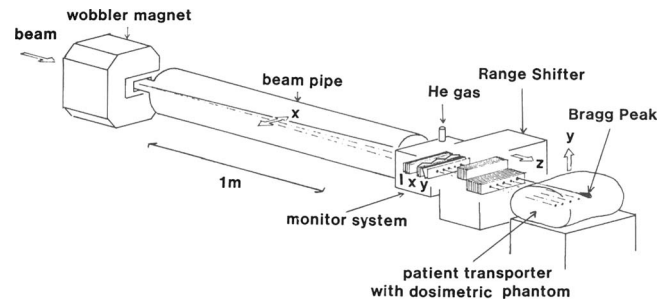


FIG. 12. Layout of the 200 MeV proton spot-scanning system at PSI. From Pedroni *et al.*, 1989.

beam is switched on again. Variation in depth is accomplished with a dynamic range shifter mounted close to the patient. The third scanning dimension is covered by (slow) vertical motion of the patient table. The device was designed to irradiate a 10 cm cube with 10 000 spots uniformly in 2 min (12 ms mean time per spot).

After performance tests at a horizontal beam line the scanning devices were mounted on a compact gantry system (Pedroni *et al.*, 1995). Patient treatments started in 1996 and a total of approximately 250 patients was reached in 2005. The positive experience with the scanning system has led to an expansion of the proton therapy facility in the following years: the PROSCAN project (now near to completion) (Schippers *et al.*, 2007) includes a new dedicated superconducting cyclotron serving both the existing spot-scanning beam line and a new isocentric gantry system. The latter is equipped with a double magnetic scanning system, which will speed up the beam delivery significantly and will permit further developments and optimization of scanning beam techniques (Pedroni *et al.*, 2004). Patient treatments at the first gantry station started again in 2007.

At GSI a fully active three-dimensional (3D) scanning beam system was developed in the early 1990s when high-energy heavy-ion beams of superior quality became available from the synchrotron SIS-18. Compared to the PSI system, a different scanning strategy, the so-called “raster-scan” concept was followed at GSI and was finally implemented for the therapy unit (Haberer *et al.*, 1993).

The intensity-controlled raster-scan system was based on the strategy of the microbeam irradiation system (Fischer, 1985), where single ions were delivered to individual spots with micrometer accuracy. In the intensity-controlled scanning a continuous path is selected over each iso-energy slice and “digitized” into a large number of voxels. When the desired dose in one voxel is reached, the beam is moved to the next voxel without turning it off. In this way, the intensity fluctuations in slowly extracted synchrotron spills can also be compensated. The pencil beam is moved in horizontal and vertical direction by fast magnetic deflection units. The treatment dose is delivered slice by slice, each slice corresponding to a constant beam energy (Fig. 13). The scan path within one slice follows a meanderlike line connecting all points of a dense grid. The spacing be-

<sup>2</sup>The application of intensity modulation techniques was first discussed for proton therapy by Lomax (1999).

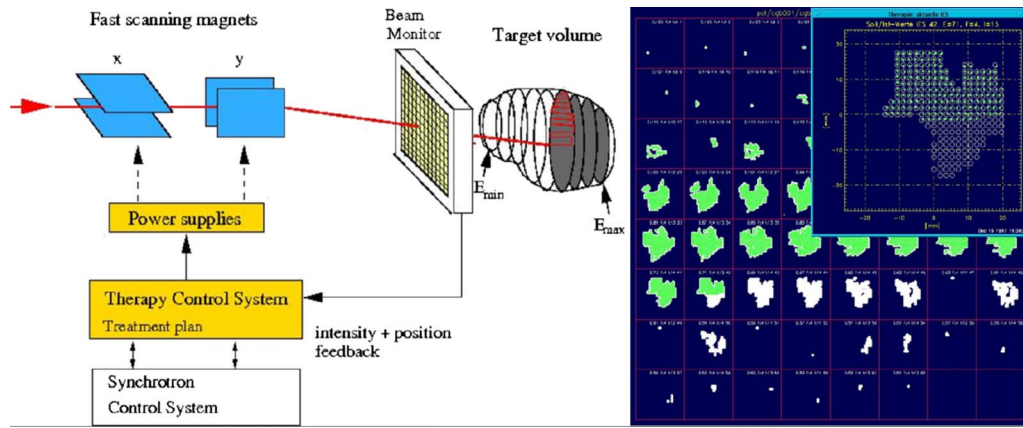


FIG. 13. (Color online) Principle of the intensity-controlled magnetic scanning system at GSI. Left: The target volume is irradiated by moving a pencil-like ion beam (80–430 MeV/u  $^{12}\text{C}$ ) with fast magnets over thin slices in depth. The required beam parameters are supplied on a pulse-to-pulse operation by the synchrotron (SIS) control system. From Haberer *et al.*, 1993. Right: Beam's-eye view of slices for a typical patient treatment plan. In each panel one slice is shown. The actually irradiated slice is seen in the magnified panel with the raster point positions indicated as open circles. The superimposed dots show the beam center positions measured online by a multiwire chamber. The spot size of the beam is larger than the circles and overlaps many positions.

tween adjacent raster points (typically 2 mm) is chosen much smaller than in spot scanning (5 mm). This makes the system less sensitive to the intensity fluctuations of synchrotron spills since many grid points contribute to the covering of a small area (Haberer *et al.*, 1993). After completion of one slice the synchrotron beam extraction is instantly interrupted and the beam energy for the next slice is selected and delivered with the next synchrotron pulse. The scanning control system is linked with the accelerator control system and requests the appropriate beam parameters for each slice irradiation during execution of the treatment plan. The accelerator data base contains predefined and optimized data sets (250 energy steps, 15 intensity steps, and seven focus widths) for the synchrotron and all magnets in the beam line. The beam monitor system has several very important functions: it controls the dose delivered to each grid position, measures the instantaneous beam position, and stops the irradiation if the measured values are outside the acceptable tolerances. Furthermore, redundant and diverse measurements of dosimetric quantities are performed in order to ensure a high degree of reliability and safety.

Patient treatments started in 1997 and were performed in close collaboration of the GSI Biophysics group with the University Clinic Heidelberg, the German Cancer Research Center (DKFZ), and the Research Center Rossendorf, Dresden. Until July 2008 in total 440 patients, most of them with radioresistant tumors in the skull base, were treated with very positive and promising clinical results (see Sec. IV). The developments and the experiences gained in the GSI pilot project had a major impact on the advanced technical design (Groß and Pavlovic, 1998; Haberer *et al.*, 2004; Heeg *et al.*, 2004) of the new clinical center HIT at Heidelberg. It will be the first clinical irradiation facility for heavy ions in Europe and will provide ion species ranging from protons to oxygen. The facility with a planned capacity of 1300 patients per year includes three

treatment rooms, one of which is equipped with a rotating gantry system—the first heavy-ion gantry worldwide.

Nowadays various companies offer scanning beam systems for clinical particle therapy facilities. The first centers using commercial scanning beam systems for patient treatments are the Hitachi proton facility at MD Anderson (Houston, Texas, July 2008), and the Rinecker proton therapy center (RPTC) in Munich (March 2009). Many others are presently under construction or in the planning stage.

### 3. Gantries

In conventional megavolt radiotherapy with electrons or photons patients are treated in supine position, i.e., in the same position as used for computer tomography (CT), magnetic resonance imaging (MRI), or positron emission tomography (PET) imaging before therapy. In this way uncontrolled organ displacements in the body with respect to the imaging data are minimized, which would otherwise spoil the precision of the treatment. The electron linac is mounted on a rotational support structure (gantry), which in combination with the rotatable patient couch allows to select the optimum beam directions and angles for the patient treatment. All commercial megavolt therapy systems include a 360° rotatable gantry and in principle all gantry angles are used.

In the early days of particle therapy the treatment beams were delivered by large proton or heavy-ion accelerators, which were designed for nuclear physics research and did not meet the requirements for an optimal treatment as in today's view. The beams were normally transported in horizontal beam lines and patients were treated in either supine or sitting position. This situation changed when the first clinical proton therapy centers were planned. It became clear that a gantry structure was advantageous in order to fully exploit the depth-dose profile and to demonstrate the superiority of par-

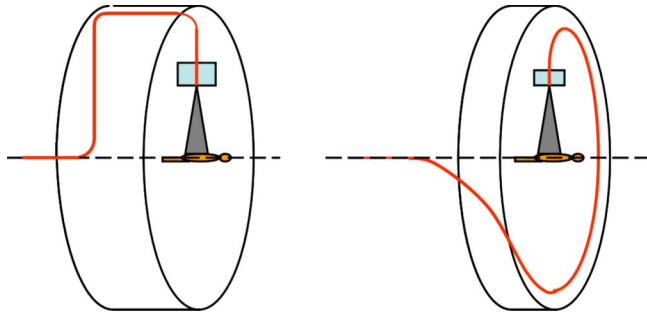


FIG. 14. (Color online) Common gantry design (left) and cork-screw gantry (right) for passive proton therapy systems. Adapted from Pedroni, 1994.

ticle therapy in comparison with modern photon therapy. For proton therapy many different gantry solutions were considered and proposed [for a classification of gantry designs, see Pedroni (1994)]. The main technical problem is the high magnetic rigidity of the beams, which for conventional magnets leads to a bending radius of more than 1 m. In the common gantry design the beam is first deflected away from the axis and then bent back to the patient with a  $180^\circ$  deflection (Fig. 14). For passive beam delivery systems a distance of 5–6 m between the scattering device and the patient is required and defines the radius of the rotating structure.

The first gantry systems for protons started operation in 1990 at the Loma Linda University Medical Center (USA), the first dedicated clinical proton therapy facility (Slater *et al.*, 1988). For these gantries the “cork-screw” design was chosen, where the beam is guided back to the axis in a plane perpendicular to the gantry axis. This solution requires a larger bending angle but saves room and shielding costs. At PSI the first gantry system with an upstream scanning system (Pedroni *et al.*, 1995) was put in operation in 1996. The eccentric design with the patient couch mounted off-axis permitted a very compact design (4 m diameter); however, some inconveniences for accessing the patient during treatment had to be accepted. The new (isocentric) gantry at PSI is designed for applying several scanning modes, including also gating and tracking facilities (Gottschalk and Pedroni, 2008). Nowadays most proton therapy centers dispose of one or several gantries, most of them using passive beam delivery systems.

For heavy ions a still higher bending power is required and leads to correspondingly large dimensions for a gantry. The magnetic rigidity of 380 MeV/u carbon ions with a range of 25 cm in water is about three times higher than for 200 MeV protons with the same range. Moreover, for scanning beams a high precision of the rotating structure is needed. In view of these technical difficulties and the large cost, alternative solutions were considered and realized in the clinical heavy-ion centers presently in operation. At HIMAC (Japan) one treatment room is equipped with a horizontal and a vertical beam line. An additional room with a  $45^\circ$  oblique beam is available at the HIBMC at Hyogo (Japan). These solutions allow one to treat a patient sequentially under

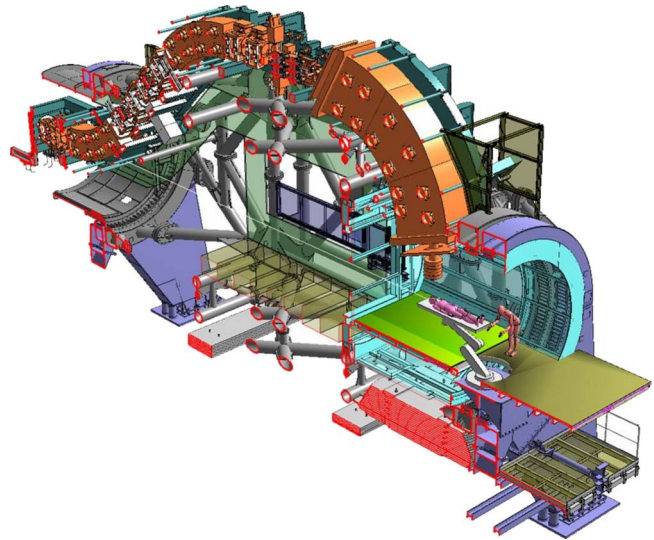


FIG. 15. (Color online) Sectional view of the heavy-ion gantry at HIT Heidelberg. Figure courtesy of MT Mechatronics GmbH (Mainz, Germany).

different angles. Together with the rotation of the patient table the treatment requirements can be reasonably met for most cases. Similar solutions were chosen for the new heavy-ion therapy centers CNAO in Pavia (Italy), the Gunma University Medical Center (Japan), and the Particle Therapy Center in Marburg (Germany) which are under construction.

Another interesting solution was proposed by Kats and Druzhinin (2004). Using a fixed, large-gap magnet deflecting the beam only in the vertical plane in combination with a vertical movement of the patient table many angles are accessible without rotating parts.

The first rotating (isocentric) gantry system for heavy ions was constructed at the HIT center (Germany) and is presently under commissioning. The rotating structure built by MT Mechatronics GmbH (Mainz, Germany) is about 20 m long with a diameter of 13 m and a total weight of 670 tons (Fig. 15). It is equipped with an upstream horizontal and vertical scanning system located in front of the last  $90^\circ$  bending magnet. The maximum beam energy is 430 MeV/u for  $A/Z=2$  ions like  $^{12}\text{C}$  or  $^{16}\text{O}$ . Clinical experiences to be expected within the next years may give answers to the ongoing discussion on the necessity and the therapeutic advantages of such a gantry compared to alternative solutions.

#### 4. Irradiation of moving organs

The scanning beam technique has so far mainly been applied in areas which can be immobilized by external aids. In these cases the target volume can be considered to be fixed in the patient’s coordinate system and displacements during irradiation, e.g., by breathing, are negligible. The patient still has to be immobilized (by individual head masks, bite blocks, special frames, or vacuum fixation equipment) as tightly as possible and tolerable. Under these conditions the spatial precision of

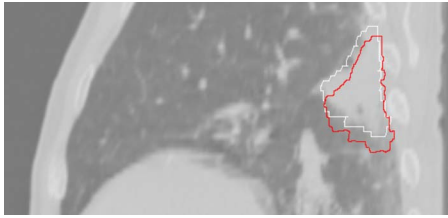


FIG. 16. (Color online) Illustration of the spatial shift of a target volume in the thorax caused by breathing. The dark and white contour lines indicate the target positions at the time of maximum inhalation and exhalation, respectively. Figure courtesy of E. Rietzel and C. Bert.

a scanning beam system can be maximally exploited, resulting in highly tumor-conformal dose applications.

This is, however, difficult for tumor sites in the thorax and abdomen where target motion due to breathing, heart pulsation, and/or pressure-related reasons (bladder and gut filling) can hardly be avoided (Fig. 16). Respiration-related target motion has largest importance in radiotherapy and is a very active field of research (Henkelmann and Mah, 1982; Ohara *et al.*, 1989; Phillips *et al.*, 1992; Okumura *et al.*, 1995; Langen and Jones, 2001) and review articles in Tepper (2004).

Motion patterns are, in general, complex, but predominantly translational in the upper-abdominal structures, while target rotation might occur, e.g., at the periphery of the lung. Translational shifts, however, may also change the radiological path length (i.e., the water-equivalent depth) of the target voxels. For particle therapy the influence of such changes is extremely high as they shift the narrow Bragg peak correspondingly, whereas for photons the depth-dose deviations are almost negligible.

Further difficulties are encountered for scanning beam systems where the superposition of beam and target motions results in dose inhomogeneities which are difficult to predict and may lead to severe underdosage or overdosage in the target volume (cold or hot spots) (Phillips *et al.*, 1992; Grözinger *et al.*, 2006; Bert *et al.*, 2008). Similar effects are faced in intensity-modulated radiation therapy (IMRT) with photons and have led to various mitigation strategies (Langen and Jones, 2001; Keall *et al.*, 2006). Their application potential in particle therapy, in particular for scanned ion beams, was subject of a number of recent investigations. In the following, a brief overview of strategies is given with special emphasis on ion-beam therapy.

(i) *Expansion* of the planned target volume (PTV) as much as required to cover the moving target volume completely at any time is a simple measure and is used for static field irradiations to cover the uncertainties of the treatment steps (e.g., patient positioning) (ICRU, 1994, 1999). It results, however, in normal-tissue dose that might limit the dose that can be given to the target volume. For scanned particle beams expansion of the PTV is not sufficient since it does not mitigate the inter-

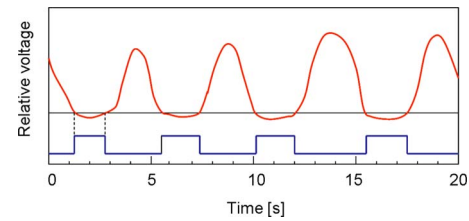


FIG. 17. (Color online) Principle of respiratory-gated irradiation. Adapted from Minohara *et al.*, 2000.

play of beam and target motion (Bert *et al.*, 2008). But expansion of the PTV is used in the gating and rescanning techniques (see below), as well as for dose applications with the broad beam technique that are not sensitive to interplay effects. Generation of the expanded target volume has to ensure that the beam energy is sufficiently high to cover the distal end of the target volume throughout the respiratory cycle (Engelsman *et al.*, 2006; Bert and Rietzel, 2007).

(ii) *Rescanning* (or *repainting*) is based on a statistical dose averaging effect by repeated irradiations of the expanded target volume, using scanned particle beams. Assuming that target motion and beam motion are uncorrelated the variance of the average dose decreases with a factor of about  $1/\sqrt{N}$  (where  $N$  is the number of scans) compared to a single irradiation (Phillips *et al.* 1992; Li and Xing, 2000; Bortfeld *et al.*, 2002). Implementation of rescanning and experimental studies are currently in progress (Pedroni *et al.*, 2004; Furukawa *et al.*, 2007). Rescanning has two major drawbacks: first, the particle fluence for each field has to be lowered such that irradiation of all fields together yields the correct dose. This will not only prolong the irradiation time but may also cause problems to the beam monitoring chambers. Second, for rescanning the field gradients are no longer defined by the beam profile but given by the amplitude of the target motion.

(iii) *Gating*, in contrast to the previous strategies, requires time-resolved monitoring of the respiration cycle. Around the point of maximum exhalation the respiratory signal shows a flat minimum (Fig. 17). Irradiation is only activated if the signal amplitude stays below a predefined limit. In this way the target motion during irradiation could be reduced to less than 10% of the free-breathing displacement (Minohara *et al.*, 2000). For scanned beams this residual motion will still cause interplay effects (Furukawa *et al.*, 2007). They can be mitigated by an increased overlap of pencil beams (Bert *et al.*, 2009). Ultimately this technique leads to much longer treatment times for the same dose deposition as compared to a continuous beam delivery. Interplay with the extraction cycle of a synchrotron further reduces the duty factor (Tsunashima *et al.*, 2008). On the other hand, overall

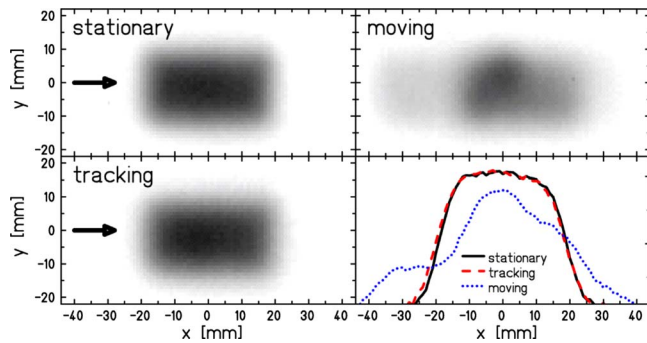


FIG. 18. (Color online) Film exposures for stationary, moving (uncompensated), and motion-compensated (tracking) irradiations. The corresponding horizontal dose profiles are shown in the lower right panel. Adapted from Bert *et al.*, 2007.

treatment times might be significantly shortened by reducing the number of treatment fractions, which might be feasible for several tumor entities (see Sec. IV.A).

- (iv) *Tracking* (or *online motion compensation*) requires a synchronous 3D compensation of the target motion in real time (Adler *et al.*, 1999; Keall *et al.*, 2001; Murphy, 2004). The beam follows the target displacements exactly at any time during irradiation. Ideally, this results in the same dose deposition as in the static case independent of the target motion. This technique was first investigated and successfully applied in the laboratory for photon IMRT using a dynamic multileaf collimator for synchronous adaptation of the photon field (Keall *et al.*, 2001).

For particles, scanning beam systems inherently offer excellent conditions for tracking. Detailed simulations (Grözinger *et al.*, 2006) have demonstrated the potential of 3D online motion compensation, which is based on three major components: monitoring of the target motion, dynamic treatment planning, and a beam delivery system permitting lateral tracing and fast range adaptation for shifting the Bragg peak correctly in depth. A promising practical approach is the segmentation of the irradiation according to different time phases of the respiration cycle. The dynamic treatment planning is based on time-resolved computer tomography (Rietzel *et al.*, 2005) and prescriptions for the transformation of the anatomical data into a reference frame (Chen *et al.*, 2007). Application to scanned carbon-ion beams was investigated by simulations (Li *et al.*, 2004; Grözinger *et al.*, 2006) as well as experimental performance tests (Bert *et al.*, 2007; Grözinger *et al.*, 2008) using an extended version of the GSI treatment planning system TRiP (Krämer *et al.*, 2000) and a modified beam control system.

As an example the lateral compensation capability is illustrated by the film exposures shown in Fig. 18. Applying online motion compensation, the dose deposition to a moving film is typically within 1% of the dose delivered to a stationary target. In these studies, the fast

range adaptation was accomplished with a passive double wedge degrader placed in front of the target.

A method for fast range adaption without any passive elements was proposed by Amaldi *et al.* (2004). Combining a cyclotron with a linac booster (“cyclinac”), including ten dual klystron modulators, fast (ms) energy variation for protons between 30 and 210 MeV can be achieved. However, this solution would require a fast tracking of the energy change for all the beam delivery system magnets which might be difficult. A prototype of the 3 GHz linac structure has been constructed and was successfully tested. For carbon ions the combination of a 300 MeV/u superconducting cyclotron with a linear accelerator with 16 modulators would be needed to reach 430 MeV/u (Amaldi and Kraft, 2007).

Recent studies on moving organ irradiations also include combined applications of the mitigation strategies (i)–(iv) discussed above. For example, combination of gating and rescanning techniques is planned to be employed at the new gantry system (gantry2) at PSI (Gottschalk and Pedroni, 2008).

These developments on rescanning, gating, and tracking techniques document the progress that has been made in finding optimal solutions for the treatment of moving targets with particle beams. As the scanning beam technology offers highest conformity for the treatment of static target volumes, an extension to the treatment of moving targets would be highly desirable. Although tracking techniques with scanning beam systems have not yet been applied to patient treatments, clinical trials seem to be in reach within the next few years.

#### D. Treatment planning and dose verification

The first step of treatment planning for any radiation therapy modality is to define and delineate the target volume on the basis of modern imaging techniques. X-ray CT provides quantitative information about the anatomical structures by recording photon attenuation images with a typical pixel resolution of 1 mm and slice thickness of 3 mm. Native CT data (without contrast agents) are essential for calculating the particle range and dose deposited in tissue and have to be recorded under the same conditions and with the same fixation aids (e.g., head mask) as used later in the treatment. Magnetic resonance imaging (MRI) and PET (Levy, 2007) are often applied in combination with CT to allow for a better definition of the target volume and organs at risk (image fusion).

Based on these images the target volume as well as critical structures are delineated manually in different slices. From these contours a 3D model of the treatment geometry is constructed, which is used to find suitable beam entrance ports under the condition that the traversal of critical structures should be avoided. For protons and heavier ions only few entrance ports (typically 2 nearly opposing fields) are necessary in most cases because of their superior depth-dose characteristics. Thereby radiosensitive organs can be spared to a maximum extent. A comparison of dose distributions for a

typical clinical case planned with IMRT techniques for both photons and protons revealed that the integral dose delivered to the patient's body was a factor of 2 lower for protons (Nill *et al.*, 2004).

### 1. Dose optimization

After target definition the dose distribution has to be adapted to the planned target volume, which ideally should be covered completely by 100% of the prescribed dose, while the dose in organs at risk should be minimized. For protons the optimization commonly is restricted to absorbed dose only, applying a constant RBE value of 1.0–1.1 (Paganetti *et al.*, 2002). For ion-beam therapy the biological effective dose has to be optimized, which is a difficult task in view of the manifold dependencies of RBE and the complex radiation field. For passive beam delivery systems it is equivalent in optimizing a set of beam shaping elements and preparing patient-specific hardware for each individual case (Chu *et al.*, 1993). At the HIMAC facility the treatment planning system HIPLAN (Endo *et al.*, 1996) has been used since 1994. For the raster-scanning project at HIMAC (Furukawa *et al.*, 2007) a new planning system was recently developed as a research version (Inaniwa *et al.*, 2008).

At GSI the novel treatment planning system TRiP (Krämer and Scholz, 2000; Krämer *et al.*, 2000; Jäkel, Krämer, *et al.*, 2001) has been developed, tailored to the challenging possibilities of the fully active raster-scan system and the application of IMPT techniques. The task of this code is to find an optimum superposition of a large number of pencil beams (typically several ten thousandths) with individual energy, position, and particle number, in order to achieve the prescribed dose (“inverse planning”). TRiP covers the beam modeling and optimization of absorbed dose as well as biologically effective dose. It is used in conjunction with the software platform VOXELPLAN (Schlegel *et al.*, 1992) developed at the German Cancer Research Center (DKFZ), which provides the standard planning tools such as segmentation of images and graphical user interfaces. The beam model included in TRiP describes the ion interaction with tissue and calculates the distribution of primary ions and secondary fragments, their energy spectra and depth-dose distributions (Krämer *et al.*, 2000).

To calculate the dose deposition including the exact position of the Bragg peak in heterogeneous tissue, the relationship between CT numbers and stopping power has to be established. The concept of water-equivalent path length (WEPL) is used to relate the traversal of an ion through a CT voxel to the corresponding path length in water. CT numbers are given in Hounsfield units (HU) defined by

$$\text{CT number } (\bar{x}) = 1000 \times \frac{\mu(\bar{x}) - \mu_W}{\mu_W}, \quad (12)$$

where  $\mu(\bar{x})$ ,  $\mu_W$  denote the x-ray absorption coefficients in tissue at location  $\bar{x}$  and in water as reference medium, respectively. There is no simple functional relationship

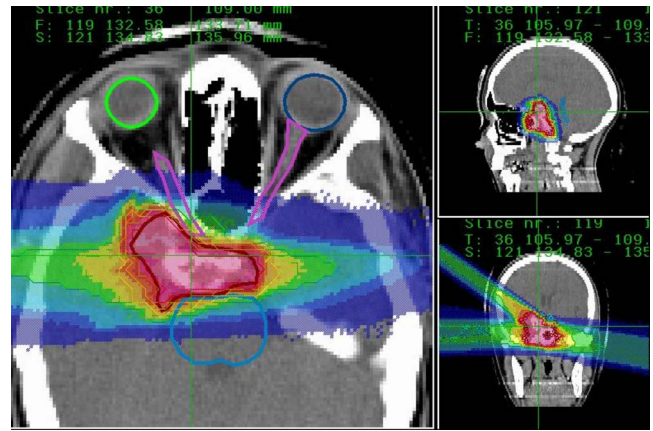


FIG. 19. (Color online) Biologically effective dose distribution optimized with the treatment planning system TRiP (Krämer *et al.*, 2000) for a skull base tumor treated at GSI Darmstadt. With three fields an excellent sparing of critical organs (brain stem and optical nerves) is achieved. Figure courtesy of O. Jäkel.

between CT number and stopping power or WEPL, but it in a first step can be approximated by linear sections (Minohara *et al.*, 1993). Methods to obtain the calibration of CT numbers were investigated systematically for protons at PSI (Schneider *et al.*, 1996; Schaffner and Pedroni 1998). For the stoichiometric calibration method it was concluded that the range of protons in the human body can be controlled to better than  $\pm 1.1\%$  in soft tissue and  $\pm 1.8\%$  in bone. This has been verified experimentally by measuring pairs of CT numbers and stopping powers for animal tissue samples. Similar investigations were carried out for carbon ions at NIRS (Matsufuji *et al.*, 1998; Kanematsu *et al.*, 2003) and at GSI (Jäkel, Jacob, *et al.*, 2001; Rietzel *et al.*, 2007). These studies have shown that for soft tissues in typical patient treatments in the head and neck region range uncertainties of 1–2 mm can be expected.

Optimization with TRiP is performed in two steps: first, only the absorbed dose is considered using various sets of input parameters (number of fields, field weighting, scanning grid, or beam spot size). When a clinically acceptable solution is found, the optimization with respect to the biologically effective dose is started as the most time-consuming computational part of planning. Because for scanned beams the composition of each voxel differs from another, voxel-specific RBE values have to be calculated. For the inclusion of local RBE values and the biological models in TRiP, see Sec. III.B.3. Due to computational limitations, until 2006 all treatment plans were calculated by single-field optimization, i.e., each contributing field was optimized separately. The recent introduction of a fast approximation of biological effects (Krämer and Scholz, 2006) allowed simultaneous optimization of multiple fields (Gemmel *et al.*, 2008), which enables better sparing of radiosensitive organs. The treatment plan shown in Fig. 19 represents a typical case of skull base tumors treated at GSI and illustrates the dose conformation and the sparing of organs at risk. The

treatment planning system TRiP, in combination with VOXELPLAN, was routinely used for carbon-ion treatments during 1997–2008 and has proven to be a reliable tool for heavy-ion therapy with scanning beams.

## 2. Heavy-ion dosimetry

To meet the special requirements of dosimetry with heavy ions and in particular for scanning beam delivery systems, new techniques had to be developed and introduced into clinical application. This includes calibration of the beam monitor, checks of lateral and depth-dose profiles, as well as the verification of complex three-dimensional dose distributions (Karger *et al.*, 2002).

The absorbed dose to water,  $D_w$  is the quantity of main interest in clinical dosimetry. It is normally measured with small cylindrical air-filled ionization chambers which are calibrated in  $^{60}\text{Co}$   $\gamma$ -radiation under reference conditions. According to the formalism described in the IAEA code of practice (IAEA, 2000) the dose to water in a proton-or heavy-ion field can be written as

$$D_w(P_{\text{eff}}) = M_{\text{corr}} N_w^{60\text{Co}} k_Q. \quad (13)$$

$P_{\text{eff}}$  denotes the effective point of measurement, i.e., the point in depth to which the measured dose refers (Jäkel *et al.*, 2000).  $M_{\text{corr}}$  is the measured charge in the air cavity corrected for deviations from the reference conditions,  $N_w^{60\text{Co}}$  is the  $^{60}\text{Co}$  calibration factor, and  $k_Q$  is a calculated beam quality correction factor. For ionization chamber dosimetry the relative standard uncertainty in the determination of  $D_w$  for carbon ions is estimated to be about 3% (IAEA, 2000), dominated by the uncertainties in the water-to-air stopping-power ratio (Paul *et al.*, 2007), and the  $w$  value, defined as the average energy required to create an electron-ion pair in the chamber gas. Measurements of the  $w$  value for  $^{12}\text{C}$  in air were reported by Kanai *et al.* (1993) and Rodriguez *et al.* (2001).

A smaller uncertainty can be achieved with water calorimetry, which is the most direct approach to determine  $D_w$  as it measures the dose in terms of its definition as the temperature rise induced by the energy absorbed in water. The feasibility of water calorimetry for radiation fields produced with scanning beam techniques has been demonstrated for proton beams at PSI (Sassowsky and Pedroni, 2005) and carbon-ion beams at GSI (Brede *et al.*, 2006). Further investigations with an improved transportable water calorimeter (Krauss, 2006) are planned in the near future. The aim of these developments is to establish water calorimetry as a primary standard for  $D_w$  in particle therapy, allowing one to calibrate ionization chambers directly in units of absorbed dose.

To facilitate the verification of complex patient treatment plans the dose distribution has to be transformed from the inhomogeneous patient geometry to water (see Sec. II.D.1). Dose measurements with a single-ionization chamber placed in a water phantom would, however, be ineffective for scanning systems, as each measurement would require repeated complete applications of the

treatment field. An optimized dose verification system (Karger *et al.*, 1999) was developed for the carbon-ion treatments with scanning beams at GSI. It consists of 24 ionization chambers mounted compactly in a block structure which is attached to the arm of a three-dimensional motor driven water phantom. The computer-controlled system allows automated positioning of the block as well as numerical and graphic comparison of the measured dose values with the treatment plan.

As demonstrated by Boon *et al.* (1998, 2000) and Schippers *et al.* (2002) scintillation screens viewed by a charge-coupled device camera can be used as a two-dimensional dosimetry system with high resolution (1 mm or better). The system is used for verification of complex dose distributions at the spot-scanning facility at PSI. For absolute dose measurements the quenching characteristic [the dependence of scintillation efficiency on the ionization density (Birks, 1951)] of the material has to be exactly known and taken into account. Investigations of quenching properties of various phosphors at PSI (Safai *et al.*, 2004) have shown that the light output of a mixture of selected materials can be adjusted by the mixing ratio, so that it reproduces the depth profile measured with ionization chambers. Another promising new approach is the development of a scintillation gas detector using gas electron multiplier (GEM) systems (Sauli, 1997). Recent measurements with 250 MeV/u carbon beams at GSI have shown a significant reduction of the quenching factor as compared to a  $\text{Gd}_2\text{O}_2\text{S}:\text{Tb}$  screen (Seravalli *et al.*, 2008).

Various methods for measuring *relative* three-dimensional dose distributions produced with protons or heavy ions have been investigated, such as ionization chamber arrays (Brusasco *et al.*, 2000; Cirio *et al.*, 2004), or MRI gel dosimetry (Ramm *et al.*, 2000). These methods allow a quick 3D reconstruction of the relative dose with good spatial resolution.

## 3. *In vivo* PET monitoring

With the availability of high-energy beams of radioactive particles at the Bevalac a new field of interesting applications in particle therapy and medical imaging was opened and pioneered at LBL, Berkeley (Chatterjee *et al.*, 1981). The basic idea was to verify the correctness of treatment plans for  $^{20}\text{Ne}$  therapy by depositing positron-emitting particles (e.g.,  $^{19}\text{Ne}$ ) at low dose exposure prior to the treatment and to measure their range in the patient tissue by imaging the 511 keV annihilation photons emitted in the decay of the positron emitters from the location they stopped at. Another promising application seemed to be the study of metabolic or flow rates by depositing positron-emitting nuclei directly into specific small volumes of the body and measuring the  $\beta^+$  activity as a function of position and time. However, the amount of activity that can be deposited at low dose is quite small (for  $^{19}\text{Ne}$  with 17 s half-life an entrance dose of 100 mGy corresponds to a deposited  $\beta^+$  activity of about 5000 Bq only) and therefore a high detection efficiency

of the PET camera is essential. Several pilot experiments employing a planar PET camera with two blocks of BGO crystals yielded promising results, including beam range measurements in a live dog (Llacer, Chatterjee, *et al.*, 1984). These measurements were hampered, however, by the rather low intensities of secondary beams and a significant activation of the BGO camera, which was ascribed to neutrons produced by the passive beam shaping system.

In 1989 the new heavy-ion synchrotron SIS-18 at GSI Darmstadt started operation and provided intense beams of high energy heavy ions. In combination with the in-flight fragment separator high-quality beams of secondary radioactive ions became available for experiments. Dedicated studies with pure high-energy beams of  $^{15}\text{O}$ ,  $^{17}\text{F}$ , and  $^{19}\text{Ne}$  were carried out to assess the performance of different PET cameras (Pawelke *et al.*, 1996). For an optimized BGO-based PET camera the maximum dose to the patient that is necessary to achieve a range accuracy better than 1 mm was found to be about 10 mGy. More recently, from similar investigations using  $^{10}\text{C}$  beams at HIMAC a peak dose of 96 mGyE was found to be required for an uncertainty of  $\pm 0.3$  mm (Iseki *et al.*, 2004).

The development of radioactive ion-beam (RIB) facilities, using in-flight separation at high energies or production at low energy combined with isotope separation online techniques and post-acceleration, has led to the proposal to apply radioactive ions instead of stable ions for tumor therapy. Detailed investigations of RIB production and applications in radiotherapy were carried out within the EULIMA study (Berger *et al.*, 1990; Ryckewaert *et al.*, 1991) and have shown that sufficient intensities [e.g.,  $1.8 \times 10^9$  ions/s for  $^{19}\text{Ne}^{2+}$  using the  $^{19}\text{F}(p,n)$  reaction with 30 MeV protons] could be extracted and transported to a beam line for further acceleration. It became clear, however, that such rather complex facilities were less suitable and too cost intensive for implementation to clinical facilities.

Most notably at the HIMAC facility much effort was put into further development of a RIB system based on the high-energy fragmentation concept (Kitagawa *et al.*, 2006). A dedicated line for secondary beams was set up including a production target, magnetic in-flight separation, and a raster-scanning system (Kanazawa *et al.*, 2002). For  $^{11}\text{C}$  a beam intensity of  $7 \times 10^6$  ions/s available in routine machine operation was reported.

Another approach for monitoring the dose delivery to the patient *in vivo* is the utilization of secondary radiation resulting from nuclear interactions of the primary ions along their stopping path in tissue (see Sec. II.A.4). This includes both *prompt* emission of photons or secondary particles like protons or neutrons and *delayed* emission of radiation from the decay of unstable nuclei formed in the target. The latter process, the production of radioactive nuclei in a thick target by an incident beam of stable ions, was called “autoactivation” (Tobias *et al.*, 1971). In first experiments with  $^{14}\text{N}$  beams at the Bevalac the depth profile of the induced positron activ-

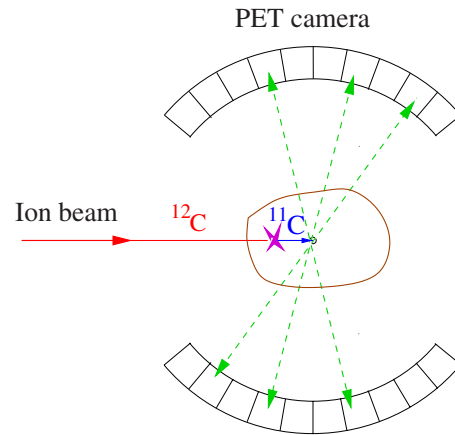


FIG. 20. (Color online) Principle of *in situ* range verification by autoactivation and PET imaging. A small fraction ( $<1\%$ ) of the incident  $^{12}\text{C}$  ions is transformed into radioactive  $^{11}\text{C}$  in high-energy fragmentation reactions. Their stopping depth is nearly the same as for the primary ions and can be monitored with a PET camera.

ity showed a sharp peak, which was attributed to the production of  $^{11}\text{C}$  as a projectile fragment.

Many years later the application of this phenomenon for *in situ* range monitoring with PET techniques (Fig. 20) was studied in more detail at GSI. The measured depth profiles of positron activity induced in a PMMA block by beams of  $^{12}\text{C}$ ,  $^{16}\text{O}$ , and  $^{20}\text{Ne}$  exhibited two different components: a flat decreasing background resulting from target fragmentation and a pronounced peak structure caused by projectile fragments (Enghardt *et al.*, 1992). The peak is formed by a complex superposition of all  $\beta^+$ -emitting isotopes formed in projectile fragmentation. The simplest  $\beta^+$ -activity profile was observed for incident  $^{12}\text{C}$  ions because in this case only  $^{11}\text{C}$  and  $^{10}\text{C}$  contribute. The relation between depth-dose distribution (Bragg curve) of the incident primary beam and the  $\beta^+$ -activity profile is shown in the upper panel of Fig. 21. For comparison, the activity profile generated with 140 MeV protons (Fig. 21, lower panel) does not show a peak structure due to the lack of projectile fragments (Parodi *et al.* 2005).

As a result of these investigations, an in-beam PET system for monitoring patient treatments with carbon-ion beams was designed and integrated into the treatment site at GSI (Pawelke *et al.*, 1997; Enghardt, Crespo, *et al.*, 2004). This system was employed routinely for monitoring almost all of the 440 patient treatments administered since 1997 and has proven to be a valuable tool for quality assurance (Enghardt, Parodi, *et al.* 2004). The data evaluation is based on a quantitative comparison of the spatial distribution reconstructed from the measured PET data with that predicted by a model calculation based on the treatment plan and taking into account the time course of irradiation. The example shown in Fig. 22 demonstrates the clinical relevance of PET monitoring in case of critical dose applications near organs at risk. The technique permits (i) monitoring the maximum ion range, (ii) verifying the field position, and

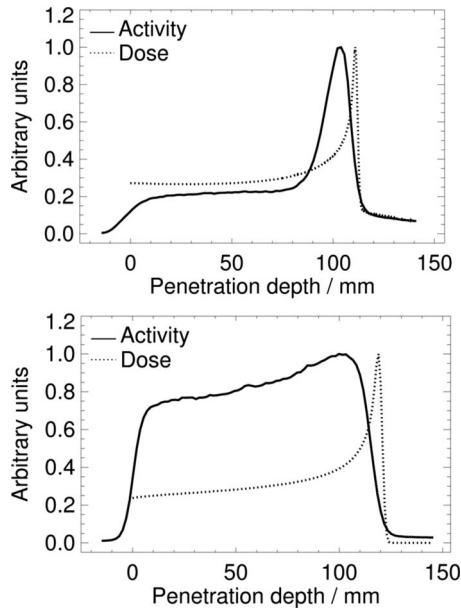


FIG. 21. Autoactivation of thick PMMA targets by beams of 260 MeV/u carbon ions (top) and 140 MeV protons (bottom). The solid line shows the depth profile of the measured  $\beta^+$ -activity. For comparison the depth-dose profile of the primary beam is shown by a dotted line. From Parodi, 2004.

(iii) detecting deviations in the patient positioning or local changes of the patient anatomy in the course of the treatments (Enghardt *et al.*, 1999).

In parallel to these developments at GSI, PET monitoring based on autoactivation was also investigated at NIRS (Chiba) (Tomitani *et al.*, 1994, 1997). Instead of the in-beam solution followed at GSI, a postirradiation (offline) imaging system using a commercial full-ring volumetric PET scanner was implemented at the carbon-ion therapy facility HIMAC, but to our knowledge was not used in clinical routine.

The optimal strategy for implementing PET monitoring into clinical centers is still controversial, see, e.g., Parodi, Bortfeld, Enghardt, *et al.* (2008). As demonstrated by Crespo *et al.* (2006) the geometrical detector arrangement and the counting statistics are the most

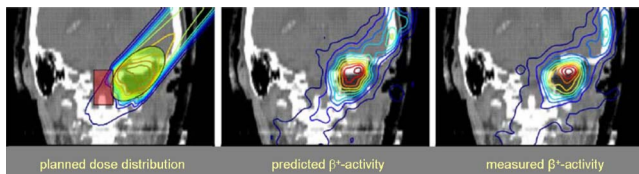


FIG. 22. (Color online) Example of in-beam PET monitoring showing the irradiation of a skull base tumor at GSI. Left: Planned dose distribution superimposed onto the CT image. The target volume and the brain stem as an organ at risk are highlighted. Middle: Predicted  $\beta^+$ -activity distribution calculated from the treatment plan and time course of the irradiation. Right: Measured  $\beta^+$ -activity distribution. By comparison with the prediction it was verified that the carbon ions were stopped before the brain stem. Adapted from Enghardt, Crespo, *et al.*, 2004.

crucial points affecting the quality of the PET images. The rather low density of the implanted activity demands highest detection sensitivity. An off-line full-ring tomograph offers better imaging performance, but valuable short-lived activity components ( $^{15}\text{O}$ ) are lost for detection. In-beam solutions, on the other hand, are restricted to limited-angle detectors with lower efficiency and their implementation is technically more difficult.

In-beam imaging is, however, preferable for another important reason: long-lived activity can be transported away from its stopping point by metabolic processes such as blood flow, and so confuse the images that are obtained (“wash-out effect”). This effect was studied experimentally (Mizuno *et al.*, 2003; Tomitani *et al.*, 2003) at the HIMAC facility by implanting secondary beams of  $^{10}\text{C}$  and  $^{11}\text{C}$  into brain and thigh muscles of rabbits and recording the time-activity curve *in situ* with a pair of Anger-type scintillation cameras (Iseki *et al.*, 2004). For both tissue types three components were found in the clearance, characterized as fast (few s), medium (few min), and slow (hours). In the case of  $^{11}\text{C}$  irradiation about half of the implanted activity was lost due to the wash-out effect and as a consequence the precision of the range determination decreased by a factor of 1.1–1.5. Recent in-beam PET studies aiming on a quantification of the wash-out effect were performed during treatments of skull base tumors with  $^{12}\text{C}$  ions at GSI (Fiedler *et al.*, 2008). It was found that the biological half-lives (170–210 s) were correlated with the local dose. The observed longer half-life in high-dose regions might be attributed to a reduced perfusion of the tumor. Furthermore, a slight decrease of the effective half-lives with the overall treatment time was observed.

PET monitoring based on autoactivation can also be applied in proton therapy (Bennett *et al.*, 1978). Its feasibility and value for treatment verification was investigated in various detailed studies; see, e.g., Litzenberg (1998), Hishikawa *et al.* (2002), and Parodi *et al.* (2002).

The lacking peak structure in the activity profile (cf. Fig. 21), which is a drawback in comparison with carbon ions, is balanced to some extent by the three times higher total induced activity per Gy for protons (Parodi *et al.*, 2002). A comprehensive quantitative patient study on the feasibility of postradiation PET for *in vivo* verification after proton treatment was performed by Parodi *et al.* (2007) at the Massachusetts General Hospital in Boston. The data analysis includes, for the first time, a model of the metabolic wash-out of positron emitters based on a previous formulation by Mizuno *et al.* (2003). The results demonstrate that this approach is essential to reproduce the measured PET images, which show a significant distortion with respect to the calculated initial activity distribution without wash-out correction. In another study, a comparison of the quality and clinical benefits of *in vivo* PET monitoring for different scenarios including both synchrotron and cyclotron facilities was presented (Parodi *et al.*, 2008).

An alternative to the application of PET techniques for *in vivo* range and dose monitoring in proton-or heavy-ion therapy might be the utilization of prompt

photon or particle radiation. In fragmentation reactions occurring along the stopping path of the primary particles prompt photons are emitted by excited nuclei as well as secondary protons,  $\alpha$  particles, and neutrons which have long ranges and can be detected outside of the patient's body (Gunzert-Marx *et al.*, 2004, 2008). As this radiation is emitted promptly, i.e., typically within less than 1 ns after the nuclear reaction, the spatial information is not affected by physiological processes unlike the PET method. As recently demonstrated for proton beams of 100–200 MeV stopping in a water phantom, the intensity of prompt photons emitted orthogonally to the beam direction exhibits a peak structure which is correlated with the Bragg peak (Min *et al.*, 2006, 2007). Similar recent results were reported with 73 MeV/u  $^{13}\text{C}$  ions stopping in a PMMA target (Testa *et al.*, 2008). Further investigations will be needed to ascertain the applicability of prompt photon (or secondary particle) detection to in-beam range and dose verification.

### E. Future directions

One of the major challenges in particle therapy is the treatment of moving organs and it consequently represents a very active field of research. Although scanning beam systems suffer from interplay effects that cause serious deteriorations of the dose distribution, these systems offer excellent conditions for an on-line motion compensation by tracking techniques. First promising results have demonstrated the feasibility of real-time tracking, but further research is required to bring this technique to clinical application. Rescanning and gating (with scanning beams), as technically less demanding mitigation strategies, might have a better chance to be implemented in the near future.

*In vivo* monitoring of dose delivery may become more important in the future in view of the millimeter precision and the high degree of tumor conformation that can be achieved with modern ion-beam technology. For a full exploitation of these advantages it has to be guaranteed that the dose is delivered correctly. Inaccuracies, e.g., in the treatment planning, patient positioning, or changes in the tissue composition may lead to uncertainties in dose application, which can only be recognized by *in vivo* monitoring. Correction of the treatment parameters based on *in vivo* imaging thus will improve the therapeutic ratio and result in better sparing of normal tissue. Additionally, *in vivo* monitoring has proven a valuable tool for quality assurance. So far, only GSI has used in-beam PET monitoring in its routine clinical program. Further investigations are needed to evaluate the full potential of this technique.

The utilization of prompt photon or particle radiation emitted in nuclear reactions of the primary ions along their stopping path in tissue has been little explored so far. New developments in particle detection such as the GEM systems offering high sensitivity and excellent position resolution may foster the development of efficient monitoring systems exploiting secondary prompt radiation.

Alternative particle accelerator concepts such as the dielectric wall accelerator and the laser driven particle accelerators represent exciting new approaches and their potential for applications in ion-beam therapy is currently being investigated. However, these technologies are presently far from application in radiotherapy and require further intense research efforts to overcome the tremendous technical difficulties.

## III. BIOLOGICAL EFFECTS OF ION IRRADIATION

### A. Relative biological effectiveness

In addition to the advantageous depth-dose profile as discussed in the previous section, heavy ions offer an even larger efficacy for tumor treatments due to the enhanced biological effect of high-LET<sup>3</sup> particles. As seen in Eq. (3) the LET (related to stopping power) depends quadratically on the projectile charge ( $Z_p^2$ ) and results in large values for heavy ions. Typically, the large energy deposition in the center of ion tracks result in more severe DNA damage with respect to low-LET irradiation. Since the ionization density of light ions is larger for the low energetic high-LET particles as present in the tumor region relative to the swift ions in the entrance channel (often referred to as “plateau”), the biological effect in the target volume is more pronounced than in the surrounding normal tissue. The most common method adapted in radiation protection of estimating the biological response of ions relative to conventional radiation is the use of weighting factors, formerly known as quality factors. However, they represent upper limits only and thus largely overestimate the effect in many cases. For an accurate estimate of the efficacy of ions, the concept of the RBE must be applied. The RBE is defined as the ratio of the dose of x rays divided by the dose of ion irradiation that results in the same biological effect. It depends on many different parameters such as the biological end point, dose, particle type, and energy as well as the tissue under consideration. As a result, the RBE is different for every location in the treatment field. Therefore, the increased biological effectiveness must be thoroughly considered for heavy ion treatment planning and poses a big challenge for correct beam delivery. Although it is appealing to characterize the larger biological effect by a single parameter, often referred to as “clinical RBE,” one must keep in mind that the RBE can vary drastically within the tumor volume. However, the RBE concept facilitates the transfer of the knowledge gathered in conventional radiotherapy to the case of heavy ions. In our context of radiotherapy, tumor control (cell survival) and normal-tissue complications are the most important biological end points. They characterize the tumor response as well as the radiation tolerance of the surrounding tissue including organs at risk.

<sup>3</sup>Photons, x rays, and  $\gamma$  rays are typically referred to as low-LET radiation. Heavier particles such as carbon ions are called high-LET due to their large stopping power.

Up to the present there have been four heavy-ion treatment facilities in operation which developed different strategies for biological treatment planning. Most of the differences can be attributed to the diverse beam delivery systems at the centers. However, the experimental progress in radiation biology also led to the development of more comprehensive models for the determination of RBE values. In the following, we define the relative biological effectiveness and discuss its dependence on various parameters relevant for carbon-ion therapy. Subsequently, we present the pioneering research performed at LBL that led to the first biologically optimized heavy-ion treatments (Blakely *et al.*, 1980; Lyman *et al.*, 1980). The description of the strategy of the worldwide second facility for carbon-ion therapy located at the HIMAC at the NIRS in Chiba, Japan, follows, which is based on an extensive data collection of cell experiments combined with their experience of radiation therapy with neutrons (Kanai *et al.*, 1999). This approach was also adapted at the HIBMC in Hyogo (Kagawa *et al.*, 2002). The most recent concept was developed at GSI and uses the LEM to determine the photon-equivalent dose (Krämer and Scholz, 2000). Additionally, we address current research topics in the framework of heavy-ion therapy such as the effect of different oxygen levels, cell transformation, and the induction of secondary cancer.

### 1. Radiation damage by photons and heavy ions

The most striking difference between photon and ion irradiation concerns the microscopic spatial energy distribution. In the case of photons the energy is transferred to the cell either by photo effect or by Compton effect—depending on the energy of the penetrating photon (Alpen, 1998). Since the cross sections for these processes are rather low, the number of ionization events per incident photon within the volume of a cell is also small. Typically only a few electrons are ejected from target molecules possibly ionizing further molecules if they have received enough energy during their primary interaction. Due to this low number of events, many photons are required to deposit a relevant dose. Since these photons are randomly distributed, the resulting ionization density can be assumed to be homogenous over the entire cell volume.

#### *a. Microscopic track structure of ion beams*

The spatial distribution of energy is entirely different for heavy ions than for photons. It is this localized energy distribution associated with ion beams that results in a typically larger biological effect induced by particles. The radial dose distribution around ions is governed by two steps. First, electrons (often named secondary or  $\delta$  electrons) are emitted in ion-atom or ion-molecule interactions by means of Coulomb interaction of the projectile and the target. Second, the liberated electrons are scattered by frequent interactions with the medium.

The dominant ionization process can be described by the binary-encounter approximation assuming that the projectile collides with a quasifree electron (Kraft and Krämer, 1993). Another source of energetic electrons originates from the Auger effect, which is the expulsion of outer electrons in the process of filling inner-shell vacancies created by direct Coulomb collisions. A third important interaction mechanism produces so-called convoy (or cusp) electrons. These electrons are either lost or picked up into unbound states of the projectile thus being sharply emitted into forward direction.

Those primary electrons induced by interaction of the projectile and the target are subsequently transported through the medium by elastic and inelastic collisions. The former merely lead to change in direction whereas in the latter process energy is transferred to the medium by either ionization or excitation. For slow electrons with energies below 50 eV at the very end of the electron track, excitation dominates. For all larger energies ionization outweighs the other processes and creates additional electrons finally adding to the total energy deposition. Interestingly, the ionization cross section of electrons in water exhibits its maximum at about 100 eV, which relates to a mean free path of a few nm. In other words, there is a high probability that two ionization events occur on each of the 2 nm separated, opposite strands of DNA.

Most of the induced electrons receive either only a small energy transfer or they are scattered in the forward direction, depositing most of the dose in the center of ion tracks. However, those electrons that are fast enough to leave the track core ( $\delta$  rays) typically undergo a large number of interactions. Due to those frequent scattering processes, the initial preference of electrons in the forward direction diminishes, resulting in a broad angular distribution. All existing models, analytical (Chatterjee and Schaefer, 1976; Katz and Cucinotta, 1999) or Monte Carlo simulations (Paretzke, 1986; Krämer, 1995), as well as experimental studies (Varma *et al.*, 1977) show a steep radially symmetric dose distribution with a negative gradient for an increasing distance  $r$ , approximately following a  $1/r^2$  dependence. Figure 23 demonstrates the highly inhomogeneous energy distribution deposited by a single carbon ion with an energy of 1 MeV/u. A Monte Carlo track structure code was used to simulate the generation of electrons and its transport in water (typically used as cell surrogate) (Krämer, 1995).

One major challenge for experimentalists to measure the relevant track structure for ion radiation biophysics concerns the liquid state of the target. Typically, measurements are performed in water vapor and rescaled to the density of liquid water, thus neglecting collective effects like target polarization or collective excitations. Recent studies for heavy ion-atom collisions on solid-state targets show considerable progress. However, they also demonstrate the technical problems involved in such experiments (Lineva *et al.*, 2008). In current Monte Carlo codes, the liquid phase is typically considered by

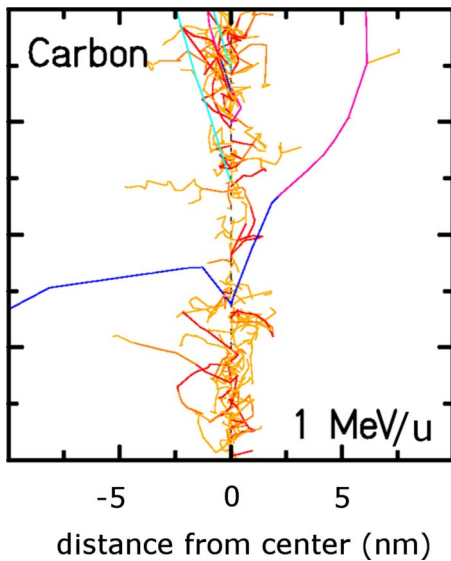


FIG. 23. (Color online) Track structure of a 1 MeV/u carbon ion simulated by the Monte Carlo code TRAX. Lines represent the paths of individual secondary electrons. Figure courtesy of Michael Krämer.

determining the macroscopic dielectric response function (Dingfelder, 2002).

#### b. DNA damage and cell inactivation

Considering the different energy distributions of photons and ions and assuming that the DNA molecule is the most sensitive target, we can qualitatively understand the larger radiation damage evoked by ions: The typical extension of the track center with the highest “local” dose is on the order of nanometers, thus resulting in a large probability of correlated nearby DNA damages like single or double strand breaks or base damages. In contrast, the approximately homogeneous dose distribution of photons generates much larger distances between neighboring damage sites. An example of the microscopic dose distributions is shown in Fig. 24. Since the cell’s repair capability is reduced for more complex DNA damage, the radiation damage of heavy ions is larger than that of photons (Nikjoo *et al.*, 1999). Typically, one distinguishes DNA damage induced by *direct* hits of the ion or its surrounding secondary electrons and *indirect* DNA damage generated by radiation-induced radicals. The contribution of indirect damage (about 70%) is larger than the DNA damage by direct hits (about 30%) for low-LET radiation. For high-LET carbon ions, the contribution of direct hits is slightly increased (Ito *et al.*, 2006).

A common way to analyze the different effects of photons and heavy ions is by means of cell survival curves. These experiments are relatively easy to perform and they have a high significance for radiation therapy because they give insight into the potential of radiation to kill tumor cells. In the standard experimental protocol (Puck and Marcus, 1956), cell proliferation is analyzed about 1–2 weeks after irradiation and cells are counted

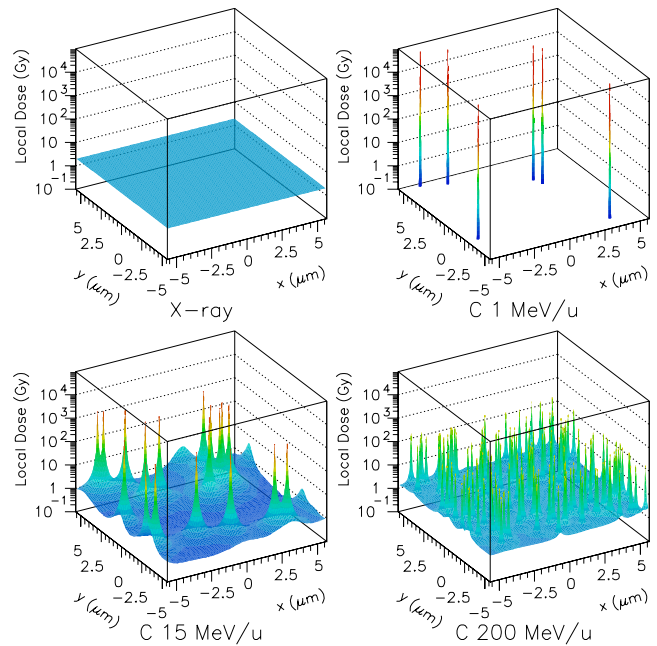


FIG. 24. (Color online) Illustration of the different microscopic dose distribution by x rays and carbon ions with different specific energies. The average macroscopic dose is 2 Gy in all cases. From Scholz, 2003.

as survivors, if they have formed a colony with more than 50 daughter cells. The surviving fraction is given by normalization to the number of seeded cells. The most common way to parametrize the cell survival  $S$  uses the linear-quadratic (LQ) model (Hall, 2000),

$$S(D) = \exp(-\alpha D - \beta D^2), \quad (14)$$

where  $D$  is the absorbed dose and  $\alpha$  and  $\beta$  are experimentally determined parameters. The ratio  $\alpha/\beta$  determines the shoulder of the survival curve and represents an important quantity in conventional radiotherapy (Fowler, 1989).

We have to keep in mind, however, that the picture just presented is greatly simplified and that the radiation effects depend on many different parameters. Some of them are summarized and quantified by the relative biological effectiveness introduced in the next section. This phenomenological factor proved to be of particular significance, since all therapy-related biological end points (i.e., cell survival, normal-tissue complications) are not yet understood in terms of a clear mechanistic reasoning.

## 2. Definition of RBE

The most common way to assess the biological response of heavy ions is by means of radiation and tissue weighting factors assigned in radiation protection (ICRP1991, 2007). The radiation weighting factor, formerly known as quality factor, takes into account the biological effect of different radiation qualities (e.g., electrons, neutrons, alpha particles, and heavy ions). For heavy particles the value is set to 20. The tissue weight-

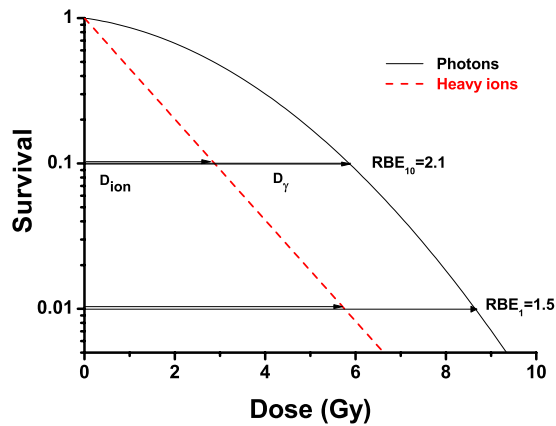


FIG. 25. (Color online) Determination of RBE for cell inactivation for 10% and 1% survival level for a typical heavy ion irradiation.

ing factor considers the radiosensitivity of different organs. In order to determine the equivalent dose (in Sievert), both weighting factors must be taken into account. These are maximum values chosen to assess the radiation risk in the most conservative way. However, they should not be confused with the RBE, which is a much more powerful and versatile concept taking into account the radiation quality and tissue-specific response as well as the biological end point and the dose level of the radiation.

The RBE is defined as the ratio of the dose of a reference radiation (typically x rays or  $\gamma$  rays) to the dose of the radiation in question (e.g., ions) to produce an identical biological effect (isoeffect),

$$\text{RBE}_{\text{iso}} = \frac{D_{\text{ref}}}{D_{\text{ion}}}. \quad (15)$$

It is important to note that the statement of a RBE value requires both the specification of the reference radiation and the level of the biological effect. In Fig. 25 we show the determination of the RBE by typical cell survival curves for x rays and heavy ions. The RBE values for cell inactivation are indicated for two effect levels, namely 10% and 1% cell survival.

The RBE is the most important quantity in biological treatment planning of heavy-ion therapy, since it determines the photon-equivalent dose by multiplication with the absorbed (physical) dose. The photon-equivalent dose, sometimes abbreviated as biological dose, quantifies the dose of conventional radiation that would yield the same biological effect as the applied radiation. It is conveniently used to compare the results of conventional radiation with other radiation qualities such as neutrons, protons, or carbon ions. The RBE can be used for many biological end points such as DNA strand breaks, mutations, or transformations. In the scope of heavy-ion therapy, however, the RBE for cell killing and normal-tissue complications are most relevant.

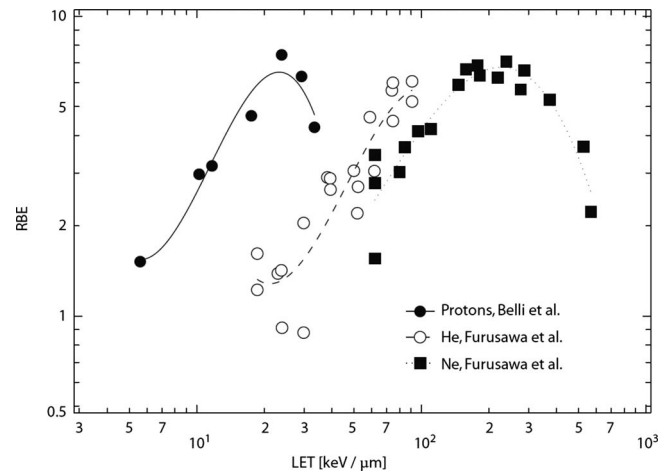


FIG. 26. Dependence of  $\text{RBE}_{\alpha} = \alpha_{\text{ion}}/\alpha$  on LET and particle type, where  $\alpha$  and  $\alpha_{\text{ion}}$  are the linear part of the survival curve for photons and ions, respectively. Data are redrawn from Belli *et al.* (1998) and Furusawa *et al.* (2000). From Scholz, 2003.

### 3. Dependencies of RBE

In contrast to proton therapy, where the low LET of protons is believed to allow the application of a single factor ( $\text{RBE}=1.1$ ) throughout the entire radiation field (Paganetti *et al.*, 2002), the situation in heavy-ion therapy is much more complex because of the large variations of LET. From the previous section, we know that the mixed radiation field of a carbon-ion SOBP is comprised not only of carbon ions with a large energy spread but also of lighter fragments. Additionally, the levels of absorbed dose can vary largely within single fractions and between different tumor sites. Therefore, we need to understand how the biological effect of heavy ions depends on the parameters relevant for radiotherapy.

First, the RBE depends on the dose level as already shown in Fig. 25. In general, it is higher for lower dose levels and lower for larger doses owing to the shoulder shape of the photon response curve (Weyrather *et al.*, 1999; Furusawa *et al.*, 2000). For application in ion therapy that means that the biological differences between conventional radiation and particle beams diminish if the dose is escalated.

Second, the response of cellular systems depends on the energy or LET of the penetrating particle. Figure 26 presenting a compilation of different cell survival experiments with V79 hamster cells (a frequently used cell line in radiobiology laboratories) reveals that the RBE increases with LET up to an ion-dependent maximum value and decreases for higher LET values (Belli *et al.*, 1998; Furusawa *et al.*, 2000). According to the higher ionization density in the track center of particles with a larger LET, the radiation damage is more severe, thus increasing the RBE. However, at a certain LET value the dose deposition is so large that a single-particle traversal sufficiently reduces the cell survival probability. In that case, the additional dose deposited by ions with a larger LET is wasted and we would not expect a larger

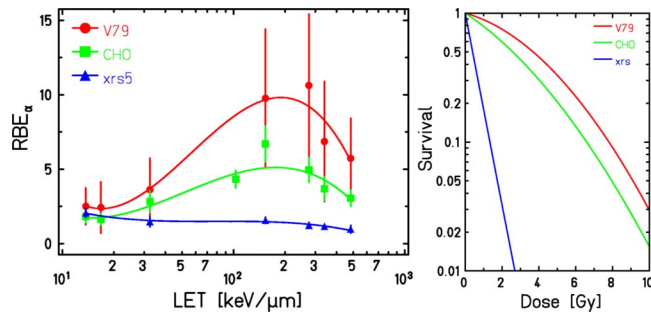


FIG. 27. (Color online) RBE dependence on the radiation sensitivity of cell lines. Left: Dependence of initial  $RBE_{\alpha}$  on the three cell lines CHO, V79, and XRS after carbon irradiation. Right: Survival curves of the same cell lines demonstrate the different radiosensitivities after x ray irradiation. Experimental data are from Weyrather *et al.* (1999).

RBE. Moreover, the RBE decreases due to the lower hitting probability, since the number of ions required for the same dose deposition is lower for particles with a higher LET. As a consequence, the ratio of cells without any particle hit (obviously being survivors) increases resulting in a lower RBE for cell killing. Notably, the LET dependence varies for different biological end points and needs to be considered cautiously.

Third, the particle type influences the position of the RBE maximum (see Fig. 26). For heavier particles, the maximum is typically shifted to higher LETs. We can understand that with the following argument: At the LET corresponding to the RBE maximum for protons, carbon ions are much faster than protons resulting in broader tracks with a reduced ionization density in the track center. Therefore, at the same LET the biological damage and thus the cell killing effect of carbon ions is smaller than for protons. In order to achieve the maximum RBE, slower ions with a correspondingly smaller track size and higher LET are required.

Last, the radiosensitivity of the irradiated cell line or tissue also determines the RBE (Weyrather *et al.*, 1999; Suzuki *et al.*, 2000). A comparison of three mammalian cell lines with different radiosensitivities is shown in Fig. 27. The RBE for carbon irradiation is highest for the V79 cell line, which is most resistant to conventional irradiation. Chinese hamster ovary (CHO) cells are more sensitive to photon radiation and show a moderate RBE, whereas for the repair-deficient CHO-mutant XRS cell line, the increased effectiveness of ions is almost negligible. In general, the difference in radiosensitivity is largely reduced for high-LET irradiation. In order to investigate the radiosensitivity of human cell lines to therapeutic carbon ions, Suzuki *et al.* determined the survival curves for more than a dozen lineages of normal and tumor cells. A compilation of these experimental data in terms of  $RBE_{\alpha}$  dependence on the  $\alpha/\beta$  ratio after conventional photon irradiation showed an increasing RBE with decreasing  $\alpha/\beta$  ratio (Elsässer *et al.*, 2008). Therefore, the RBE of carbon ions relates to the  $\alpha/\beta$  ratio determined in x-ray experiments.

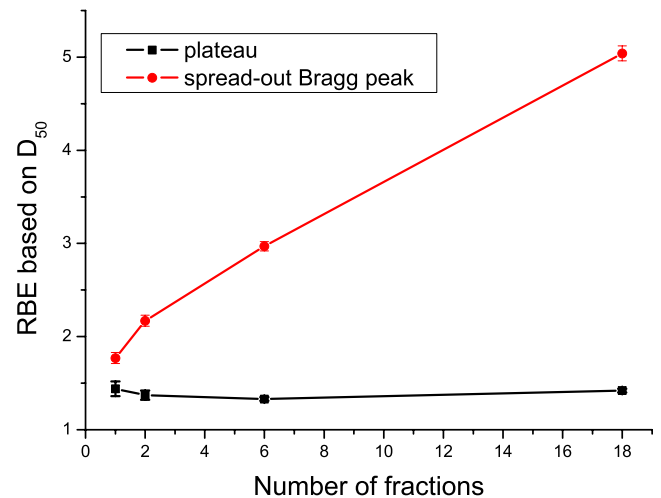


FIG. 28. (Color online) RBE values based on the dose for 50% complication probability for the radiation tolerance of the rat spinal cord after 1, 2, 6, and 18 fractions of carbon ions. Data for the spread-out Bragg peak ( $125 \text{ keV}/\mu\text{m}$ ) and the plateau ( $13 \text{ keV}/\mu\text{m}$ ) are adapted from Karger *et al.*, 2006.

#### 4. RBE determined from *in vivo* measurements

Experiments with cell lines are of high value in radiation research. However, they represent artificial systems partly neglecting cell communication or any other tissue-specific higher-order mechanisms. Especially, the radiation response of normal tissue cannot be reasonably simulated by *in vitro* experiments. Therefore, the RBE systematics described in the preceding sections should also be analyzed by *in vivo* studies.

Animal experiments for tumor control are extremely scarce (Tenforde *et al.*, 1982). Nevertheless, the main RBE trends were also found *in vivo*. Koike *et al.* (2002) demonstrated that the RBE for tumor growth delay of murine fibrosarcoma induced by carbon ions increases with increasing LET and decreases with dose per delivered fraction. Recently, the same trends were detected for prostate tumors implanted in the leg of rats (Peschke, private communication).

At each heavy-ion-therapy center, animal studies of normal-tissue complications were performed in order to verify the quality of the irradiation facility (Leith *et al.*, 1982; Zacharias *et al.*, 1997; Ando *et al.*, 1998). In these studies, the RBE dependence on dose level, LET, and particle type were confirmed. Generally, also *in vivo* the RBE increased for lower dose levels, lower LET, and lighter ions. As an example, the experimental data for the tolerance of the rat spinal cord after fractionated carbon-ion irradiations (Fig. 28) demonstrates the LET and dose dependence (Karger *et al.*, 2006). The RBE increases with the number of fractions (equivalent to a lower dose per fraction) and is larger in the Bragg peak with its higher dose-averaged LET. For intercomparison between different proton and carbon treatment facilities the crypt cell assay was developed to study the radiation tolerance of the intestine. It was found that the RBE between irradiations at HIMAC and GSI, respectively, agreed within a few percent (Uzawa *et al.*, 2009). Addi-

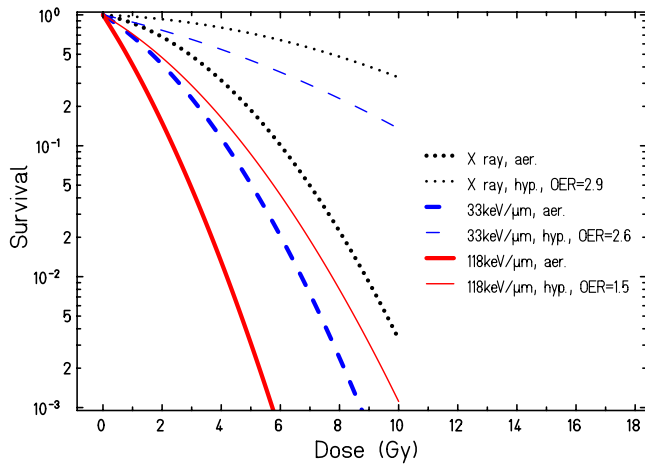


FIG. 29. (Color online) Influence of the oxygen level on cell survival of human kidney T-1 cells for carbon ions with different LET. Lines are based on experimental data by [Blakely et al. \(1979\)](#).

tionally, the RBE of carbon ions was significantly higher than for protons.

### 5. Dependence on oxygen status

In radiation therapy, the treatment of hypoxic tumors poses a specific challenge. When tumors are growing in size, new blood vessels need to be generated to supply oxygen to the cells in the tumor core. Often these vessels are not generated fast enough or they might also be of minor quality. Those effects of poor angiogenesis result in a lower oxygen level as compared to healthy cells. Especially in the center of large tumors, hypoxic regions occur frequently. It is known that these hypoxic conditions lead to a larger radioresistance, however, a widely accepted mechanistic explanation for this effect is still missing. The oxygen effect is quantified by the oxygen enhancement ratio (OER),

$$\text{OER} = \frac{D_{\text{hypoxic}}}{D_{\text{aerobic}}}, \quad (16)$$

where  $D_{\text{hypoxic}}$  and  $D_{\text{aerobic}}$  are the doses with reduced and normal oxygen supply, respectively, resulting in the same biological or clinical effect. Contrary to RBE, the OER is a dose-modifying factor and independent of dose. Typically, it is about 3 for conventional radiation, whereas it is significantly reduced for ion irradiation. Figure 29 shows the results of cell survival studies carried out at LBL in the 1970s as a preparation for the first heavy-ion treatments ([Blakely et al., 1979](#)). The difference between hypoxic and normoxic cells is reduced for high-LET particles and the survival curves converge. The OER decreases with decreasing particle energy, and for high-LET particles it is close to 1. This behavior is in line with the general observation that cell line-specific differences diminish after ion irradiation. In numerous other cell experiment during the last decades, this behavior was validated for a large range of ions and cell lineages ([Barendsen et al., 1966](#); [Bewley, 1968](#); [Furusawa](#)

[et al., 2000](#); [Staab et al., 2004](#)). It was found that the minimum OER is lower for heavier ions such as carbon or neon than for light ions (e.g., helium). Supposedly, the potential higher radiation damage of ions by direct hits compared to indirect radical-induced hits reduces the oxygen effect. Along with a reduction of the OER the RBE is further enhanced in the SOBP. Therefore, heavy particles such as carbon ions offer enormous potential for curing tumors with hypoxic regions.

### B. Biophysical models in heavy-ion therapy

From the previous considerations it is clear that a mere optimization of the physical dose is not adequate for heavy-ion-beam therapy. In contrast to proton therapy, where the beam shaping devices are designed to generate a homogenous physical dose along the spread-out Bragg peak ([Coutrakon et al., 1991](#)), for carbon ions, the absorbed dose in the target needs to be shaped in order to achieve a homogenous *photon-equivalent* dose. For this purpose, the concept of the RBE proves extremely helpful. By properly predicting the RBE for each position in the treatment field, the required physical dose can be determined and the appropriate primary particle fluence can be applied. However, those complex dependencies of RBE previously described covering a wide range of parameters require biophysical modeling, since it is not feasible to experimentally determine the RBE for all possible parameter combinations even for *in vitro* measurements. Unfortunately, the poor general understanding of the processes that govern the value of the RBE—like initial physical and chemical damage induction and their associated repair processes—impedes the preferential mechanistic modeling of the biological response. Although promising approaches exist for the primary physical and chemical processes ([Nikjoo et al., 1994](#); [LaVerne, 2000](#); [Champion et al., 2005](#)) as well as for the subsequent repair pathways ([Cucinotta et al., 2008](#)), these are not yet suitable for application in treatment planning and their future application is uncertain at this time. The lack of knowledge about basic mechanisms, and the absence of rigid quantitative data necessary as input for the models, prohibit the achievement of required model accuracy. Therefore, simplified models needed to be developed to include the RBE either based on some experimental heavy-ion data or by transferring the experience with conventional radiation to the case of ions.

The complexity of the RBE issue also impacts the definition of the biologically or clinically relevant dose. Since the RBE values used in therapy are not known in advance and critically depend on the applied biophysical model, no common definition has been achieved yet. The relevant dose has been named and determined differently at every heavy-ion treatment center. A homogenization of the different approaches initiated by the International Commission on Radiological Units is in progress and will help to find a common definition. In the following, we use the expressions frequently used by the original authors and emphasize on their rationale.

We use the unit “GyE” (Gray Equivalent) for the biologically or clinically related dose in order to express the desire to compare the doses used in particle therapy to those reported in conventional radiotherapy.

The approach at LBL was based on a large data set of measured RBE values which was exploited as input to design the beam shaping devices (Chapman *et al.*, 1977, 1978; Blakely *et al.*, 1980; Lyman *et al.*, 1980). At HIMAC and HIBMC, a similar method is applied to shape the ridge filter system to account for the declining slope of the physical dose along the target volume (Kanai *et al.*, 1997; Kagawa *et al.*, 2002). However, the absolute dose level is determined by adjusting the RBE for carbon ions at the distal part of the SOBP to coincide with the RBE used in neutron therapy (Kanai *et al.*, 1999). The most recent approach applied at GSI relies on the local effect model, which predicts RBE values using the photon dose-response curve of the system, the physical dose distribution around single ion tracks, and the cell nucleus as the sensitive target (Scholz and Kraft, 1994; Scholz *et al.*, 1997). In the following we describe these models that have been already implemented in heavy-ion therapy, before we summarize alternative approaches.

### 1. Biological optimization at LBL

In contrast to the treatment facility at GSI and the future European projects, the beam delivery system based on fixed ion energies requires the application of passive scattering and beam shaping techniques. At LBL, ridge filters were used to shape 4–14 cm long SOBPs in 2 cm increments (Lyman *et al.*, 1980). Since filter design and handling is complicated and time consuming, there is a desire to keep the number of such filters as low as possible. However, due to the different biological systems, particle types and doses, it was clear that it would not be appropriate to use the same set of filters for all treatments. Therefore, extensive cell studies were performed at LBL to optimize the ridge filter design.

The Berkeley rationale of beam shaping was the aim of a photon-equivalent dose based on 66% cell survival (Lyman *et al.*, 1980), which was assumed to be equivalent to the typical dose delivery of 2 Gy per fraction in conventional radiation treatments. Based on numerous cell survival measurements for different particles and LET values (Blakely *et al.*, 1980) and knowledge about the composition of the particle field (Lyman and Howard, 1977; Chen *et al.*, 1979), and a consideration of normal-tissue complications (Woodruff *et al.*, 1984; Lyman and Wolbarst, 1987; Zink *et al.*, 1988), the linear-quadratic model [see Eq. (14)] was applied to calculate the estimated biological response at each water-equivalent depth. Since most of the available cell studies present the RBE at a survival level of 10% and 50%, the LQ model was applied to calculate such values and compare them to existing experimental data. In general, good agreement was found (Lyman *et al.*, 1980). It turned out that different ridge filters need to be used for helium,

neon, and argon ions. However, the same set of filters was used for neon and carbon ions, respectively, since the estimated RBE difference was considered small enough. Although the measurements suggested an influence of the cell type, it was concluded that the deviations between different tumor types are only small and the errors associated with the application of the same filter set are on a few-percent level only (Petti, Lyman, and Castro, 1991; Petti, Lyman, Renner, *et al.*, 1991). Additionally, the application of opposing treatment fields partly levels the RBE distribution and reduces the uncertainty.

### 2. HIMAC approach

Following the pioneering studies at LBL, Kanai *et al.* developed a new strategy to include the biological effectiveness of ions. Based on the experience NIRS had gathered with neutron therapy prior to the start of heavy-ion treatments, the rationale was to find the ion type that most closely resembles their fast neutron beams. By cell inactivation experiments (Fukumura *et al.*, 1997; Kanai *et al.*, 1999), they found that the RBE values of monoenergetic 65 keV/ $\mu\text{m}$  carbon ions coincide with those of the clinical neutron beam. Therefore, the use of carbon ions facilitates the application of the same treatment protocols proven to be effective in neutron therapy.

The design of the SOBP at HIMAC is based on measurements of the human salivary gland (HSG) tumor cell line. It is argued that HSG cells are representative for a variety of biological species and that the RBE values do not significantly differ at the 10% survival level supposed to be typical for daily dose prescriptions. Therefore, they fitted HSG data for numerous LET values to the LQ model and used the following formula to determine the linear-quadratic parameters  $\alpha_{mix}$  and  $\beta_{mix}$  of the mixed radiation field of the SOBP:

$$\begin{aligned}\alpha_{mix} &= \sum f_i \alpha_i, \\ \sqrt{\beta_{mix}} &= \sum f_i \sqrt{\beta_i},\end{aligned}\tag{17}$$

where  $f_i$  is the relative dose contribution of the  $i$ th beam component to the total dose. The design of the ridge filter was optimized in order to achieve a homogeneous biological response. Measurements validating the flat photon-equivalent dose for 10% cell survival along the Bragg peak for several different cell lines is exemplarily shown in Fig. 30 for a 6 cm SOBP. Other experiments verifying the SOBP design include osteosarcoma cells and crypt cells of the mouse jejunum (Kubota *et al.*, 1995; Kanai *et al.*, 1999).

Once the SOBP design was fixed and the flat dose distribution along the target volume was established, cell experiments applying the ridge filters were conducted to find the neutron-equivalent position within the spread-out Bragg peak. Figure 31 demonstrates that at 80 keV/ $\mu\text{m}$  the RBE of 2.1 resembles the neutron RBE for 10% survival of the HSG cell line. However, for neu-

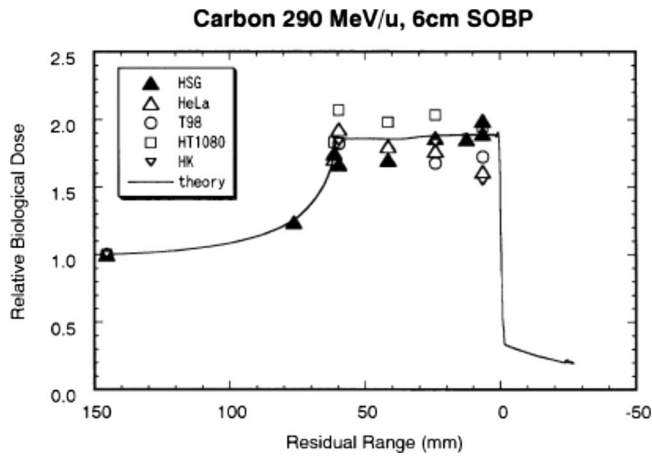


FIG. 30. Distribution of the photon-equivalent dose along a 60 mm spread-out Bragg peak used at HIMAC. Experimental data for several different cell lines are depicted. From Kanai *et al.*, 1999.

tron radiotherapy at NIRS, the RBE was determined to be 3. Therefore, the absolute RBE for carbon-ion treatments was fixed such that for the neutron-equivalent LET of 80 keV/μm the RBE is 3, which is 50% larger than the *in vitro* RBE of 2.0. The position of the neutron-equivalent beam is 8 mm upstream of the distal

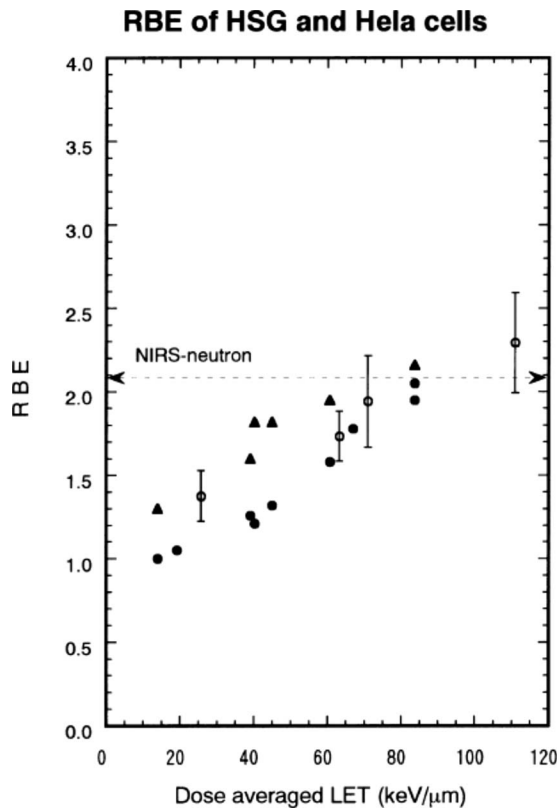


FIG. 31. LET dependence for RBE of 10% survival for HSG and HeLa cells after irradiation by 290 MeV/u carbon ions using a ridge filter to extend the Bragg peak. The dashed line depicts the corresponding value of the NIRS neutron beam for HSG cells. From Kanai *et al.*, 1999.

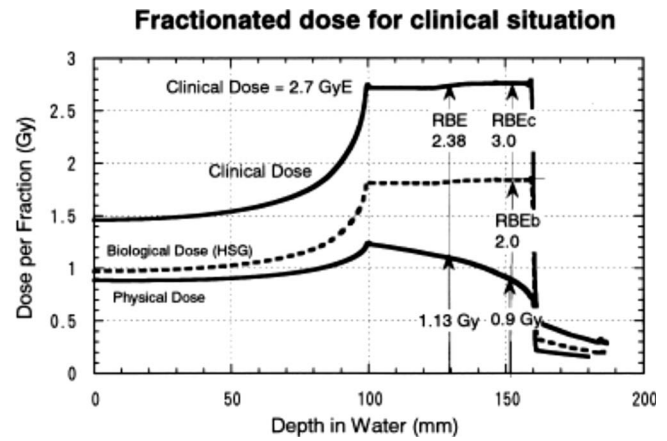


FIG. 32. Schematics to demonstrate the determination of the absolute clinical dose for carbon-ion treatments. The RBE of 3.0 belongs to the neutron-equivalent beam, whereas the clinical RBE is given in the SOBPs center. From Kanai *et al.*, 1999.

end of the SOBPs as shown in Fig. 32. Based on the RBE of 3 as observed in the clinical neutron trials, the dose at the neutron-equivalent point is chosen as 0.9 Gy, resulting in a so-called *clinical* dose of 2.7 GyE; this corresponds to the effective dose also used in the neutron trials and thus allows a direct comparison of the carbon and neutron trials. The RBE of the clinical carbon-ion treatment is reported at the center of the SOBPs, where it is smaller, typically between 2.1 and 2.8, depending on the extension of the SOBPs that covers the tumor volume. This method of RBE determination is applied regardless of the dose level, number of fractions, or the tissue under consideration. The term *biological dose* shown in Fig. 32 refers to the RBE for 10% survival of HSG cells as determined by experimental *in vitro* data.

### 3. Local effect model (GSI)

The implementation of active energy variation and raster scanning for carbon ions (Haberer *et al.*, 1993) opened the pathway for individually optimized tumor conformity for each patient without the need of additional customized passive beam shaping devices. This breakthrough in beam delivery poses a new challenge for biological treatment planning in order to fully exploit the new potential. For this purpose, the local effect model was developed at GSI (Scholz and Kraft, 1996). It calculates RBE values for each position in the treatment field and facilitates the application of complex 3D volumes with a homogenous photon-equivalent dose.

#### a. Basic assumptions

The local effect model relates the response of biological systems following ion irradiation to the corresponding response after x-ray irradiation. It assumes that the biological effect of irradiation is entirely determined by the spatial local dose distribution inside the cell nucleus. The accumulated local dose in the cell nucleus from different tracks is calculated for small subvolumes individually using a track structure model. With knowledge of

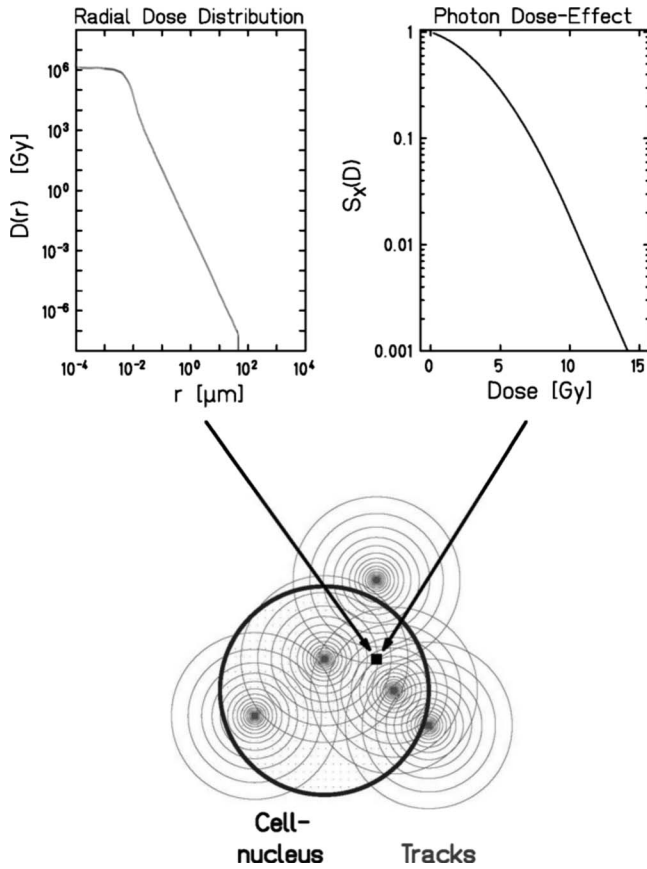


FIG. 33. Schematics of the local effect model. From [Elsässer and Scholz, 2007](#).

the deposited dose, the resulting biological damage is extrapolated from data of x-ray experiments for each subvolume and integrated over the entire cell nucleus. Since for particle irradiation the dose distribution is highly inhomogeneous, the three-dimensional local dose  $d(x, y, z)$  is considered to calculate the average number of lethal events,

$$N_{ion} = \int_V dV v_{ion}[d(x, y, z)], \quad (18)$$

where  $v_{ion}$  denotes the lethal event density after ion radiation within the volume  $V$ , and the survival after ion irradiation is  $S = \exp(-N_{ion})$ . According to the main idea of the LEM, the *local* effect is independent of the radiation quality and  $v_{ion}(d) = v_x(d) = \ln[S_x(d)/V]$ :

$$N_{ion} = \int_V dV \frac{\ln\{S_x[d(x, y, z)]\}}{V}, \quad (19)$$

Equation (19) represents the most general formulation of the local effect model and illustrates the relation of the biological effect of particle irradiation to the effect of photon irradiation. Figure 33 shows the basic idea and the three input quantities. The positions of ion tracks are randomly distributed over the cell nucleus according to Poisson statistics. In the following, we summarize the three constituents of the LEM.

It is assumed that the sensitive sites are distributed homogeneously over the cell nucleus and that they exhibit the same radiosensitivity. The target is thus modeled by a cylinder with an effective area  $A = r_n^2$ , which is smaller than the arithmetic mean of the size distribution of cell nuclei ([Scholz and Kraft, 1996](#)) accounting for inhomogeneities in DNA density.

The linear-quadratic model [see Eq. (14)] is used to parametrize the cell inactivation curve, since it is well accepted and most widely used in literature. However, experiments suggest that a purely linear-quadratic model overestimates the radiation effect for high doses ([Fertil et al., 1994](#); [Park et al., 2008](#)), and a modification must be introduced to account for this behavior. Therefore, a threshold dose  $D_t$  is introduced to describe the dose, above which the dose-response curve turns from the shouldered form into a purely exponential part, similar to the suggestion of a recent thorough analysis of photon dose response curves ([Astrahan, 2008](#)). For even higher doses exceeding a few hundred Gy, additional cluster effects due to the enormous ionization densities in the track center are considered resulting in additional double strand breaks due to nearby single strand breaks ([Elsässer and Scholz, 2007](#)),

$$S(D) = \begin{cases} \exp(-\alpha D - \beta D^2), & D \leq D_t \\ S_t \exp\{-s[\eta(D)D - D_t]\}, & D > D_t, \end{cases} \quad (20)$$

where  $\alpha, \beta$  denote the linear-quadratic components,  $s = \alpha + 2\beta D_t$  is the slope of the exponential tail for doses above  $D_t$ ,  $S_t$  is the survival at threshold dose  $D_t$ , and  $\eta$  quantifies the cluster effect.

The local effect model uses an amorphous track structure description which assumes that the track consists of an inner part with a constant initial dose attached to an outer part following a  $1/r^2$  dependence. It can be expressed by

$$D(r) = \begin{cases} \lambda \text{LET}/r_{min}^2, & r < r_{min} \\ \lambda \text{LET}/r^2, & r_{min} \leq r \leq r_{max} \\ 0, & r_{max}, \end{cases} \quad (21)$$

where LET denotes the linear energy transfer and  $\lambda$  is a normalization constant to assure that the radial integral reproduces the LET for a medium with density  $\rho$ . The maximum radius  $r_{max}$  is determined by those  $\delta$  electrons with the highest energy. It was found by [Kiefer and Straaten \(1986\)](#) that  $r_{max}$  only depends on the energy  $E$  (in MeV/u) and can be parametrized by  $r_{max} = \gamma E^\delta$ ;  $\gamma = 0.062 \mu\text{m} (\text{MeV/u})^{-1.7}$ ,  $\delta = 1.7$ , with  $r_{max}$  in  $\mu\text{m}$ , and  $E$  in MeV/u. The minimum or core radius  $r_{min}$  is constant for earlier versions of the LEM, namely  $r_{min} = 0.3 \text{ nm}$  for the recent cluster version and  $r_{min} = 10 \text{ nm}$  for the original model. The latter uses the large radius to implicitly account for radical diffusion ([Elsässer and Scholz, 2007](#)). In these LEM representations we have assumed an energy-independent core radius. However, by applying Bohr's principle of adiabatic invariance to determine the core radius, it was shown that the minimum track core depends on the ion velocity:  $r_{min} = \beta_{ion} r_c$ , with  $\beta_{ion} = v/c$ ,

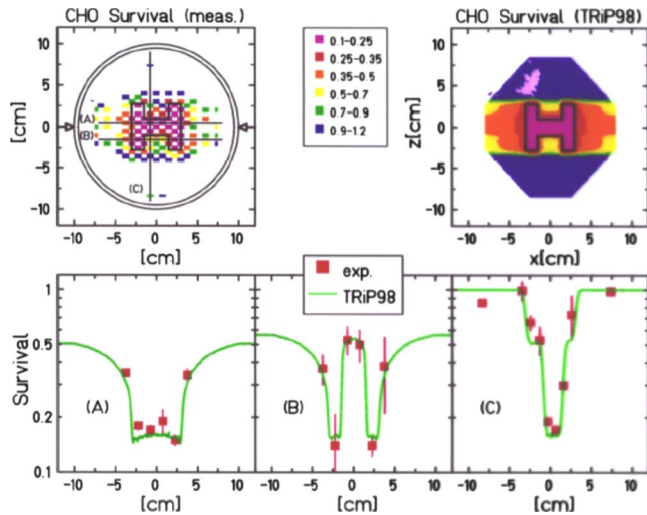


FIG. 34. (Color online) Validation of the treatment planning system with CHO cells in a therapylike scenario with an organ at risk close to the tumor volume (represented by the H-shaped structure). Upper left: Measured survival data. Upper right: Calculated survival. Lower row: Survival along cuts through the irradiated volume. From Krämer, Wang, and Weyrather, 2003.

where  $v$  is the velocity of the particle,  $c$  is the speed of light, and  $r_c$  describes the largest extension of the inner part of the track in the relativistic limit of  $v=c$ . In a recent approach of LEM, it was found that  $r_c=40$  nm gives the best agreement with experimental data (Elsässer *et al.*, 2008).

#### b. Integration into the treatment planning system

The LEM as described above can be applied to calculate the dose response for all relevant parameters using the linear-quadratic model with the ion-specific parameters  $\alpha_{\text{ion}}$  and  $\beta_{\text{ion}}$ . Since the simulations usually take a long time, it is favorable to use approximations to reduce the computation time. Therefore, a method was developed to rapidly determine  $\beta_{\text{ion}}$  from the corresponding initial slope of the dose response curve  $\alpha_{\text{ion}}$  (Scholz *et al.*, 1997). Since the radiation field comprises different particles with a large range of energies, the LQ parameters are required for all their combinations. For this purpose, the treatment planning system TRiP used at GSI stores values of  $\alpha_{\text{ion}}$  for 40 different energies for each particle in tables. These data are used as input to the RBE calculations for mixed fields (Krämer and Scholz, 2000; Krämer *et al.*, 2000). The main task here is to derive the LQ parameters for mixed radiation fields from the parameters  $\alpha_{\text{ion}}$  and  $\beta_{\text{ion}}$  obtained for monoenergetic ions. Recently, an approximation was introduced to rapidly determine the LQ parameters of any given mixed particle field (Krämer and Scholz, 2006). This method is a prerequisite for multiple-field optimization (Gemmel *et al.*, 2008), which has been routinely applied for most of the patients treated at GSI in 2008. In Fig. 34, cell survival experiments with a mammalian cell line (CHO) are shown for a complex target volume with sur-

rounding OAR. It demonstrates the validity of the LEM to calculate the photon-equivalent dose even in complex radiation fields as well as the impressive sparing of the OAR. During the last decade, numerous additional *in vitro* experiments were carried out to demonstrate the applicability of the LEM (Mitaroff *et al.*, 1998; Krämer and Scholz, 2000; Krämer, Weyrather, and Scholz, 2003).

#### c. Choice of parameters for clinical treatments

In the LEM, the radiosensitivity of the irradiated normal and tumor tissue is parameterized by its  $\alpha$  and  $\beta$  values after conventional radiation. For application of the LEM to real cancer treatments, two questions need to be addressed: Is it possible to transfer the positive results of *in vitro* experiments to the more complicated clinical case? And, are the necessary input data available?

In Secs. III.A.3 and III.A.4 it was elaborated that the RBE depends on the radiosensitivity of the irradiated tissue or cell line. The cell experiments reported by Suzuki *et al.* (2000) indicate that the initial RBE ( $\alpha_{\text{ion}}/\alpha$ ) depends on the  $\alpha/\beta$  ratio of the tissue after x-ray irradiation. Additionally, this trend was reproduced by the LEM for the same data set as well as in theoretical investigations (Scholz and Elsässer, 2007). Moreover, the absolute values of  $\alpha$  and  $\beta$  were found to be less important. This general behavior opens up the pathway for a possible transfer to the clinical case, since it is probable that the RBE systematic found for *in vitro* data also holds true for *in vivo* and clinical data, since many other characteristics were found to be the same independent on the experimental system (see Sec. III.A.4). The reduction of the required input information on the  $\alpha/\beta$  ratios increases the range of applicable tissues, since the  $\alpha/\beta$  ratio is known for many tumor and normal tissues.

Using this concept, several animal studies were conducted at GSI to investigate whether the response of normal tissue to carbon ions can be predicted by the LEM based on photon data. Good agreement was found for the RBE of skin reactions in minipigs after fractionated irradiation (5F) with carbon ions (Zacharias *et al.*, 1997); see Fig. 35. In this particular experiment, the primary aim was to determine the absorbed dose levels for carbon ions, which would result in the same skin reaction as the photon dose fields given to the same animals at the same time as the carbon fields. The model calculations were based on  $\alpha/\beta$  values for skin reactions after photon irradiation obtained from *in vivo* studies. For the investigations on the radiation tolerance of the rat spinal cord (see Fig. 28), the initial LEM predictions showed deviations of up to 30% for the spread-out Bragg peak (Karger *et al.*, 2006). However, the recent consideration of an energy-dependent core radius reduced the model discrepancy to the few-percent level (Elsässer *et al.*, 2008).

#### 4. Alternative approaches

After the thorough discussion of those approaches that have been actually used in heavy-ion therapy, in this

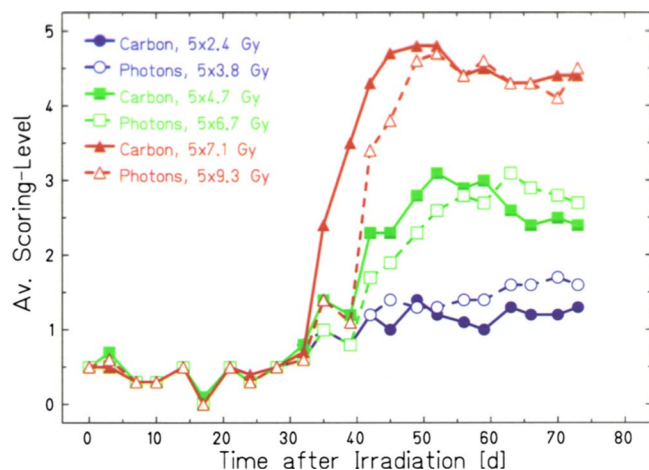


FIG. 35. (Color online) Skin reaction after irradiation with x rays and carbon ions. The scoring level indicates the severity of the skin reaction [for details see Zacharias *et al.* (1997)]. Using the predictions of LEM, the doses for carbon-ion irradiation were adjusted to result in the same biological effect as the photon fields applied simultaneously. From Scholz and Elsässer, 2007; adapted from Zacharias *et al.*, 1997.

section we summarize other biophysical models. These were developed to predict the RBE of ions with a possible application in particle therapy treatment planning in mind and focus on cell inactivation as biological end point.

The Katz approach (Katz *et al.*, 1971; Katz and Sharma, 1974) is similar to the LEM in the sense that both models use the photon dose response as an input to their calculations. Additionally it also uses an amorphous track structure model to simulate the dose deposition of single particles. The relevant sensitive target is assumed to be smaller than the cell nucleus which is comprised of many of such targets. The main idea of the Katz approach is the division of radiation action into two different inactivation modes, the ion-kill and  $\gamma$ -kill, respectively, postulating two different mechanisms for the central part of the track (ion-kill) and the outer  $\delta$  rays ( $\gamma$ -kill). The representation of cell inactivation after photon irradiation is based on the multihit single target (MTSH) theory, an alternative way to parametrize cell survival curves. The MTSH accounts for a purely exponential slope at high doses and postulates a vanishing slope in the limit of low doses. Recently, the Katz model was used to calculate cell inactivation along a SOBP based on experimental *in vitro* data (Waligorski *et al.*, 2006). Despite good model agreement, the requirement of four free parameters and a diminishing slope for low doses of x rays (equivalent with an RBE approaching infinity) impedes the clinical application of the Katz model.

The theory of dual radiation action (TDRA) (Kellerer and Rossi, 1972) is based on the concepts of microdosimetry, which relates the radiation damage to the microscopic energy distribution in micrometer-sized targets. According to TDRA, the typical shoulder shape of survival curves originates from the interaction of suble-

thal lesions at higher doses thus increasing the radiation effect. The physically measured energy distribution is related to the biological response by means of weighting functions generated from experimental heavy-ion data (Loncol *et al.*, 1994). Since these functions are different for each biological end point and dose level, the concept of TDRA is not favorable for heavy-ion therapy.

A promising concept was recently developed at NIRS based on the microdosimetric kinetic model (MKM) (Hawkins, 1994, 2003). Similar to LEM, it uses the dose response of low-LET radiation as input. However, the description of the survival curve follows the conventional LQ model even for large doses. The microdosimetric energy distribution in submicrometer-sized targets is measured and used as model input (Kase *et al.*, 2006). Alternatively, it can be calculated by means of a track structure model (Kase *et al.*, 2008). The MKM achieves good results for monoenergetic *in vitro* cell measurements for each cell line. Therefore, it is a good candidate for implementation in treatment planning, although a successful transfer to clinical applications remains to be shown.

### C. Implications for treatment planning

A crucial and challenging task for heavy-ion treatment planning is the predictive determination of RBE values at each position in the treatment field. The preceding sections showed that RBE values may vary by more than one order of magnitude along the radiation field. In particular, the dose dependence needs to be considered carefully. If carbon-ion treatments involve many fields from different directions, the expected biological gain might be wasted, since the large RBE at a low absorbed entrance dose might outweigh the RBE resulting from high-dose high-LET radiation in the tumor volume. Moreover, for hypofractionation schemes with dose levels exceeding 10 Gy per fraction, the gain due to the biological effect of ions is assumed to be reduced. Although application of different fractionation strategies should follow the same principles as applied in conventional radiotherapy (Fowler, 1989), the determination of the dose per fraction needs to be calculated properly (Karger *et al.*, 2008).

The results reported by Elsässer *et al.* (2008) indicate that the biological effectiveness of ions is related to the radiosensitivity of photons or x rays, which can be characterized by the  $\alpha/\beta$  ratio (see Sec. III.B.3). This perception primarily implies that the most beneficial carbon ion treatments are expected for tumor tissues with a low  $\alpha/\beta$  ratio surrounded by normal tissues characterized by a relatively large  $\alpha/\beta$  ratio. This combination increases the therapeutic ratio even more than it is enhanced by considering the same radiosensitivity for the tumor and normal tissue. As an example, calculations performed with TRiP using different tissues for the tumor, brain (both assumed to have a  $\alpha/\beta$  ratio of 2), and skin ( $\alpha/\beta = 5.9$ ) showed that the photon-equivalent dose in the entrance channel is reduced by about 50% for the skin as compared to brain or chordoma tissue. However, for the

opposite ratio, namely, a high  $\alpha/\beta$  for the tumor and low for normal tissue, the biological effectiveness of heavy ions might reduce the therapeutic ratio. Therefore, careful consideration of the radiobiological properties of the irradiated tissues is essential for the full benefit of heavy ion treatments.

For the optimum choice of the ion species, these dependencies are also of utmost importance. State-of-the-art accelerators are capable of providing swift ions starting from protons up to neon, allowing for plenty of room for optimization (Brahme, 2004; Amaldi and Kraft, 2007). Biological models for treatment planning should guide these considerations, although the final judgement will be provided by clinical data. At GSI, the decision for carbon ions was supported by cell measurements showing the largest ratio between high- and low-LET particles for carbon ions relative to oxygen and neon (Scholz, 2003). The fundamental reason is the slope of the RBE-LET dependence, being the steepest for carbon ions. However, for lighter particles like boron, lithium, or helium a significant increase in RBE is also expected for an SOBP, however, starting at a more distal position. For a careful consideration of the best treatment option, physical aspects like fragmentation, straggling, and scattering need to also be considered.

#### D. Future directions

The crucial criteria for the comprehensive applicability of a biologically optimized treatment planning system for heavy-ion therapy is a sufficient RBE accuracy for all incident tissues using a number of adjustable or unknown parameters that is as small as possible. Currently, the application of different biophysical models results in different predictions of the photon-equivalent dose for the same cancer or tissue type. Also no investigation of RBE values derived from clinical values has been performed yet. Therefore, a reasonable statement on the systematic errors of RBE predictions in carbon-ion therapy is not feasible and needs to be determined as soon as relevant clinical data are available. However, we should keep in mind that in conventional radiotherapy the required error margin does not relate to the biological effect but rather to the absorbed dose and, hence, the requested maximal errors need to be larger. Therefore, we cannot state a simple number for the systematic error (which very much depends on the biological system, dose level, etc.). Considering the uncertainties for hypoxic regions, the situation is similar to conventional therapy, namely, that the variations in radiosensitivity are not fully reflected by the physical dose. Especially for carbon ions, the difference in radiosensitivity is greatly reduced, thus keeping the additional uncertainty small.

The experiment-based approach at HIMAC provides reasonable RBE estimates to shape the SOBP and was shown to facilitate excellent clinical results (Tsujii *et al.*, 2004). However, the concentration on a single cell line and survival level causes inaccuracies for uncommon treatment protocols as well as tissues with radiobiologi-

cal characteristics greatly different from the reference cell system. It was found that the clinical RBE for hypofractionated nonsmall cell lung cancer with a large dose per fraction is smaller than predicted (Kanai *et al.*, 2006). Also, the necessity of different methods to determine RBE values for different tissues was addressed recently at HIMAC within the scope of eye cancer treatments, where the shape of the SOBP is based on the human malignant melanoma (HMV-I) cell line (Koyama-ito *et al.*, 2007).

At GSI, the LEM considers most of the RBE dependencies previously discussed and is the biophysical basis of the outstanding clinical results. However, a thorough analysis of its accuracy based on clinical results is pending. Since during the last decade an underestimation of the therapeutic ratio was detected by means of cell and animal experiments, the LEM was recently amended to address these inaccuracies. Still, the universal application of the LEM including light ions like proton or helium needs further improvements, since significant systematic deviations of the model predictions relative to measurements are observed for these light ions. Additionally, the tissue-specific parameter  $D_t$  requires input from high LET information either by a few experimental data points or by transferring knowledge from tissues with similar radiobiological properties. In the future, direct determination of the parameter  $D_t$  as well as a further improvement of its accuracy will foster the application of treatment planning based on the LEM to new tumor sites and different ion species.

An obvious field of future research concerns the explicit consideration of hypoxic regions in RBE calculations. Extensive studies were conducted elucidating the mechanistic principles of the oxygen effect (Dewhurst *et al.*, 2008) and possible improved imaging techniques (Macapinlac, 2008). We have also summarized in Sec. III.A.5 that numerous *in vitro* experiments have been performed since the early days of heavy-ion therapy. However, the two approaches actually used in treatment planning do not take the OER explicitly into account.

Due to the longer lifetime and reduced treatment age, the second cancer risk is of growing concern in radiation therapy (Allan and Travis, 2005), especially for the use of particles. On the one hand, the excellent tumor conformity and its related small irradiated volumes considerably reduces the total dose delivered to patients. On the other hand, for proton therapy the cancer risk of secondary neutrons needs to be clarified and for heavier ions, the RBE for cancer induction is probably increased. Therefore, the positive effect of small treatment fields might be partially outweighed by a higher effectiveness of particles for second cancer risk. Unfortunately, there are only very few data available assessing the cancer risk based on cell transformation experiments (Bettega, 2004) or animal studies (Ando, Koike, Oohira, *et al.*, 2005). However, due to the success of the carbon-ion therapy facilities and the desire of NASA to take mankind to Mars, the research in heavy-ion radiobiology has gained enormous momentum and we can expect a steady increase of understanding (Durante and Cuci-

notta, 2008). In order to incorporate cancer risk estimates into heavy-ion treatment planning, novel models need to be established, possibly using the same basic principles as in the local effect model, by transferring knowledge gained from conventional treatments to ion therapy.

#### IV. CLINICAL EXPERIENCES

##### A. Clinical trials investigating heavy-ion radiation therapy

Most of the patients treated with carbon-ion RT so far have been included in prospective clinical phase I–III trials. Taking into account radiobiological aspects, the highest benefit of carbon-ion RT by means of increased biological effectiveness and minimization of toxicity can be expected for radioresistant tumors, which are located within radiosensitive normal tissues.

RBE depends on several factors such as tissue type, dose level, atomic number, and energy of particles traversing a cell nucleus. Different biological end points like cell killing within the target volume and toxicity to normal tissues have to be taken into consideration. In systems with a high repair capacity characterized by low  $\alpha/\beta$  ratios and a pronounced shoulder of the cell survival curves, high RBE values could be found in experiments. On the other hand, systems with a poor repair capacity showed low RBE values. When a patient is treated with carbon-ion RT, different tissues with different repair capacities are typically included in the target volume. For the same beam within the same target volume various RBE values may coexist for different end-points. Therefore, RBE has to be accounted for during the treatment planning process.

Historical clinical neutron data have been useful in identifying tumor entities that might benefit from carbon-ion RT and in defining clinical trials. In a second step, dose finding studies have been performed to determine the optimal target doses with respect to the tolerance of dose-limiting normal tissues surrounding the tumors.

At NIRS in Chiba, Japan, a large clinical research program was started in 1994. Carbon-ion RT was investigated within dose escalation trials and, thereafter, in clinical phase II trials for a number of different tumor entities. A focus of research was put on toxicity to normal tissues. Using passive beam delivery systems with the beam passing through a compound scattering system or magnetic wobbling systems, toxicity was mainly observed in the entrance channels of the radiation fields. The dose limiting toxicity of carbon-ion RT was therefore acute toxicity to soft tissues and skin in most of the trials performed at the NIRS.

For a number of tumors high local control rates were found after carbon-ion RT. Promising results were reported for high risk prostate cancer, non-small-cell lung cancer, several skull base tumors of the bone, and chondrogenic tumors as well as hepatocellular carcinoma, malignant salivary gland tumors, malignant melanoma,

and adenocarcinomas of the head and neck region (Tsujii *et al.*, 2004).

In locally advanced head and neck tumors, radiation therapy is part of interdisciplinary treatment concepts. Most patients with head and neck tumors are treated for squamous cell carcinomas. Carbon-ion RT has been found to be beneficial especially for the less common histological subtypes such as adenocarcinomas, adenoid cystic carcinomas, and malignant melanomas (Mizoe *et al.*, 2004). These histological subtypes are known to be relatively resistant to conventional photon RT.

At NIRS, 36 patients with locally advanced head and neck tumors have been enrolled in a dose escalation trial investigating carbon-ion RT. Eleven patients had squamous cell carcinomas, five had malignant melanomas, nine had adenoid cystic carcinomas, four had adenocarcinomas, and seven patients had other histologies. Total doses between 52.8 and 70.2 GyE were delivered in 16 or 18 fractions within 4–6 weeks. Five year local control rates achieved with carbon-ion RT were 100% for malignant melanoma, 50% for adenoid cystic carcinoma, and 34% for squamous cell carcinoma, respectively. Local control rates were found to be favorable in comparison to conventional photon RT especially in nonsquamous cell tumors like malignant melanoma, adenoid cystic carcinoma, and adenocarcinoma (Mizoe *et al.*, 2004).

At GSI, only patients with locally advanced adenoid cystic carcinomas have been chosen for a clinical phase I-II trial investigating a combination treatment of photon IMRT and a carbon-ion boost to the macroscopic tumor. This histological subtype belongs to the group of high grade malignant salivary gland tumors and was chosen for a clinical phase I-II trial because of the relatively high RBE values of up to 8 after high-LET irradiation in these tumors (Battermann *et al.*, 1981). Twenty-nine patients with inoperable, incompletely resected, or recurrent adenoid cystic carcinoma have been included in the trial. Treatment planning for carbon-ion RT included biological plan optimization using the TRiP treatment planning software (Scholz *et al.*, 1997; Krämer and Scholz, 2000). A target dose of 18 GyE of carbon-ion RT was applied in six fractions of 3.0 GyE. Additionally, patients received photon treatment with a median total dose of 54 Gy using conventional fractionation. The 4-year locoregional control and overall survival rates were 77% and 75.8%, respectively. Severe late toxicity grade 4 was observed in one patient, only. While locoregional control rates and overall survival rates were comparable to historical neutron data, toxicity seemed to be reduced after carbon-ion RT. When results were compared to data collected for an adenoid cystic carcinoma series treated with photon IMRT alone, local control rates tended to be higher after combination therapy with photons and carbon ions (Schulz-Ertner *et al.*, 2005).

Carbon-ion RT has also been investigated in chordomas, chondrosarcomas, and osteosarcomas. These histological subtypes of soft tissue and tumors of the bone are known to be very unresponsive to conventional RT necessitating irradiation with high tumor doses, typically

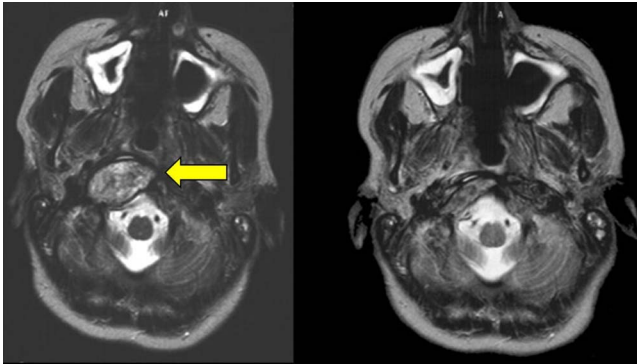


FIG. 36. (Color online) Axial MRI scan of a skull base chordoma prior to RT (left) and tumor regression 6 weeks after irradiation (right).

exceeding the tolerance doses of neighboring normal-tissue structures. Between 1997 and 2005, 96 patients with chordomas have been treated with a full course of carbon-ion RT with a median total tumor dose of 60 GyE at GSI. A local control of 70% at 5 years could be achieved, while highest local control probability rates after modern photon RT are reported to be as low as 50% in chordomas. Overall survival after carbon-ion RT was 88.5% at 5 years. Severe late toxicity was observed in less than 5% of all patients, while overall treatment time could be significantly reduced to 3 weeks. When the local control rates observed after carbon-ion RT at GSI in chordomas were compared with the data available for proton RT in the literature, a clear dose-response relationship could be found and the optimal dose could be estimated to be between 75 and 85 GyE (Schulz-Ertner *et al.*, 2007). Similar advantages of carbon-ion RT could be shown for chondrosarcomas of the skull base. The local control rate was 89.8% at 5 years after carbon-ion RT in 54 patients (Schulz-Ertner *et al.*, 2007). An example of tumor regression is shown in Fig. 36.

At NIRS, 57 patients with inoperable bone and soft tissue sarcomas were treated within a phase I-II dose escalation trial. Carbon-ion beams were applied passively using compensators and collimators. Total doses between 52.8 and 73.6 GyE were applied in 16 fractions within 4 weeks. The overall local control rate was 73% at 3 years, the overall survival rate was 46%. Results were promising especially for 15 patients with inoperable osteosarcoma of the trunk for which an overall survival rate of 45% at 3 years was obtained (Kamada *et al.*, 2002). Imai *et al.* reported a 5-year local control rate of 96% for a subset of 30 patients with unresectable sacral chordomas treated with carbon-ion RT using total doses between 70.4 and 73.6 GyE (Imai *et al.*, 2004).

Using conventional RT with photons or proton RT, hypofractionation is limited by the tolerance of normal tissue included in the planning target volume. It has been shown for neutrons, which are high-LET beams as well, that increasing the fraction size leads to lower RBE for the tumor and less pronounced for normal tissues (Denekamp *et al.*, 1997). Similar results have been ob-

served for carbon-ion beams (Ando, Koike, Uzawa, *et al.*, 2005). Moreover, it has been shown in clinical trials performed at the NIRS that hypofractionation is feasible for several tumor entities. In dose escalation and phase II trials, hypofractionation of carbon-ion RT has been established at the NIRS for stage I lung cancer and hepatocellular carcinoma.

Surgical resection is the treatment of choice for localized non-small-cell lung cancer (NSCLC), but primary RT is considered in medically inoperable patients. Due to the high radiosensitivity of the lung parenchyma and the reduced lung function in most of these patients, the benefit of RT has always to be weighted against the associated risk of further impairment of lung function. Carbon-ion RT represents a RT modality that can be focussed precisely to the tumor. A first phase I-II study was conducted from 1994 to 1999 to determine the optimal dose in stage I NSCLC. Irradiation was applied in 18 fractions within 6 weeks in 47 patients and nine fractions within 3 weeks in 34 patients. The optimal dose fractionation scheme of carbon-ion RT in stage I NSCLC was determined to be 68.4–79.2 GyE given in nine fractions. The 5-year local control probability was 84%, three out of 81 patients developed grade 3 toxicity to normal lung tissue (Miyamoto *et al.*, 2003). As a next step, a phase II study investigating 72.0 GyE within nine fractions in 3 weeks was carried out in 50 patients at NIRS. The local control rate was 94.7%. The 5-year overall and cause-specific survival rates were 50% and 75.7%, respectively. Hypofractionated carbon-ion RT given in four fractions yielded similar local control rates in a phase I-II trial performed in 79 patients (Miyamoto *et al.*, 2007). Furthermore, single dose irradiation using carbon-ion RT is currently being investigated for stage I NSCLC patients. Single total doses of at least 28.0 GyE are applied in this dose escalation trial, which is still ongoing (Tsujii *et al.*, 2007, 2008).

So far, there are no data available comparing proton and carbon-ion RT with modern stereotactic photon RT. A comparative study is particularly warranted for large-sized T2 tumors.

Another important potential indication for hypofractionated carbon-ion RT is hepatocellular carcinoma. Twenty-four patients with 24 lesions were treated with a 15 fractions regimen within 5 weeks. Further phase I-II trials were carried out in order to confirm the safety and efficacy of short-course therapy regimes such as 12 fractions within 3 weeks, eight fractions within 2 weeks and four fractions within 1 week. In these trials, dose was escalated by increasing the fraction dose in increments of 10% from 3.3 to 5.3 GyE (15 fractions), 4.5 to 5.8 GyE (12 fractions), 6.0 to 7.5 GyE (eight fractions), and 12.0 to 13.2 GyE (four fractions). The total dose ranged from 49.5 to 79.5 GyE (15 fractions), 54.0 to 69.6 GyE (12 fractions), and 48.0 to 58.0 GyE (eight fractions). Carbon-ion RT yielded local control and overall survival rates comparable to proton RT (Kato *et al.*, 2004). While there was no significant difference among the different fractionation regimen, the gen-

eral tendency was that local control rate improved with shorter irradiation periods. As a result of a dose escalation trial, which proved the safety and efficacy of a regimen of four fractions within 1 week with a total dose of 52.8 GyE, this fractionation scheme has been adopted for a subsequent phase II trial. Forty-four patients were treated with 52.8 GyE within four fractions within this phase II trial. Local control rate was 95% at 3 years and overall survival was 35% at 5 years (Tsujii *et al.*, 2007).

Hypofractionated carbon-ion RT has also been investigated in patients with locally advanced prostate cancer and soft tissue sarcomas. A fractionation scheme of 16–20 fractions within 4–5 weeks was employed at the facility in Chiba. Given the relatively high photon and proton doses needed to control prostate cancer, prostate cancer cells can be assumed to be relatively radioresistant to conventional photon RT. The  $\alpha/\beta$  ratio was found to be very low in the range of 1.5 Gy, while a higher radiosensitivity is assumed for dose-limiting late reactions of the rectal wall (Fowler, 2005). Therefore, the delivery of higher single doses is currently under discussion even for photon irradiation. High-LET beams such as carbon ions do not only provide the physical advantage of an inverted dose profile, which enables a steep dose gradient towards the anterior rectal wall, but also offer biologic advantages by means of an enhanced biologic effectiveness in tumors with low  $\alpha/\beta$  ratios.

After determination of the optimal carbon-ion dose for prostate cancer within a dose escalation trial, carbon-ion RT has been investigated within a prospective phase II trial at a fixed dose of 66 GyE in 20 fractions given within 5 weeks (Akakura *et al.*, 2004; Tsujii *et al.*, 2005). 175 patients received this fixed regimen of 66.0 GyE/20 fractions of carbon-ion RT within a phase II trial. No patient developed severe late toxicity. Biochemical disease free survival and overall survival rates were 87% and 91% at 4 years, respectively, although the majority of patients had high risk tumors (Ishikawa *et al.*, 2006). The favorable outcome after carbon-ion RT in prostate cancer patients is assumed to be related to an elevated relative biological effectiveness of carbon-ion RT in prostate cancer cells. Besides, hypofractionation has been proven to be feasible, thus reducing the overall treatment time. Nevertheless, the promising results obtained with carbon-ion RT need confirmation in controlled clinical trials with large patient numbers comparing carbon-ion RT with photon IMRT and proton RT, taking also into account toxicity and quality of life. Further hypofractionation of carbon-ion RT appears attractive and might be realized with further optimization of the beam delivery and by combination with new methods for tumor tracking in the future.

## B. Future directions

From the clinical point of view, further research is required to quantify the benefit from therapy with protons and heavy ions in different tumor situations, and to determine the ideal ion species and fractionation scheme.

These questions can be answered only in clinical studies performed at hospital based ion therapy facilities.

So far, not much experience has been gained with combination therapies of carbon-ion RT, chemotherapeutic agents, and other modifiers of the radiation response. Almost all clinical trials investigated carbon-ion RT alone so far. Since modern treatment concepts contain chemotherapy as essential part of the treatment, the combination of carbon-ion RT with different chemotherapeutic agents will be an important research field in the near future. One of the main clinical problems using active beam delivery techniques is the physiological movement of targets and breath dependent changes in the normal tissues surrounding the tumor region. These changes might influence the range of carbon-ion beams and limit the application of scanned carbon-ion beams. Potential strategies currently under investigation include motion management for active particle beam delivery with gating and fast rescanning (see Sec. II.C.4). Furthermore, different tumor tracking methods are under development as well for particle therapy. Technological improvements in the fields of treatment planning, accelerator technology, patient positioning, image guidance, adaptive radiation therapy, PET monitoring, and biological dosimetry will help to fully exploit the potential of carbon-ion RT in the treatment of oncological patients in the future.

## V. CONCLUSION

Since the pioneering work at LBL Berkeley, where in 1975 heavy ions were applied in cancer treatment for the first time, rapid progress in accelerator technology has contributed significantly to the further development of ion-beam therapy as a precision tool in radiooncology. The following generation of heavy-ion accelerators, the SIS-18 synchrotron at GSI and the HIMAC facility at NIRS, Chiba provided excellent beam quality and highly reliable performance, which was essential for the further development of radiotherapy with ion beams. An important step was the design and installation of scanning beam systems for proton beams at PSI and carbon ions at GSI, providing optimum conditions for the application of IMPT and enabling highly tumor-conformal treatments with improved sparing of normal tissue and organs at risk.

In parallel, extensive radiobiological studies have led to an improved understanding of the biological effectiveness of heavy ions. Comprehensive strategies and models for biological treatment planning have been developed and implemented in the treatment planning systems. These tremendous achievements advanced the better exploitation of the specific advantage of heavy ions, characterized by the effective combination of physical and biological benefits.

The increasing number of excellent clinical results provide evidence that carbon-ion therapy should be beneficial in numerous tumor entities, however, more data will be needed for a better assessment of the role of heavy ions in modern radiation therapy. Interesting re-

sults can be expected from the dedicated ion-beam center HIT which started patient treatments in November 2009 and allows for the first time to compare clinical results of proton and heavy-ion treatments under the same irradiation conditions. Various other heavy-ion therapy centers presently under construction in Italy, Japan, Germany, and China will follow within a few years' time and make this precise and effective modality of treatment available to a large number of patients.

## ACKNOWLEDGMENTS

We would like to thank all colleagues of the heavy-ion therapy group (GSI Darmstadt/Kopfclinik Heidelberg/DKFZ Heidelberg/FZ Dresden) for the very fruitful collaboration over more than ten years in the pilot project at GSI, where many of the results presented in this review were obtained. We particularly thank Gerhard Kraft for his enthusiasm and countless stimulating discussions. His tireless efforts have paved the way for the first heavy-ion therapy unit in Europe. Critical comments and valuable suggestions on the manuscript from Christoph Bert, Ellie Blakely, Peter Heeg, Oliver Jäkel, Michael Krämer, Katia Parodi, Eike Rietzel, Michael Scholz, and Uli Weber are gratefully acknowledged.

## REFERENCES

- Adler, J. R., M. J. Murphy, S. D. Chang, and S. L. Hancock, 1999, "Image-guided robotic radiosurgery," *Neurosurgery* **44**, 1299–1307.
- Agosteo, S., C. Birattari, M. Caravaggio, M. Silari, and G. Tosi, 1998, "Secondary neutron and photon dose in proton therapy," *Radiother. Oncol.* **48**, 293–305.
- Ahlen, S. P., 1980, "Theoretical and experimental aspects of the energy loss of relativistic heavily ionizing particles," *Rev. Mod. Phys.* **52**, 121–173.
- Akakura, K., H. Tsujii, S. Morita, H. Tsuji, T. Yagishita, S. Isaka, H. Ito, H. Akaza, M. Hata, M. Fujime, M. Harada, and J. Shimazaki, 2004, "Phase I/II clinical trials of carbon ion therapy for prostate cancer," *Prostate* **58**, 252–258.
- Allan, J. M., and L. B. Travis, 2005, "Mechanisms of therapy-related carcinogenesis," *Nat. Rev. Cancer* **5**, 943–955.
- Allkofer, O. C., and W. Heinrich, 1974, "Attenuation of cosmic ray heavy nuclei fluxes in the upper atmosphere by fragmentation," *Nucl. Phys. B* **71**, 429–438.
- Alpen, E. L., 1998, *Radiation Biophysics* (Academic, San Diego).
- Amaldi, U., and G. Kraft, 2007, "European developments in radiotherapy with beams of large radiobiological effectiveness," *J. Radiat. Res. Suppl.* **48**, A27–A41.
- Amaldi, U., *et al.*, 2004, "LIBO-A linac-booster for proton therapy: Construction and tests of a prototype," *Nucl. Instrum. Methods Phys. Res. A* **521**, 512–529.
- Ando, K., S. Koike, K. Nojima, Y. J. Chen, C. Ohira, A. Ando, N. Kobayashi, T. Ohbuchi, W. Shimizu, and T. Kanai, 1998, "Mouse skin reactions following fractionated irradiation with carbon ions," *Int. J. Radiat. Biol.* **74**, 129–138.
- Ando, K., S. Koike, C. Oohira, T. Ogiu, and F. Yatagai, 2005, "Tumor induction in mice locally irradiated with carbon ions: A retrospective analysis," *J. Radiat. Res. (Tokyo)* **46**, 185–190.
- Ando, K., S. Koike, A. Uzawa, N. Takai, T. Fukawa, Y. Furusawa, M. Aoki, and Y. Miyato, 2005, "Biological gain of carbon-ion radiotherapy for the early response of tumor growth delay and against early response of skin reaction in mice," *J. Radiat. Res. (Tokyo)* **46**, 51–57.
- Astrahan, M., 2008, "Some implications of linear-quadratic-linear radiation dose-response with regard to hypofractionation," *Med. Phys.* **35**, 4161–4172.
- Badano, L., M. Benedikt, P. J. Bryant, M. Crescenti, P. Holy, P. Knaus, A. Meier, M. Pullia, and S. Rossi, 1999, *Proton Ion Medical Machine Study (PIMMS), Part I* (CERN, Geneva), cern/ps 1999-010.
- Badano, L., M. Benedikt, P. J. Bryant, M. Crescenti, P. Holy, P. Knaus, A. Meier, M. Pullia, and S. Rossi, 2000, *Proton Ion Medical Machine Study (PIMMS), Part II* (CERN, Geneva), cern/ps 2000-007.
- Barendsen, G. W., C. J. Koot, G. R. van Kersen, D. K. Bewley, S. B. Field, and C. J. Parnell, 1966, "The effect of oxygen on impairment of the proliferative capacity of human cells in culture by ionizing radiations of different LET," *Int. J. Radiat. Biol.* **10**, 317–327.
- Barkas, H. W., 1963, *Nuclear Research Emulsions* (Academic, New York), Vol. 1.
- Battermann, J. J., K. Breur, G. A. Hart, and H. A. van Peperzeel, 1981, "Observations on pulmonary metastases in patients after single doses and multiple fractions of fast neutrons and cobalt-60 gamma rays," *Eur. J. Cancer* **17**, 539–548.
- Belli, M., F. Cera, R. Cherubini, V. M. Dalla, A. M. Haque, F. Ianzini, G. Moschini, O. Saporita, G. Simone, M. A. Tabocchini, and P. Tiveron, 1998, "RBE-LET relationships for cell inactivation and mutation induced by low energy protons in V79 cells: Further results at the LNL facility," *Int. J. Radiat. Biol.* **74**, 501–509.
- Bennett, G. W., J. O. Archambeau, B. E. Archambeau, J. I. Meltzer, and C. L. Wingate, 1978, "Visualization and transport of positron emission from proton activation *in vivo*," *Science* **200**, 1151–1153.
- Berger, G., M. Bouvy, T. Daras, E. Kaerts, M. Loiselet, and G. Ryckewaert, 1990, *Proceedings of the 2nd European Particle Accelerator Conference*, edited by P. M. P. Mandrillon (Editions Frontières, Gif-sur-Yvette, France), pp. 1793–1795.
- Bert, C., A. Gemmel, N. Saito, and E. Rietzel, 2009, "Gated irradiation with scanned particle beams," *Int. J. Radiat. Oncol., Biol., Phys.* **73**, 1270–1275.
- Bert, C., S. O. Grözinger, and E. Rietzel, 2008, "Quantification of interplay effects of scanned particle beams and moving targets," *Phys. Med. Biol.* **53**, 2253–2265.
- Bert, C., and E. Rietzel, 2007, "4D treatment planning for scanned ion beams," *Radiat. Oncol.* **2**, 24.
- Bert, C., N. Saito, A. Schmidt, N. Chaudhri, D. Schardt, and E. Rietzel, 2007, "Target motion tracking with a scanned particle beam," *Med. Phys.* **34**, 4768–4771.
- Bethe, H., 1930, "Zur theorie des durchgangs schneller korpuskularstrahlen durch materie," *Ann. Phys.* **397**, 325–400.
- Bettega, D., 2004, "Cell transformation by light charged particles: Review of available data," *Radiother. Oncol.* **73**, S155–S157.
- Bewley, D. K., 1968, "A comparison of the response of mammalian cells to fast neutrons and charged particle beams," *Radiat. Res.* **34**, 446–458.
- Bichsel, H., and T. Hiraoka, 1992, "Energy loss of 70 MeV

- protons in elements," *Nucl. Instrum. Methods Phys. Res. B* **66**, 345–351.
- Bichsel, H., T. Hiraoka, and K. Omata, 2000, "Aspects of fast-ion dosimetry," *Radiat. Res.* **153**, 208–219.
- Binns, P. J., and J. H. Hough, 1997, "Secondary dose exposures during 200 MeV proton therapy," *Radiat. Prot. Dosim.* **70**, 441–444.
- Birks, J. B., 1951, "The specific fluorescence of anthracene and other organic materials," *Phys. Rev.* **84**, 364–365.
- Blakely, E. A., C. A. Tobias, F. Q. Ngo, and S. B. Curtis, 1980, "Physical and cellular radiobiological properties of heavy ions in relation to cancer therapy applications," report (unpublished).
- Blakely, E. A., C. A. Tobias, T. C. Yang, K. C. Smith, and J. T. Lyman, 1979, "Inactivation of human kidney cells by high-energy monoenergetic heavy-ion beams," *Radiat. Res.* **80**, 122–160.
- Bloch, F., 1933a, "Bremsvermögen von Atomen mit mehreren elektronen," *Z. Phys. A: Hadrons Nucl.* **81**, 363–376.
- Bloch, F., 1933b, "Zur bremsung rasch bewegter teilchen beim durchgang durch materie," *Ann. Phys.* **408**, 285–320.
- Böhne, D., 1992, "Light ion accelerators for cancer therapy," *Radiat. Environ. Biophys.* **31**, 205–218.
- Bohr, N., 1940, "Scattering and stopping of fission fragments," *Phys. Rev.* **58**, 654–655.
- Boon, S. N., P. van Luijk, T. Bohringer, A. Coray, A. Lomax, E. Pedroni, B. Schaffner, and J. M. Schippers, 2000, "Performance of a fluorescent screen and CCD camera as a two-dimensional dosimetry system for dynamic treatment techniques," *Med. Phys.* **27**, 2198–2208.
- Boon, S. N., P. van Luijk, J. M. Schippers, H. Meertens, J. M. Denis, S. Vynckier, J. Medin, and E. Grusell, 1998, "Fast 2D phantom dosimetry for scanning proton beams," *Med. Phys.* **25**, 464–475.
- Bortfeld, T., K. Jokivarsi, M. Goitein, K. J. and S. B. Jiang, 2002, "Effects of intra-fraction motion on IMRT dose delivery: Statistical analysis and simulation," *Phys. Med. Biol.* **47**, 2203–2220.
- Bothe, W., 1921, "Das allgemeine fehlergesetz, die schwankungen der feldstärke in einem dielektrikum und die zerstreung der a-Strahlen," *Z. Phys. A: Hadrons Nucl.* **5**, 63–69.
- Bragg, W., 1905, "On the a-particles of radium and their loss of range in passing through various atoms and molecules," *Philos. Mag.* **10**, 318–340.
- Brahme, A., 2004, "Recent advances in light ion radiation therapy," *Int. J. Radiat. Oncol., Biol., Phys.* **58**, 603–616.
- Brede, H. J., K. D. Greif, O. Hecker, P. Heeg, J. Heese, D. T. L. Jones, H. Kluge, and D. Schardt, 2006, "Absorbed dose to water determination with ionization chamber dosimetry and calorimetry in restricted neutron, photon, proton and heavy-ion radiation fields," *Phys. Med. Biol.* **51**, 3667–3682.
- Brusasco, C., B. Voss, D. Schardt, M. Krämer, and G. Kraft, 2000, "A dosimetry system for fast measurement of 3D depth-dose profiles in charged-particle tumor therapy with scanning techniques," *Nucl. Instrum. Methods Phys. Res. B* **168**, 578–592.
- Calabretta, L., G. Cuttone, M. Maggiore, M. Re, and D. Rifugiato, 2006, "A novel superconducting cyclotron for therapy and radioisotope production," *Nucl. Instrum. Methods Phys. Res. A* **562**, 1009–1012.
- Caporaso, G. J., *et al.*, 2007, "Compact accelerator concept for proton therapy," *Nucl. Instrum. Methods Phys. Res. B* **261**, 777–781.
- Champion, C., A. L'hoir, M. F. Politis, P. D. Fainstein, R. D. Rivarola, and A. Chetioui, 2005, "A Monte Carlo code for the simulation of heavy-ion tracks in water," *Radiat. Res.* **163**, 222–231.
- Chapman, J. D., E. A. Blakely, K. C. Smith, and R. C. Urta-sun, 1977, "Radiobiological characterization of the inactivating events produced in mammalian cells by helium and heavy ions," *Int. J. Radiat. Oncol., Biol., Phys.* **3**, 97–102.
- Chapman, J. D., E. A. Blakely, K. C. Smith, R. C. Urta-sun, J. T. Lyman, and C. A. Tobias, 1978, "Radiation biophysical studies with mammalian cells and a modulated carbon ion beam," *Radiat. Res.* **74**, 101–111.
- Chatterjee, A., E. L. Alpen, C. A. Tobias, J. Llacer, and J. Alonso, 1981, "High energy beams of radioactive nuclei and their biomedical applications," *Int. J. Radiat. Oncol., Biol., Phys.* **7**, 503–507.
- Chatterjee, A., and H. J. Schaefer, 1976, "Microdosimetric structure of heavy ion tracks in tissue," *Radiat. Environ. Biophys.* **13**, 215–227.
- Chen, G. T., J. H. Kung, and E. Rietzel, 2007, "Four-dimensional imaging and treatment planning of moving targets," *Front. Radiat. Ther. Oncol.* **40**, 59–71.
- Chen, G. T., R. P. Singh, J. R. Castro, J. T. Lyman, and J. M. Quivey, 1979, "Treatment planning for heavy ion radiotherapy," *Int. J. Radiat. Oncol., Biol., Phys.* **5**, 1809–1819.
- Chen, G. T. Y., J. R. Castro, and J. M. Quivey, 1981, "Heavy charged particle radiotherapy," *Annu. Rev. Biophys. Bioeng.* **10**, 499–529.
- Chu, W. T., B. A. Ludewigt, and T. R. Renner, 1993, "Instrumentation for treatment of cancer using proton and light-ion beams," *Rev. Sci. Instrum.* **64**, 2055–2122.
- Cirio, R., *et al.*, 2004, "Two-dimensional and quasi-three-dimensional dosimetry of hadron and photon beams with the Magic Cube and the Pixel Ionization Chamber," *Phys. Med. Biol.* **49**, 3713–3724.
- Collot, J., Y. Mori, P. Mandrillon, F. Méot, and R. Edgecock, 2008, "The rise of the FFAG," *CERN Cour.* **48**, 21–23.
- Coutrakon, G., M. Bauman, D. Lesyna, D. Miller, J. Nusbaum, J. Slater, J. Johanning, J. Miranda, J. P. M. DeLuca, and J. Siebers, 1991, "A prototype beam delivery system for the proton medical accelerator at Loma Linda," *Med. Phys.* **18**, 1093–1099.
- Crespo, P., G. Shakirin, and W. Enghardt, 2006, "On the detector arrangement for in-beam PET for hadron therapy monitoring," *Phys. Med. Biol.* **51**, 2143–2163.
- Cucinotta, F. A., J. M. Pluth, J. A. Anderson, J. V. Harper, and P. O'Neill, 2008, "Biochemical kinetics model of DSB repair and induction of gamma-H2AX foci by non-homologous end joining," *Radiat. Res.* **169**, 214–222.
- Denekamp, J., T. Waites, and J. F. Fowler, 1997, "Predicting realistic RBE values for clinically relevant radiotherapy schedules," *Int. J. Radiat. Biol.* **71**, 681–694.
- Dewhirst, M. W., Y. Cao, and B. Moeller, 2008, "Cycling hypoxia and free radicals regulate angiogenesis and radiotherapy response," *Nat. Rev. Cancer* **8**, 425–437.
- Dingfelder, M., 2002, "Cross section calculations in condensed media: Charged particles in liquid water," *Radiat. Prot. Dosim.* **99**, 23–28.
- Durante, M., and F. A. Cucinotta, 2008, "Heavy ion carcinogenesis and human space exploration," *Nat. Rev. Cancer* **8**, 465–472.
- Elsässer, T., A. Gemmel, M. Scholz, D. Schardt, and M. Krämer, 2009, "The relevance of very low energy ions for

- heavy-ion therapy," *Phys. Med. Biol.* **54**, N101–N106.
- Elsässer, T., M. Krämer, and M. Scholz, 2008, "Accuracy of the local effect model for the prediction of biologic effects of carbon ion beams *in vitro* and *in vivo*," *Int. J. Radiat. Oncol., Biol., Phys.* **71**, 866–872.
- Elsässer, T., and M. Scholz, 2007, "Cluster effects within the local effect model," *Radiat. Res.* **167**, 319–329.
- Endo, M., H. Koyama-ito, S. Minohara, N. Miyahara, H. Tomura, T. Kanai, K. Kawachi, H. Tsuji, and K. Morita, 1996, "HIPLAN-a heavy ion treatment planning system at HIMAC," *J. Jpn. Soc. Ther. Radiol. Oncol.* **8**, 231–238.
- Endo, S., K. Tanaka, M. Takada, Y. Onizuka, N. Miyahara, T. Sato, M. Ishikawa, N. Maeda, N. Hayabuchi, K. Shizuma, and M. Hoshi, 2007, "Microdosimetric study for secondary neutrons in phantom produced by a 290 MeV/nucleon carbon beam," *Med. Phys.* **34**, 3571–3578.
- Engelsman, M., E. Rietzel, and H. M. Kooy, 2006, "Four-dimensional proton treatment planning for lung tumors," *Int. J. Radiat. Oncol., Biol., Phys.* **64**, 1589–1595.
- Enghardt, W., P. Crespo, F. Fiedler, R. Hinz, K. Parodi, J. Pawelke, and F. Pönisch, 2004, "Charged hadron tumour therapy monitoring by means of PET," *Nucl. Instrum. Methods Phys. Res. A* **525**, 284–288.
- Enghardt, W., J. Debus, T. Haberer, B. G. Hasch, R. Hinz, O. Jäkel, M. Krämer, K. Lauckner, J. Pawelke, and F. Pönisch, 1999, "Positron emission tomography for quality assurance of cancer therapy with light ion beams," *Nucl. Phys. A* **654**, 1047c–1050c.
- Enghardt, W., K. Parodi, P. Crespo, F. Fiedler, J. Pawelke, and F. Pönisch, 2004, "Dose quantification from in-beam positron emission tomography," *Radiother. Oncol.* **73**, S96–S98.
- Enghardt, W., *et al.*, 1992, "The spatial distribution of positron-emitting nuclei generated by relativistic light ion beams in organic matter," *Phys. Med. Biol.* **37**, 2127–2131.
- Fano, U., 1963, "Penetration of protons, alpha particles, and mesons," *Annu. Rev. Nucl. Sci.* **13**, 1–66.
- Fertil, B., I. Reydellet, and P. J. Deschavanne, 1994, "A benchmark of cell survival models using survival curves for human cells after completion of repair of potentially lethal damage," *Radiat. Res.* **138**, 61–69.
- Fiedler, F., M. Priegnitz, R. Jülich, J. Pawelke, P. Crespo, K. Parodi, F. Pönisch, and W. Enghardt, 2008, "In-beam PET measurements of biological half-lives of  $^{12}\text{C}$  irradiation induced beta<sup>+</sup>-activity," *Acta Oncol.* **47**, 1077–1086.
- Fischer, B. E., 1985, "The scanning heavy ion microscope at GSI," *Nucl. Instrum. Methods Phys. Res. B* **10-11**, 693–696.
- Fowler, J. F., 1989, "The linear-quadratic formula and progress in fractionated radiotherapy," *Br. J. Radiol.* **62**, 679–694.
- Fowler, J. F., 2005, "The radiobiology of prostate cancer including new aspects of fractionated radiotherapy," *Acta Oncol.* **44**, 265–276.
- Friedländer, E. M., and H. H. Heckmann, 1985, "Relativistic heavy-ion collisions: experiments," in *Treatise on Heavy-Ion Science*, edited by D. A. Bromley (Plenum, New York), Vol. 4, pp. 403–562.
- Fukutsu, K., T. Kanai, Y. Furusawa, and K. Ando, 1997, "Response of mouse intestine after single and fractionated irradiation with accelerated carbon ions with a spread-out Bragg peak," *Radiat. Res.* **148**, 168–174.
- Furukawa, T., T. Inaniwa, S. Sato, T. Tomitani, S. Minohara, K. Noda, and T. Kanai, 2007, "Design study of a raster scanning system for moving target irradiation in heavy-ion radiotherapy," *Med. Phys.* **34**, 1085–1097.
- Furusawa, Y., K. Fukutsu, M. Aoki, H. Itsukaichi, K. Eguchi-Kasai, H. Ohara, F. Yatagai, T. Kanai, and K. Ando, 2000, "Inactivation of aerobic and hypoxic cells from three different cell lines by accelerated (3)He-, (12)C- and (20)Ne-ion beams," *Radiat. Res.* **154**, 485–496.
- Gemmel, A., B. Hasch, M. Ellerbrock, W. K. Weyrather, and M. Krämer, 2008, "Biological dose optimization with multiple ion fields," *Phys. Med. Biol.* **53**, 6991–7012.
- Goldhaber, A. S., and H. H. Heckman, 1978, "High energy interactions of nuclei," *Annu. Rev. Nucl. Part. Sci.* **28**, 161–205.
- Golovkov, M., D. Aleksandrov, L. Chulkov, G. Kraus, and D. Schardt, 1997, "Fragmentation of 270 AMeV carbon ions in water," in *Advances in Hadrontherapy*, International Congress Series No. 1144 (Elsevier Science, New York), pp. 316–324.
- Gottschalk, B., 2006, "Neutron dose in scattered and scanned proton beams: In regard to Eric J. Hall (Int J Radiat Oncol Biol Phys 2006;65:1–7)," *Int. J. Radiat. Oncol., Biol., Phys.* **66**, 1594–1594.
- Gottschalk, B., A. M. Koehler, R. J. Schneider, J. M. Sisterson, and M. S. Wagner, 1993, "Multiple Coulomb scattering of 160 MeV protons," *Nucl. Instrum. Methods Phys. Res. B* **74**, 467–490.
- Gottschalk, B., and E. Pedroni, 2008, "Treatment delivery systems," in *Proton and Charged Particle Radiotherapy*, edited by T. F. DeLaney, and H. M. Kooy (Lippincott Williams and Wilkins, Philadelphia), Chap. 5, pp. 33–49.
- Gottschalk, B., and M. S. Wagner, 1989, "Contoured scatterer for proton dose flattening," Harvard Cyclotron Laboratory Technical Note.
- Groß, K. D., and M. Pavlovic, 1998, Eds., *Proposal for a Dedicated Ion Beam Facility for Cancer Therapy* (GSI, Darmstadt).
- Grözinger, S. O., C. Bert, T. Haberer, G. Kraft, and E. Rietzel, 2008, "Motion compensation with a scanned ion beam: A technical feasibility study," *Radiat. Oncol.* **3**, 34.
- Grözinger, S. O., E. Rietzel, Q. Li, C. Bert, T. Haberer, and G. Kraft, 2006, "Simulations to design an online motion compensation system for scanned particle beams," *Phys. Med. Biol.* **51**, 3517–3531.
- Gunzert-Marx, K., H. Iwase, D. Schardt, and R. S. Simon, 2008, "Secondary beam fragments produced by 200 MeV/u  $^{12}\text{C}$  ions in water and their dose contributions in carbon ion radiotherapy," *New J. Phys.* **10**, 075003.
- Gunzert-Marx, K., D. Schardt, and R. S. Simon, 2004, "Fast neutrons produced by nuclear fragmentation in treatment irradiations with  $^{12}\text{C}$  beam," *Radiat. Prot. Dosim.* **110**, 595–600.
- Haberer, T., W. Becher, D. Schardt, and G. Kraft, 1993, "Magnetic scanning system for heavy ion therapy," *Nucl. Instrum. Methods Phys. Res. A* **330**, 296–305.
- Haberer, T., J. Debus, H. Eickhoff, O. Jäkel, D. Schulz-Ertner, and U. Weber, 2004, "The Heidelberg ion therapy center," *Radiother. Oncol., Suppl. 2* **73**, S186–S190.
- Haettner, E., H. Iwase, and D. Schardt, 2006, "Experimental fragmentation studies with  $^{12}\text{C}$  therapy beams," *Radiat. Prot. Dosim.* **122**, 485–487.
- Hall, E., 2000, *Radiobiology for the Radiologist*, 5th ed. (Lippincott Williams and Wilkins, Philadelphia).
- Hall, E. J., 2006, "Intensity-modulated radiation therapy, protons, and the risk of second cancers," *Int. J. Radiat. Oncol., Biol., Phys.* **65**, 1–7.

- Hall, E. J., and D. J. Brenner, 2006, "In reply to Drs. Macklis Gottschalk, Paganetti *et al.*," *Int. J. Radiat. Oncol., Biol., Phys.* **66**, 1595–1595.
- Hawkins, R. B., 1994, "A statistical theory of cell killing by radiation of varying linear energy transfer," *Radiat. Res.* **140**, 366–374.
- Hawkins, R. B., 2003, "A microdosimetric-kinetic model for the effect of non-Poisson distribution of lethal lesions on the variation of RBE with LET," *Radiat. Res.* **160**, 61–69.
- Heeg, P., H. Eickhoff, and T. Haberer, 2004, "Conception of heavy ion beam therapy at Heidelberg University (HICAT)," *Z. Med. Phys.* **14**, 17–24.
- Henkelmann, R. M., and K. Mah, 1982, "How important is breathing in radiation therapy of the thorax?," *Int. J. Radiat. Oncol., Biol., Phys.* **8**, 2005–2010.
- Highland, V. L., 1975, "Some practical remarks on multiple scattering," *Nucl. Instrum. Methods Phys. Res.* **129**, 497–499.
- Highland, V. L., 1979, "Erratum," *Nucl. Instrum. Methods Phys. Res.* **161**, 171.
- Hirao, Y., *et al.*, 1992, "Heavy ion synchrotron for medical use-HIMAC project at NIRS-Japan-," *Nucl. Phys. A* **538**, 541–550.
- Hishikawa, Y., K. Kagawa, M. Murakami, H. Sakai, T. Akagi, and M. Abe, 2002, "Usefulness of positron-emission tomographic images after proton therapy," *Int. J. Radiat. Oncol., Biol., Phys.* **53**, 1388–1391.
- Hüfner, J., 1985, "Heavy fragments produced in proton-nucleus and nucleus-nucleus collisions at relativistic energies," *Phys. Rep.* **125**, 129–185.
- IAEA, 2000, "Absorbed dose determination in external beam radiotherapy," Technical Reports Series 398.
- ICRP1991, 2007, "ICRP 1990 Recommendations of the International Commission on Radiological Protection," *ICRP Publication* (Pergamon, Oxford), Vol. 60.
- ICRU, 1993, ICRU Report 51, "Quantities and Units in Radiation Protection Dosimetry" (International Commission on Radiation Units and Measurements, Bethesda, MD).
- ICRU, 1994, ICRU Report 50, "Prescribing, Recording and Reporting Photon Beam Therapy," *Med. Phys.* **21**, 833–834.
- ICRU, 1999, Report 62, "Prescribing, Recording and Reporting Photon Beam Therapy, Supplement to ICRU Report 50" (International Commission on Radiation Units and Measurements, Bethesda, MD).
- ICRU, 2007, ICRU Report 78, "Prescribing, Recording and Reporting Proton-Beam Therapy," *J. ICRU* **7** (2).
- Imai, R., T. Kamada, H. Tsuji, T. Yanagi, M. Baba, T. Miyamoto, S. Kato, S. Kandatsu, J. E. Mizoe, H. Tsujii, and S. Tazetaki, 2004, "Carbon ion radiotherapy for unresectable sacral chordomas," *Clin. Cancer Res.* **10**, 5741–5746.
- Inaniwa, T., T. Furukawa, S. Sato, T. Tomitani, M. Kobayashi, S. Minohara, K. Noda, and T. Kanai, 2008, "Development of treatment planning for scanning irradiation at HIMAC," *Nucl. Instrum. Methods Phys. Res. B* **266**, 2194–2198.
- Iseki, Y., T. Kanai, M. Kanazawa, A. Kitagawa, H. Mizuno, T. Tomitani, M. Suda, and E. Urakabe, 2004, "Range verification system using positron emitting beams for heavy-ion radiotherapy," *Phys. Med. Biol.* **49**, 3179–3195.
- Ishikawa, H., H. Tsuji, T. Kamada, T. Yanagi, J.-E. Mizoe, T. Kanai, S. Morita, M. Wakatsuki, J. Shimazaki, and H. Tsujii, 2006, "Carbon ion radiation therapy for prostate cancer: Results of a prospective phase II study," *Radiother. Oncol.* **81**, 57–64.
- Ito, A., H. Nakano, Y. Kusano, R. Hirayama, Y. Furusawa, C. Murayama, T. Mori, Y. Katsumura, and K. Shinohara, 2006, "Contribution of indirect action to radiation-induced mammalian cell inactivation: Dependence on photon energy and heavy-ion LET," *Radiat. Res.* **165**, 703–712.
- Iwase, H., K. Gunzert-Marx, E. Haettner, D. Schardt, F. Guetermuth, M. Krämer, and G. Kraft, 2007, "Experimental and theoretical study of the neutron dose produced by carbon ion therapy beams," *Radiat. Prot. Dosim.* **126**, 615–618.
- Jäkel, O., G. H. Hartmann, P. Heeg, and D. Schardt, 2000, "Effective point of measurement of cylindrical ionization chambers for heavy charged particles," *Phys. Med. Biol.* **45**, 599–607.
- Jäkel, O., C. Jacob, D. Schardt, C. P. Karger, and G. H. Hartmann, 2001, "Relation between carbon ion ranges and x-ray CT numbers," *Med. Phys.* **28**, 701–703.
- Jäkel, O., M. Krämer, C. P. Karger, and J. Debus, 2001, "Treatment planning for heavy ion radiotherapy: Clinical implementation and application," *Phys. Med. Biol.* **46**, 1101–1116.
- Kagawa, K., M. Murakami, Y. Hishikawa, M. Abe, T. Akagi, T. Yanou, G. Kagiya, Y. Furusawa, K. Ando, K. Nojima, M. Aoki, and T. Kanai, 2002, "Preclinical biological assessment of proton and carbon ion beams at Hyogo Ion Beam Medical Center," *Int. J. Radiat. Oncol., Biol., Phys.* **54**, 928–938.
- Kamada, T., H. Tsujii, H. Tsuji, T. Yanagi, J. E. Mizoe, T. Miyamoto, H. Kato, S. Yamada, S. Morita, K. Yoshikawa, S. Kandatsu, and A. Tateishi, 2002, "Efficacy and safety of carbon ion radiotherapy in bone and soft tissue sarcomas," *J. Clin. Oncol.* **20**, 4466–4471.
- Kanai, T., Y. Furusawa, K. Fukutsu, H. Itsukaichi, K. Eguchi-Kasai, and H. Ohara, 1997, "Irradiation of mixed beam and design of spread-out Bragg peak for heavy-ion radiotherapy," *Radiat. Res.* **147**, 78–85.
- Kanai, T., K. Kawachi, H. Matsuzawa, and T. Inada, 1983, "Three-dimensional beam scanning for proton therapy," *Nucl. Instrum. Methods Phys. Res. A* **214**, 491–496.
- Kanai, T., T. Kohno, S. Minohara, M. Sudou, E. Takada, F. Soga, K. Kawachi, and A. Fukumura, 1993, "Dosimetry and measured differential W values of air for heavy ions," *Radiat. Res.* **135**, 293–301.
- Kanai, T., N. Matsufuji, T. Miyamoto, J. Mizoe, T. Kamada, H. Tsuji, H. Kato, M. Baba, and H. Tsujii, 2006, "Examination of GyE system for HIMAC carbon therapy," *Int. J. Radiat. Oncol., Biol., Phys.* **64**, 650–656.
- Kanai, T., *et al.*, 1999, "Biophysical characteristics of HIMAC clinical irradiation system for heavy-ion radiation therapy," *Int. J. Radiat. Oncol., Biol., Phys.* **44**, 201–210.
- Kanazawa, M., *et al.*, 2002, "Application of an RI-beam for cancer therapy: *In-vivo* verification of the ion-beam range by means of positron imaging," *Nucl. Phys. A* **701**, 244–252.
- Kanematsu, N., N. Matsufuji, R. Kohno, S. Minohara, and T. Kanai, 2003, "A CT calibration method based on the polybinary tissue model for radiotherapy treatment planning," *Phys. Med. Biol.* **48**, 1053–1064.
- Karger, C. P., O. Jäkel, and G. H. Hartmann, 1999, "A system for three-dimensional dosimetric verification of treatment plans in intensity-modulated radiotherapy with heavy ions," *Med. Phys.* **26**, 2125–2132.
- Karger, C. P., O. Jäkel, P. Heeg, and G. H. Hartmann, 2002, "Clinical dosimetry for heavy ion therapy," *Z. Med. Phys.* **12**, 159–169.
- Karger, C. P., O. Jäkel, M. Scholz, P. Peschke, and J. Debus, 2008, "What is the clinically relevant relative biologic effectiveness? A warning for fractionated treatments with high lin-

- ear energy transfer radiation: In regard to Dasu and Toma-  
DAsu. (*Int J Radiat Oncol Biol Phys* 2008;70:867–874).” *Int. J. Radiat. Oncol., Biol., Phys.* **70**, 1614–1615.
- Karger, C. P., P. Peschke, R. Sanchez-Brandelik, M. Scholz, and J. Debus, 2006, “Radiation tolerance of the rat spinal cord after 6 and 18 fractions of photons and carbon ions: Experimental results and clinical implications,” *Int. J. Radiat. Oncol., Biol., Phys.* **66**, 1488–1497.
- Kase, Y., T. Kanai, N. Matsufuji, Y. Furusawa, T. Elsasser, and M. Scholz, 2008, “Biophysical calculation of cell survival probabilities using amorphous track structure models for heavy-ion irradiation,” *Phys. Med. Biol.* **53**, 37–59.
- Kase, Y., T. Kanai, Y. Matsumoto, Y. Furusawa, H. Okamoto, T. Asaba, M. Sakama, and H. Shinoda, 2006, “Microdosimetric measurements and estimation of human cell survival for heavy-ion beams,” *Radiat. Res.* **166**, 629–638.
- Kato, H., *et al.*, 2004, “Results of the first prospective study of carbon ion radiotherapy for hepatocellular carcinoma with liver cirrhosis,” *Int. J. Radiat. Oncol., Biol., Phys.* **59**, 1468–1476.
- Kats, M., and B. Druzhinin, 2004, “Simple planar system,” *Proceedings of RuPAC XIX, Dubna, 2004* (unpublished), p. 115.
- Katz, R., B. Ackerson, M. Homayoonfar, and S. C. Sharma, 1971, “Inactivation of cells by heavy ion bombardment,” *Radiat. Res.* **47**, 402–425.
- Katz, R., and F. A. Cucinotta, 1999, “Tracks to therapy,” *Radiat. Meas.* **31**, 379–388.
- Katz, R., and S. C. Sharma, 1974, “Heavy particles in therapy: An application of track theory,” *Phys. Med. Biol.* **19**, 413–435.
- Keall, P., S. Vedam, R. George, C. Bartee, J. Siebers, F. Lerma, E. Weiss, and T. Chung, 2006, “The clinical implementation of respiratory-gated intensity-modulated radiotherapy,” *Med. Dosim.* **31**, 152–162.
- Keall, P. J., V. R. Kini, S. S. Vedam, and R. Mohan, 2001, “Motion adaptive x-ray therapy: A feasibility study,” *Phys. Med. Biol.* **46**, 1–10.
- Kellerer, A. M., and H. H. Rossi, 1972, “The theory of dual radiation action,” *Curr. Top. Radiat. Res. Q.* **8**, 85–158.
- Kiefer, J., and H. Straaten, 1986, “A model of ion track structure based on classical collision dynamics,” *Phys. Med. Biol.* **31**, 1201–1209.
- Kim, J., and H. Blosser, 2001, *Cyclotrons and their Applications 2001*, edited by F. Marti, AIP Conf. Proc. No. 600 (AIP, Melville, NY), pp. 345–347.
- Kitagawa, A., *et al.*, 2006, “Medical application of radioactive nuclear beams at HIMAC,” *Rev. Sci. Instrum.* **77**, 03C105-3.
- Koehler, A. M., R. J. Schneider, and J. M. Sisterson, 1975, “Range modulators for protons and heavy ions,” *Nucl. Instrum. Methods Phys. Res.* **131**, 437–440.
- Koehler, A. M., R. J. Schneider, and J. M. Sisterson, 1977, “Flattening of proton dose distributions for large-field radiotherapy,” *Med. Phys.* **4**, 297–301.
- Koike, S., *et al.*, 2002, “Relative biological effectiveness of 290 MeV/u carbon ions for the growth delay of a radioresistant murine fibrosarcoma,” *J. Radiat. Res. (Tokyo)* **43**, 247–255.
- Kox, S., *et al.*, 1987, “Trends of total reaction cross sections for heavy ion collisions in the intermediate energy range,” *Phys. Rev. C* **35**, 1678.
- Koyama-ito, H., T. Kanai, S. Minohara, H. Tsuji, and H. Tsujii, 2007, “Carbon ion therapy for ocular melanoma: Planning orthogonal two-port treatment,” *Phys. Med. Biol.* **52**, 5341–5352.
- Kraft, G., 2000, “Tumor therapy with heavy charged particles,” *Prog. Part. Nucl. Phys.* **45**, S473–S544.
- Kraft, G., and M. Krämer, 1993, “Linear energy transfer and track structure,” *Adv. Radiat. Biol.* **17**, 1–51.
- Krämer, M., 1995, “Calculations of heavy-ion track structure,” *Nucl. Instrum. Methods Phys. Res. B* **105**, 14–20.
- Krämer, M., O. Jäkel, T. Haberer, G. Kraft, D. Schardt, and U. Weber, 2000, “Treatment planning for heavy-ion radiotherapy: Physical beam model and dose optimization,” *Phys. Med. Biol.* **45**, 3299–3317.
- Krämer, M., and M. Scholz, 2000, “Treatment planning for heavy-ion radiotherapy: Calculation and optimization of biologically effective dose,” *Phys. Med. Biol.* **45**, 3319–3330.
- Krämer, M., and M. Scholz, 2006, “Rapid calculation of biological effects in ion radiotherapy,” *Phys. Med. Biol.* **51**, 1959–1970.
- Krämer, M., J. F. Wang, and W. Weyrather, 2003, “Biological dosimetry of complex ion radiation fields,” *Phys. Med. Biol.* **48**, 2063–2070.
- Krämer, M., W. K. Weyrather, and M. Scholz, 2003, “The increased biological effectiveness of heavy charged particles: From radiobiology to treatment planning,” *Technol. Cancer Res. Treat.* **2**, 427–436.
- Krauss, A., 2006, “The PTB water calorimeter for the absolute determination of absorbed dose to water in 60Co radiation,” *Metrologia* **43**, 259–272.
- Kubota, N., M. Suzuki, Y. Furusawa, K. Ando, S. Koike, T. Kanai, F. Yatagai, M. Ohmura, H. Tatsuzaki, S. Matsubara, and T. Inada, 1995, “A comparison of biological effects of modulated carbon-ions and fast neutrons in human osteosarcoma cells,” *Int. J. Radiat. Oncol., Biol., Phys.* **33**, 135–141.
- Kumazaki, Y., T. Akagi, T. Yanou, D. Suga, Y. Hishikawa, and T. Teshima, 2007, “Determination of the mean excitation energy of water from proton beam ranges,” *Radiat. Meas.* **42**, 1683–1691.
- Langen, K. M., and D. T. L. Jones, 2001, “Organ motion and its management,” *Int. J. Radiat. Oncol., Biol., Phys.* **50**, 265–278.
- LaVerne, J. A., 2000, “Track effects of heavy ions in liquid water,” *Int. J. Radiat. Oncol., Biol., Phys.* **153**, 487–496.
- Leith, J. T., M. McDonald, P. Powers-Risius, S. F. Bliven, and J. Howard, 1982, “Response of rat spinal cord to single and fractionated doses of accelerated heavy ions,” *Radiat. Res.* **89**, 176–193.
- Levy, R. P., 2007, “PET-CT: Evolving role in hadron therapy,” *Nucl. Instrum. Methods Phys. Res. B* **261**, 782–785.
- Li, J. G., and L. Xing, 2000, “Inverse planning incorporating organ motion,” *Med. Phys.* **27**, 1573–1578.
- Li, Q., S. O. Grözinger, T. Haberer, E. Rietzel, and G. Kraft, 2004, “Online compensation of target motion with scanned particle beams: Simulation environment,” *Phys. Med. Biol.* **49** (14), 3029–3046.
- Lineva, N., C. Kozhuharov, S. Hagemann, M. Krämer, and G. Kraft, 2008, “Investigation of low-energy electrons emitted from solid-state targets in heavy-ion-atom collisions,” *GSI-Report 2008-1* (GSI Scientific Report 2007), p. 281 (unpublished).
- Linz, U., and J. Alonso, 2007, “What will it take for laser driven proton accelerators to be applied to tumor therapy?,” *Phys. Rev. ST Accel. Beams* **10**, 094801.
- Litzenberg, D. W., 1998, “On-line monitoring and PET imag-

- ing of the positron-emitting activity created in tissue by proton radiotherapy beams," *Med. Phys.* **25**, 254–254.
- Llacer, J., A. Chatterjee, E. L. Alpen, W. Saunders, S. Andreae, and H. C. Jackson, 1984, "Imaging by injection of accelerated radioactive particle beams," *IEEE Trans. Med. Imaging* **3**, 80–90.
- Llacer, J., J. B. Schmidt, and C. A. Tobias, 1990, "Characterization of fragmented heavy-ion beams using a three-stage telescope detector: Measurements of 670-MeV/amu 20Ne beams," *Med. Phys.* **17**, 151–157.
- Llacer, J., C. A. Tobias, W. R. Holley, and T. Kanai, 1984, "On-line characterization of heavy-ion beams with semiconductor detectors," *Med. Phys.* **11**, 266–278.
- Lomax, A., 1999, "Intensity modulation methods for proton radiotherapy," *Phys. Med. Biol.* **44**, 185–205.
- Loncol, T., V. Congrove, J. M. Denis, J. Gueulette, A. Mazal, H. G. Menzel, P. Pihet, and R. Sabbattier, 1994, "Radiobiological effectiveness of radiation beams with broad LET spectra: Microdosimetric analysis using biological weighting functions," *Radiat. Prot. Dosim.* **52**, 347–352.
- Lyman, J. T., and J. Howard, 1977, "Dosimetry and instrumentation for helium and heavy ions," *Int. J. Radiat. Oncol., Biol., Phys.* **3**, 81–85.
- Lyman, J. T., J. Howard, L. Kanstein, and J. R. Alonso, 1980, "Radiological physics of heavy charged-particle beams used for therapy," report (unpublished).
- Lyman, J. T., and A. B. Wolbarst, 1987, "Optimization of radiation therapy, III: A method of assessing complication probabilities from dose-volume histograms," *Int. J. Radiat. Oncol., Biol., Phys.* **13**, 103–109.
- Lynch, W. G., 1987, "Nuclear fragmentation in proton- and heavy-ion-induced reactions," *Annu. Rev. Nucl. Part. Sci.* **37**, 493–535.
- Macapinlac, H. A., 2008, "Clinical applications of positron emission tomography/computed tomography treatment planning," *Semin Nucl. Med.* **38**, 137–140.
- Maccabee, H. D., and M. A. Ritter, 1974, "Fragmentation of high-energy oxygen-ion beams in water," *Radiat. Res.* **60**, 409–421.
- Macklis, R., 2006, "In regards to Hall: Intensity-modulated radiation therapy, protons, and the risk of second cancers (Int J Radiat Oncol Biol Phys 2006;65:1–7)," *Int. J. Radiat. Oncol., Biol., Phys.* **66**, 1593–1594.
- Maggiore, M., L. Calabretta, M. D. Giacomo, D. Rifuggiato, D. Battaglia, and L. Piazza, 2006, "Conceptual design of the RF accelerating cavities for a superconducting cyclotron," *Nucl. Instrum. Methods Phys. Res. A* **557**, 414–420.
- Mangles, S. P. D., *et al.*, 2004, "Monoenergetic beams of relativistic electrons from intense laser-plasma interactions," *Nature (London)* **431**, 535–538.
- Matsufuji, N., A. Fukumura, M. Komori, T. Kanai, and T. Kohno, 2003, "Influence of fragment reaction of relativistic heavy charged particles on heavy-ion radiotherapy," *Phys. Med. Biol.* **48**, 1605–1623.
- Matsufuji, N., M. Komori, H. Sasaki, K. Akiu, M. Ogawa, A. Fukumura, E. Urakabe, T. Inaniwa, T. Nishio, T. Kohno, and T. Kanai, 2005, "Spatial fragment distribution from a therapeutic pencil-like carbon beam in water," *Phys. Med. Biol.* **50**, 3393–3403.
- Matsufuji, N., H. Tomura, Y. Futami, H. Yamashita, A. Higashi, S. Minohara, M. Endo, and T. Kanai, 1998, "Relationship between CT number and electron density, scatter angle and nuclear reaction for hadron-therapy treatment planning," *Phys. Med. Biol.* **43**, 3261–3275.
- Min, C. H., C. H. Kim, M. Y. Youn, and J. W. Kim, 2006, "Prompt gamma measurements for locating the dose fall-off region in the proton therapy," *Appl. Phys. Lett.* **89**, 183517-3.
- Min, C. H., J. W. Kim, M. Y. Youn, and C. H. Kim, 2007, "Determination of distal dose edge location by measuring right-angled prompt-gamma rays from a 38-MeV proton beam," *Nucl. Instrum. Methods Phys. Res. A* **580**, 562–565.
- Minohara, S., T. Kanai, M. Endo, and K. Kawachi, 1993, "Effects of object size on a function to convert x-ray CT numbers into the water equivalent path length of charged particle beam," *Proceedings of the Third Workshop on Physical and Biological Research with Heavy Ions (NIRS Publication NIRS-M-99)*, pp. 14–15.
- Minohara, S., T. Kanai, M. Endo, K. Noda, and M. Kanazawa, 2000, "Respiratory gated irradiation system for heavy-ion radiotherapy," *Int. J. Radiat. Oncol., Biol., Phys.* **47**, 1097–1103.
- Mitaroff, A., W. Kraft-Weyrather, O. B. Geiss, and G. Kraft, 1998, "Biological verification of heavy ion treatment planning," *Radiat. Environ. Biophys.* **37**, 47–51.
- Miyamoto, T., *et al.*, 2003, "Carbon ion radiotherapy for stage I non-small cell lung cancer," *Radiother. Oncol.* **66**, 127–140.
- Miyamoto, T., *et al.*, 2007, "Curative treatment of Stage I non-small-cell lung cancer with carbon ion beams using a hypofractionated regimen," *Int. J. Radiat. Oncol., Biol., Phys., Suppl.* **67**, 750–758.
- Mizoe, J. E., H. Tsujii, T. Kamada, Y. Matsuoka, H. Tsuji, Y. Osaka, A. Hasegawa, N. Yamamoto, S. Ebihara, and A. Konno, 2004, "Dose escalation study of carbon ion radiotherapy for locally advanced head-and-neck cancer," *Int. J. Radiat. Oncol., Biol., Phys.* **60**, 358–364.
- Mizuno, H., *et al.*, 2003, "Washout measurement of radioisotope implanted by radioactive beams in the rabbit," *Phys. Med. Biol.* **48**, 2269–2281.
- Molière, 1948, "Theorie der streuung schneller geladener teilchen II, mehrfach-und vielfachstreuung," *Z. Naturforsch. A* **3A**, 78–97.
- Murphy, M. J., 2004, "Tracking moving organs in real time," *Semin. Radiat. Oncol.* **14**, 91–100.
- Nikjoo, H., P. O'Neill, M. Terrissol, and D. T. Goodhead, 1994, "Modelling of radiation-induced DNA damage: The early physical and chemical event," *Int. J. Radiat. Biol.* **66**, 453–457.
- Nikjoo, H., P. O'Neill, M. Terrissol, and D. T. Goodhead, 1999, "Quantitative modelling of DNA damage using Monte Carlo track structure method," *Radiat. Environ. Biophys.* **38**, 31–38.
- Nil, S., T. Bortfeld, and U. Oelfke, 2004, "Inverse planning of intensity modulated proton therapy," *Z. Med. Phys.* **14**, 35–40.
- Noda, K., *et al.*, 1996, "Slow beam extraction by a transverse RF field with AM and FM," *Nucl. Instrum. Methods Phys. Res. A* **374**, 269–277.
- Ohara, K., T. Okumura, M. Akisada, T. Inada, T. Mori, H. Yokota, and M. J. B. Caraguas, 1989, "Irradiation synchronized with the respiration gate," *Int. J. Radiat. Oncol., Biol., Phys.* **17**, 853–857.
- Okumura, T., H. Tsuji, and H. Tsujii, 1995, "Compensation of target motion," in *Ion Beams in Tumor Therapy* (Chapman and Hall, London), pp. 308–315.
- Paganetti, H., T. Bortfeld, and T. F. Delaney, 2006, "Neutron dose in proton radiation therapy: In regard to Eric J. Hall (Int J Radiat Oncol Biol Phys 2006;65:1–7)," *Int. J. Radiat. Oncol., Biol., Phys.* **66**, 1594–1595.

- Paganetti, H., A. Niemierko, M. Ancukiewicz, L. E. Gerweck, M. Goitein, J. S. Loeffler, and H. D. Suit, 2002, "Relative biological effectiveness (RBE) values for proton beam therapy," *Int. J. Radiat. Oncol., Biol., Phys.* **53**, 407–421.
- Paretzke, H. G., 1986, "Physical events of heavy ion interactions with matter," *Adv. Space Res.* **6**, 67–73.
- Park, C., L. Papiez, S. Zhang, M. Story, and R. D. Timmerman, 2008, "Universal survival curve and single fraction equivalent dose: Useful tools in understanding potency of ablative radiotherapy," *Int. J. Radiat. Oncol., Biol., Phys.* **70**, 847–852.
- Parodi, K., 2004, "On the feasibility of dose quantification with in-beam PET data in radiotherapy with  $^{12}\text{C}$  and proton beams," Ph.D. thesis (Technische Universität Dresden, Fakultät Mathematik und Naturwissenschaften).
- Parodi, K., T. Bortfeld, W. Enghardt, F. Fiedler, A. Knopf, H. Paganetti, J. Pawelke, G. Shakirin, and H. Shih, 2008, "PET imaging for treatment verification of ion therapy: Implementation and experience at GSI Darmstadt and MGH Boston," *Nucl. Instrum. Methods Phys. Res. A* **591**, 282–286.
- Parodi, K., T. Bortfeld, and T. Haberer, 2008, "Comparison between in-beam and offline positron emission tomography imaging of proton and carbon ion therapeutic irradiation at synchrotron- and cyclotron-based facilities," *Int. J. Radiat. Oncol., Biol., Phys.* **71**, 945–956.
- Parodi, K., W. Enghardt, and T. Haberer, 2002, "In-beam PET measurements of  $\text{b}^+$  radioactivity induced by proton beams," *Phys. Med. Biol.* **47**, 21–36.
- Parodi, K., H. Paganetti, H. A. Shih, S. Michaud, J. S. Loeffler, T. F. Delaney, N. J. Liebsch, J. E. Munzenrider, A. J. Fischman, A. Knopf, and T. Bortfeld, 2007, "Patient study of in vivo verification of beam delivery and range, using positron emission tomography and computed tomography imaging after proton therapy," *Int. J. Radiat. Oncol., Biol., Phys.* **68**, 920–934.
- Parodi, K., F. Pönisch, and W. Enghardt, 2005, "Experimental study on the feasibility of in-beam PET for accurate monitoring of proton therapy," *IEEE Trans. Nucl. Sci.* **52**, 778–786.
- Paul, H., 2007, "The mean ionization potential of water, and its connection to the range of energetic carbon ions in water," *Nucl. Instrum. Methods Phys. Res. B* **255**, 435–437.
- Paul, H., O. Geithner, and O. Jäkel, 2007, "The ratio of stopping powers of water and air for dosimetry applications in tumor therapy," *Nucl. Instrum. Methods Phys. Res. B* **256**, 561–564.
- Pawelke, J., L. Byars, W. Enghardt, W. D. Fromm, H. Geissel, B. G. Hasch, K. Lauckner, P. Manfrass, D. Schardt, and M. Sobiella, 1996, "The investigation of different cameras for in-beam PET imaging," *Phys. Med. Biol.* **41**, 279–296.
- Pawelke, J., W. Enghardt, T. Haberer, B. G. Hasch, R. Hinz, M. Krämer, E. Lauckner, and M. Sobiella, 1997, "In-beam PET imaging for the control of heavy-ion tumour therapy," *IEEE Trans. Nucl. Sci.* **44**, 1492–1498.
- Pedroni, E., 1994, "Beam delivery," in *Advances in Hadrontherapy*, International Congress Series No. 1077 (Elsevier Science, New York), pp. 434–452.
- Pedroni, E., R. Bacher, H. Blattmann, T. Böhringer, A. Coray, A. Lomax, S. Lin, G. Munkel, S. Scheib, and U. Schneider, 1989, "Proton therapy status reports, PSI Life Sciences Newsletter 1989/1990," in *PSI Annual Report Annex II*, pp. 5–12 (unpublished).
- Pedroni, E., R. Bacher, H. Blattmann, T. Böhringer, A. Coray, A. Lomax, S. Lin, G. Munkel, S. Scheib, U. Schneider, and A. Tourovsky, 1995, "The 200-MeV proton therapy project at the Paul Scherrer Institute: Conceptual design and practical realization," *Med. Phys.* **22**, 37–53.
- Pedroni, E., R. Bearpark, T. Böhringer, and A. Coray, 2004, "The PSI Gantry 2: A second generation proton scanning gantry," *Z. Med. Phys.* **14**, 25–34.
- Petti, P. L., and A. J. Lennox, 1994, "Hadronic radiotherapy," *Annu. Rev. Nucl. Part. Sci.* **44**, 155–197.
- Petti, P. L., J. T. Lyman, and J. R. Castro, 1991, "Sensitivity of helium beam-modulator design to uncertainties in biological data," *Med. Phys.* **18**, 506–512.
- Petti, P. L., J. T. Lyman, T. R. Renner, J. R. Castro, J. M. Collier, I. K. Daftari, and B. A. Ludewigt, 1991, "Design of beam-modulating devices for charged-particle therapy," *Med. Phys.* **18**, 513–518.
- Pfotenhauer, S. M., *et al.*, 2008, "Spectral shaping of laser generated proton beams," *New J. Phys.* **10**, 033034.
- Phillips, M. H., E. Pedroni, H. Blattmann, T. Boehringer, A. Coray, and S. Scheib, 1992, "Effects of respiratory motion on dose uniformity with a charged particle scanning method," *Phys. Med. Biol.* **37**, 223–233.
- Pshenichnov, I., I. Mishustin, and W. Greiner, 2005, "Neutrons from fragmentation of light nuclei in tissue-like media: A study with the GEANT4 toolkit," *Phys. Med. Biol.* **50**, 5493–5507.
- PTCOG, 2009, <http://ptcog.web.psi.ch>
- Puck, T. T., and P. I. Marcus, 1956, "Action of x-rays on mammalian cells," *J. Exp. Med.* **103**, 653–666.
- Ramm, U., U. Weber, M. Bock, M. Krämer, A. Bankamp, M. Damrau, C. Thilman, H. D. Bottcher, L. R. Schad, and G. Kraft, 2000, "Three-dimensional BANGTM gel dosimetry in conformal carbon ion radiotherapy," *Phys. Med. Biol.* **45**, N95–N102.
- Rietzel, E., G. T. Y. Chen, N. C. Choi, and C. G. Willet, 2005, "Four-dimensional image-based treatment planning: Target volume segmentation and dose calculation in the presence of respiratory motion," *Int. J. Radiat. Oncol., Biol., Phys.* **61**, 1535–1550.
- Rietzel, E., D. Schardt, and T. Haberer, 2007, "Range accuracy in carbon ion treatment planning based on CT-calibration with real tissue samples," *Radiat. Oncol.* **2**, 14.
- Rodriguez, J., D. Schardt, C. Brusasco, B. Voss, and U. Weber, 2001, "W-value measurements for carbon ions," GSI-Report 2001-1 (GSI Scientific Report 2000), p. 158 (unpublished).
- Rossi, B., 1952, *High-Energy Particles*, Prentice-Hall Physics Series (Prentice-Hall, Englewood Cliffs, NJ).
- Ryckewaert, G., M. Loiselet, N. Postiau, M. Bouvy, G. Berger, T. Daras, and E. Kaerts, 1991, "The production and acceleration of radioactive ion beams of  $^{11}\text{C}$ ,  $^{13}\text{N}$ ,  $^{15}\text{O}$ ,  $^{18}\text{F}$ ,  $^{19}\text{Ne}$  for postacceleration in the EULIMA accelerators." EULIMA Final Report, pp. 76–80 (unpublished).
- Safai, S., S. Lin, and E. Pedroni, 2004, "Development of an inorganic scintillating mixture for proton beam verification dosimetry," *Phys. Med. Biol.* **49**, 4637–4655.
- Sassowsky, M., and E. Pedroni, 2005, "On the feasibility of water calorimetry with scanned proton radiation," *Phys. Med. Biol.* **50**, 5381–5400.
- Sauli, F., 1997, "GEM: A new concept for electron amplification in gas detectors," *Nucl. Instrum. Methods Phys. Res. A* **386**, 531–534.
- Schaffner, B., and E. Pedroni, 1998, "The precision of proton range calculations in proton radiotherapy treatment planning: experimental verification of the relation between CT-HU and proton stopping power," *Phys. Med. Biol.* **43**, 1579–1592.

- Schall, I., D. Schardt, H. Geissel, H. Irnich, E. Kankeleit, G. Kraft, A. Magel, M. F. Mohar, G. Münzenberg, F. Nickel, C. Scheidenberger, and W. Schwab, 1996, "Charge-changing nuclear reactions of relativistic light-ion beams ( $5 \leq Z \leq 10$ ) passing through thick absorbers," *Nucl. Instrum. Methods Phys. Res. B* **117**, 221–234.
- Schardt, D., I. Schall, H. Geissel, H. Irnich, G. Kraft, A. Magel, M. F. Mohar, G. Münzenberg, F. Nickel, C. Scheidenberger, W. Schwab, and L. Sihver, 1996, "Nuclear fragmentation of high-energy heavy-ion beams in water," *Adv. Space Res.* **17**, 87–94.
- Schardt, D., P. Steidl, M. Krämer, U. Weber, K. Parodi, and S. Brons, 2008, "Precision Bragg-curve measurements for light-ion beams in water," GSI-Report 2008-1 (GSI Scientific Report 2007), p. 373 (unpublished).
- Schimmerling, W., J. Miller, M. Wong, M. Rapkin, J. Howard, H. G. Spieler, and B. V. Jarret, 2008, "The fragmentation of 670 AMeV neon-20 as a function of depth in water," *Radiat. Res.* **120**, 36.
- Schimmerling, W., T. S. Subramanian, W. J. McDonald, S. N. Kaplan, A. Sadoff, and G. Gabor, 1983, "Beam analysis spectrometer for relativistic heavy ions," *Nucl. Instrum. Methods Phys. Res.* **205**, 531–543.
- Schippers, J. M., S. N. Boon, and P. van Luijk, 2002, "Applications in radiation therapy of a scintillating screen viewed by a CCD camera," *Nucl. Instrum. Methods Phys. Res. A* **477**, 480–485.
- Schippers, J. M., R. Dölling, J. Duppich, G. Goitein, M. Jermann, A. Mezger, E. Pedroni, H. W. Reist, and V. Vrankovic, 2007, "The SC cyclotron and beam lines of PSI's new proton-therapy facility PROSCAN," *Nucl. Instrum. Methods Phys. Res. B* **261**, 773–776.
- Schlegel, W., O. Pastyr, T. Bortfeld, G. Becker, L. Schad, G. Gademann, and W. Lorenz, 1992, "Computer systems and mechanical tools for stereotactically guided conformation therapy with linear accelerators," *Int. J. Radiat. Oncol., Biol., Phys.* **24**, 781–787.
- Schneider, U., S. Agosteo, E. Pedroni, and J. Besserer, 2002, "Secondary neutron dose during proton therapy using spot scanning," *Int. J. Radiat. Oncol., Biol., Phys.* **53**, 244–251.
- Schneider, U., E. Pedroni, and A. Lomax, 1996, "The calibration of CT Hounsfield units for radiotherapy treatment planning," *Phys. Med. Biol.* **41**, 111–124.
- Scholz, M., 2003, "Effects of ion radiation on cells and tissues," *Adv. Polym. Sci.* **62**, 96–155.
- Scholz, M., and T. Elsässer, 2007, "Biophysical models in ion beam therapy," *Adv. Space Res.* **40**, 1381–1391.
- Scholz, M., A. M. Kellerer, W. Kraft-Weyrather, and G. Kraft, 1997, "Computation of cell survival in heavy ion beams for therapy. The model and its approximation," *Radiat. Environ. Biophys.* **36**, 59–66.
- Scholz, M., and G. Kraft, 1994, "Calculation of heavy ion inactivation probability based on track structure, x-ray sensitivity and target size," *Radiat. Prot. Dosim.* **52**, 29–33.
- Scholz, M., and G. Kraft, 1996, "Track structure and the calculation of biological effects of heavy charged particles," *Adv. Space Res.* **18**, 5–14.
- Schulz-Ertner, D., C. P. Karger, A. Feuerhake, A. Nikoghosyan, S. E. Combs, O. Jäkel, L. Edler, M. Scholz, and J. Debus, 2007, "Effectiveness of carbon ion radiotherapy in the treatment of skull-base chordomas," *Int. J. Radiat. Oncol., Biol., Phys.* **68**, 449–457.
- Schulz-Ertner, D., A. Nikoghosyan, B. Didinger, M. Munter, O. Jäkel, C. P. Karger, and J. Debus, 2005, "Therapy strategies for locally advanced adenoid cystic carcinomas using modern radiation therapy techniques," *Cancer* **104**, 338–344.
- Seravalli, E., M. de Boer, F. Geurink, J. Huizenga, R. Kreuger, J. M. Schippers, C. W. E. Eijk, and B. Voss, 2008, "A scintillating gas detector for 2D dose measurements in clinical carbon beams," *Phys. Med. Biol.* **53**, 4651–4665.
- Serber, R., 1947, "Nuclear reactions at high energies," *Phys. Rev.* **72**, 1114–1115.
- Shapiho, M. M., and R. Silberberg, 1970, "Heavy cosmic ray nuclei," *Annu. Rev. Nucl. Sci.* **20**, 323–392.
- Shavers, M. R., S. B. Curtis, J. Miller, and W. Schimmerling, 1990, "The fragmentation of 670 AMeV neon-20 as a function of depth in water, II. One-generation transport theory," *Radiat. Res.* **124**, 117–130.
- Shavers, M. R., K. Frankel, J. Miller, W. Schimmerling, and L. W. Townsend, 1993, "The fragmentation of 670 AMeV neon-20 as a function of depth in water, III. Analytical multigeneration transport theory," *Radiat. Res.* **136**, 1–14.
- Sigmund, P., 2004, *Stopping of Heavy Ions*, 204th ed. Springer Tracts of Modern Physics (Springer, Berlin).
- Sihver, L., D. Schardt, and T. Kanai, 1998, "Depth-dose distributions of high-energy carbon, oxygen and neon beams in water," *Jpn. J. Med. Physics* **18**, 1–21.
- Sihver, L., C. H. Tsao, R. Silberberg, T. Kanai, and A. F. Barghouty, 1993, "Total reaction and partial cross section calculations in proton-nucleus ( $Z_t \leq 26$ ) and nucleus-nucleus reactions ( $Z_p$  and  $Z_t \leq 26$ )," *Phys. Rev. C* **47**, 1225–1236.
- Slater, J. M., D. W. Miller, and J. O. Archambeau, 1988, "Development of a hospital-based proton beam treatment center," *Int. J. Radiat. Oncol., Biol., Phys.* **14**, 761–775.
- Staab, A., D. Zukowski, S. Walenta, M. Scholz, and W. Mueller-Klieser, 2004, "Response of Chinese hamster v79 multicellular spheroids exposed to high-energy carbon ions," *Radiat. Res.* **161**, 219–227.
- Suzuki, M., Y. Kase, T. Kanai, and K. Ando, 2000, "Correlation between cell killing and residual chromatin breaks measured by PCC in six human cell lines irradiated with different radiation types," *Int. J. Radiat. Biol.* **76**, 1189–1196.
- Tenforde, T. S., S. M. Afzal, S. S. Parr, J. Howard, J. T. Lyman, and S. B. Curtis, 1982, "Cell survival in rat rhabdomyosarcoma tumors irradiated *in vivo* with extended-peak silicon ions," *Radiat. Res.* **92**, 208–216.
- Tepper, J. E., 2004, "Seminars in radiation oncology," *Semin. Radiat. Oncol.* **14**, 1–100.
- Testa, E., M. Bajard, M. Chevallier, D. Dauvergne, F. L. Foulher, N. Freud, J. M. Letang, J. C. Poizat, C. Ray, and M. Testa, 2008, "Monitoring the Bragg peak location of 73 MeV/u carbon ions by means of prompt gamma-ray measurements," *Appl. Phys. Lett.* **93**, 093506.
- Tobias, C. A., 1967, "Heavy charged particles in cancer therapy, radiobiology and radiotherapy," National Cancer Institute Monograph No. 24.
- Tobias, C. A., A. Chatterjee, and A. R. Smith, 1971, "Radioactive fragmentation of N7+ ion beam observed in a beryllium target," *Phys. Lett. A* **37**, 119–120.
- Tomitani, T., M. Kanazawa, K. Yoshikawa, T. Kanai, A. Fukumura, Y. Wada, and I. Shinoda, 1997, "Effect of target fragmentation on the imaging of autoactivation of heavy ions," *J. Jpn. Soc. Ther. Radiol. Oncol. Suppl.* **9**, 79–82.
- Tomitani, T., K. Yoshikawa, M. Kanazawa, Y. Wada, and T. Kanai, 1994, "Preliminary measurements of auto activation of  $^{12}\text{C}$  beams with a commercially available PET," *Proceeding*

- of NIRS International Seminar on the Application of Heavy Ion Accelerator to Radiation Therapy of Cancer in Connection with the XXI PTCOG Meeting, 1994, NIRS-M-103/HIMAC-008, edited by T. K. Takada (National Institute of Radiological Sciences, Chiba-shi, Japan), pp. 125–130.
- Tomitani, T., *et al.*, 2003, “Washout studies of  $^{11}\text{C}$  in rabbit thigh muscle implanted by secondary beams of HIMAC,” *Phys. Med. Biol.* **48**, 875–889.
- Torikoshi, M., S. Minohara, N. Kanematsu, M. Komori, M. Kanazawa, K. Noda, N. Myahara, H. Ito, M. Endo, and T. Kanai, 2007, “Irradiation system for HIMAC,” *J. Radiat. Res. (Tokyo)* **48**, A15–A25.
- Tsai, Y. S., 1974, “Pair production and bremsstrahlung of charged leptons,” *Rev. Mod. Phys.* **46**, 815–851.
- Tsao, C. H., R. Silberberg, A. F. Barghouty, L. Sihver, and T. Kanai, 1993, “Scaling algorithm to calculate heavy-ion spallation cross sections,” *Phys. Rev. C* **47**, 1257–1262.
- Tsuji, H., T. Yanagi, H. Ishikawa, T. Kamada, J.-E. Mizoe, T. Kanai, S. Morita, and H. Tsujii, 2005, “Hypofractionated radiotherapy with carbon ion beams for prostate cancer,” *Int. J. Radiat. Oncol., Biol., Phys.* **63**, 1153–1160.
- Tsujii, H., *et al.*, 2004, “Overview of clinical experiences on carbon ion radiotherapy at NIRS,” *Radiother. Oncol.* **73**, S41–S49.
- Tsujii, H., *et al.*, 2007, “Clinical results of carbon ion radiotherapy at NIRS,” *J. Radiat. Res. (Tokyo)* **48**, A1–A13.
- Tsujii, H., *et al.*, 2008, “Clinical advantages of carbon-ion radiotherapy,” *New J. Phys.* **10**, 075009.
- Tsunashima, Y., S. Vedam, L. Dong, M. Umezawa, T. Sakae, M. Bues, P. Balter, A. Smith, and R. Mohan, 2008, “Efficiency of respiratory-gated delivery of synchrotron-based pulsed proton irradiation,” *Phys. Med. Biol.* **53**, 1947–1959.
- Uzawa, A., K. Ando, S. Koike, Y. Furusawa, Y. Matsumoto, N. Takai, R. Hirayama, M. Watanabe, M. Scholz, T. Elsässer, and P. Peschke, 2009, “Comparison of biological effectiveness of carbon-ion beams in Japan and Germany,” *Int. J. Radiat. Oncol. Biol. Phys.* **73**, 1545–1551.
- Varma, M. N., J. W. Baum, and A. V. Kuehner, 1977, “Radial dose, LET, and W for  $^{16}\text{O}$  ions in  $\text{N}_2$  and tissue-equivalent gases,” *Radiat. Res.* **70**, 511–518.
- Vavilov, P. V., 1957, “Ionizational losses of high energy heavy particles,” *Zh. Eksp. Teor. Fiz.* **32**, 920–923. [*Sov. Phys. JETP* **5**, 749–751 (1957)].
- Waligorski, M. P., M. Hollmark, and J. Lesiak, 2006, “A simple track structure model of ion beam radiotherapy,” *Radiat. Prot. Dosim.* **122**, 471–474.
- Wambersie, A., P. Chauvel, G. Gademann, J.-P. Gérard, and R. Sealy, 1992, “Cancer treatment with light ions in Europe,” report (unpublished).
- Weber, U., 1996, “Volumenkonforme Bestrahlung mit Kohlenstoff-Ionen zur Vorbereitung einer Strahlentherapie,” Ph.D. thesis [Gesamthochschule Kassel (Germany), Fachbereich Physik].
- Weber, U., and G. Kraft, 1999, “Design and construction of a ripple filter for a smoothed depth dose distribution in conformal particle therapy,” *Phys. Med. Biol.* **44**, 2765–2775.
- Weber, U., and G. Kraft, 2009, “Comparison of carbon ions versus protons,” *Cancer J.* **15**, 325–332.
- Weyrather, W. K., S. Ritter, M. Scholz, and G. Kraft, 1999, “RBE for carbon track-segment irradiation in cell lines of differing repair capacity,” *Int. J. Radiat. Biol.* **75**, 1357–1364.
- Wilson, J. W., L. W. Townsend, and F. F. Badavi, 1987, “Galactic HZE propagation through the earth’s atmosphere,” *Radiat. Res.* **109**, 173–183.
- Wilson, J. W., L. W. Townsend, H. B. Bidasaria, W. Schimmerling, M. Wong, and J. Howard, 1984, “Neon-20 depth-dose relations in water,” *Health Phys.* **46**, 1101–1111.
- Wilson, J. W., L. W. Townsend, S. L. Lamkin, and B. D. Ganapol, 1990, “A closed-form solution to HZE-propagation,” *Radiat. Res.* **122**, 223–228.
- Wilson, R. R., 1946, “Radiological use of fast protons,” *Radiology* **47**, 487–491.
- Woodruff, K. H., J. R. Castro, J. M. Quivey, W. M. Saunders, G. T. Chen, J. T. Lyman, S. Pitluck, C. A. Tobias, R. E. Walton, and T. C. Peters, 1984, “Postmortem examination of 22 pancreatic carcinoma patients treated with helium ion irradiation,” *Cancer* **53**, 420–425.
- Xu, X. G., B. Bednarz, and H. Paganetti, 2008, “A review of dosimetry studies on external-beam radiation treatment with respect to second cancer induction,” *Phys. Med. Biol.* **53**, R193–R241.
- Yan, X., U. Titt, A. M. Koehler, and W. D. Newhauser, 2002, “Measurement of neutron dose equivalent to proton therapy patients outside of the proton radiation field,” *Nucl. Instrum. Methods Phys. Res. A* **476**, 429–434.
- Zacharias, T., W. Dorr, W. Enghardt, T. Haberer, M. Krämer, R. Kumpf, H. Rothig, M. Scholz, U. Weber, G. Kraft, and T. Herrmann, 1997, “Acute response of pig skin to irradiation with  $^{12}\text{C}$ -ions or 200 kV X-rays,” *Acta Oncol.* **36**, 637–642.
- Ziegler, J. F., J. P. Biersack, and M. D. Ziegler, 2008, *SRIM—The Stopping and Range of Ions in Matter* (SRIM, Chester, MD).
- Zink, S. R., J. T. Lyman, J. R. Castro, G. T. Chen, J. M. Collier, and W. M. Saunders, 1988, “Treatment planning study for carcinoma of the esophagus: Helium ions versus photons,” *Int. J. Radiat. Oncol., Biol., Phys.* **14**, 993–1000.